**UNIVERSITĀTSmedizin.**
MAINZ

# Characterizing the Tumor Microenvironment upon Transcutaneous Immunization by Single-Cell RNA-Sequencing – Implications for Cancer Immunotherapy

**Dissertation**

Zur Erlangung des Grades

Doktor der Naturwissenschaften

Am Fachbereich Biologie

der Johannes Gutenberg-Universität Mainz

vorgelegt von

Joschka Matthias Bartneck

geboren am 13.01.1994

in Lahnstein

Mainz, April 2023

Aus der III. Med. Klinik der

Universitätsmedizin der Johannes Gutenberg-Universität Mainz

Dekan:                                  Prof. Dr. Eckhard Thines

1. Berichterstatter:                 Prof. Dr. med. Markus P. Radsak

2. Berichterstatter:                 Prof. Dr. Eckhard Thines

Tag der mündlichen Prüfung:        07.07.2023

# Index

<u>Declaration:</u>

It is planned to publish parts of this work in two separated publications. The first part relates to the optimization of the Dithranol-Imiquimod-based transcutaneous immunization method DIVA, aiming to induce protection against MC38mOVA tumor cells in a prophylactic setting (4.1 - 4.2). The second part relates to the characterization of the Tumor Microenvironment upon Dithranol-Imiquimod-based transcutaneous immunization and the identification of a suitable target for the therapeutic treatment of immunosuppressive mechanisms in the Tumor microenvironment (4.3 - 4.7).

# Abbreviations

| | |
|---|---|
| ABC | Avidin-biotin enzyme complex |
| ACK | Ammonium chloride potassium |
| AEC | 3-Amino-9-ethylcarbazole |
| ANOVA | Analysis of variance |
| APC | Antigen presenting cell |
| APC (fluorophore) | Allophycocyanin |
| Arg1 | Arginase 1 |
| BB | Brilliant Blue |
| BM | Bone marrow |
| BSA | Bovine serum albumin |
| BUV | Brilliant ultraviolet |
| BV | Brilliant violet |
| CAR | Chimeric antigen receptor T cell |
| CCL | Chemokine (C-C motif) ligand |
| CCR | CC chemokine receptor |
| CD | Cluster of differentiation |
| (c)DC | (conventional) Dendritic cell |
| CD40L | CD40 Ligand |
| CFSE | Carboxyfluorescein succinimidyl ester |
| cMoP | common Monocyte progenitor |
| CTL | cytotoxic T lymphocyte |
| CTLA-4 | Cytotoxic T-lymphocyte protein 4 |
| DAC | German Pharmaceutics codex |
| DIVA | Dithranol-Imiquimod-based vaccination |
| DIVA$^2$ | Boost DIVA |
| dLN | draining lymph node |
| DMSO | dimethyl sulfoxide |
| DNA | Deoxyribonucleic acid |
| EDTA | Ethylenediaminetetraacetic acid |
| eGFP | enhanced Green fluorescent protein |
| ELISpot | Enzyme-linked immuno-sorbent spot assay |
| ETOH | Ethanol |
| FasL | Fas Ligand |
| FCS | Fetal calf serum |
| FSC | Forward scatter light |
| G-CSF | Granulocyte-CSF |
| GM-CSF | Granulocyte Macrophage Colony-stimulating factor |
| HIF | Hypoxia-inducible factors |
| ICB | Immune checkpoint blockade |
| ICI | Immune checkpoint inhibitor |
| IDO | Indoleamine 2,3-dioxygenase |
| IFN | Interferon |
| Ig | Immunoglobulin |
| IL | Interleukin |
| ILC | Innate lymphoid cell |
| IMDM | Iscove's Modified Dulbecco's Medium |
| iNKT | invariant NKT cell |
| iNOS | Nitric oxide synthase 2 |
| ITIM | immunoreceptor tyrosine-based inhibitory motif |
| ITSM | Immunoreceptor Tyrosine-based Switch Motif |
| Lag3 | Lymphocyte-activation gene 3 |
| Ly6C | Lymphocyte antigen 6C2 |
| Ly6G | Lymphocyte antigen G6D |
| M-CSF | Macrophage-CSF |
| MACS | Magnetic activated cell separation |
| MC38mOVA | MC38 membranous Ovalbumin |
| MDSC | Myeloid derived suppressor cell |
| MEM | Minimum essential medium |
| MHC | Major histocompatibility complex |
| moDC | Monocyte-derived Dendritic cell |
| mRNA | messenger Ribonucleic acid |

| | |
|---|---|
| ndLN | non-draining lymph node |
| NK cell | Natural killer cell |
| NKG2D(L) | natural killer group 2, member D (ligand) |
| NKT cell | Natural killer T cell |
| OT-I | MHC I Ovalbumin-specific CD8+ T cells |
| Ova | Ovalbumin |
| PBS | Phosphate buffered saline |
| PD-1 | Programmed cell death protein 1 |
| PD-L1 | Programmed cell death 1 ligand 1 |
| PE | Phycoerythrin |
| PE-Cy | Phycoerythrin cyanine |
| PMA | Phorbol-12-myristat-13-acetate |
| rpm | Revolutions per minute |
| RPMI | Roswell Park Memorial institute |
| SALT | Skin associated lymphoid tissue |
| SCF | Stem cell factor |
| SFU | Spot forming unit |
| Sirpα | Signal-regulatory protein alpha |
| SSC | Side scatter light |
| t-SNE | t-distributed stochastic neighbor embedding |
| TADC | Tumor associated Dendritic cell |
| TAM | Tumor associated macrophage |
| TCI | Transcutaneous immunization |
| TCR | T cell receptor |
| TGF-β | Transforming growth factor β |
| Th1 | T helper cell type 1 |
| Tigit | T Cell Immunoreceptor With Ig and ITIM Domains |
| TIL | Tumor infiltrating leukocyte |
| Tim3 | Hepatitis A Virus Cellular Receptor 2 |
| TME | Tumor microenvironment |
| TNF | Tumor necrosis factor |
| TRAIL | TNF-related apoptosis-inducing ligand |
| Treg | Regulatory T cell |
| TRM | Tissue-resident macrophage |
| VEGF | Vascular endothelial growth factor |
| VEGFR2 | VEGF receptor 2 |
| WHO | World health organization |

## SI-Units

| | |
|---|---|
| *g* | gravitation acceleration |
| g | gram |
| mg | milligram |
| μg | microgram |
| ng | nanogram |
| l | Liter |
| ml | milliliter |
| μl | microliter |
| mm | millimeter |
| μm | mikrometer |
| nm | nanometer |
| mm$^2$ | square millimeter |
| mm$^3$ | cubic millimeter |
| °C | degree celsius |
| sec | second |
| min | minute |
| h | hour |
| bar | pressure unit |
| mbar | millibar |

# 1   Introduction

## 1.1   The Tumor microenvironment and anti-tumor immunity

### 1.1.1   Formation of tumors

In an organism, the transformation of healthy cells into tumor cells occurs ubiquitously in every types of tissue. This process is driven by tumorigenic factors such as carcinogens, radiation, viral infections, chronic inflammation or inherited genetic mutations (Schreiber et al. 2011). The first barrier against the establishment of such degenerated cells is formed by intrinsic tumor suppression mechanisms such as the induction of senescence, DNA repair or apoptotic pathways in the tumor cells (DeGregori 2011). However, if intrinsic tumor suppression is not sufficient to prevent the outgrowth of these cells, extrinsic tumor suppression is necessary. The interaction of the innate and adaptive immune system can prevent tumor formation from such degenerated cells in different ways. In this context, tumor cells or tumors in early stages are eliminated before they can become clinically relevant.

The innate immune response is based on the recognition of pathogen-associated molecular patterns (PAMPs) or damage-associated molecular patterns (DAMPs) expressed by stressed tumor cells at an early stage. Pattern recognition receptors (PRRs) on the cell surface of innate immune cells enable the recognition of PAMPs or DAMPs. (Cheng et al. 2013). Myeloid immune cells such as monocytes, macrophages and Neutrophils play an important role in this process. Activation of PRRs on their surface induces cytolytic and phagocytic effector mechanisms, thereby eliminating tumor cells (Lebegge et al. 2020). Furthermore, Natural Killer (NK) cells recognize tumor cells via activating receptors which induces secretion of perforin and granzyme-containing granules by the NK cells leading to apoptosis in tumor cells. Dendritic cells (DCs) form a link between the innate and adaptive immune defense. They take up tumor antigens released by eliminated tumor cells in the tissue and present them to naïve cluster of differentiation (CD)8$^+$ T cells via cross-presentation on major histocompatibility complex (MHC) class I molecules (den Haan et al. 2000). Priming of CD8$^+$ T cells by DCs massively increases the number of tumor-specific CD8$^+$ T cells. The binding of co-stimulatory molecules between DCs and T cells during T cell priming amplifies the activating signal, crucial for a strong T cell proliferation. Activated T cells can induce apoptosis of tumor cells by secreting perforin and granzyme-containing granules. Furthermore, they secrete interferon (IFN)-$\gamma$, contributing to the proliferation-inhibiting effect of NK cells (Cheng et al. 2013). Since tumor cells also present tumor antigens on their cell surface via MHC I molecules, the tumor-specific CD8$^+$ T cells can recognize and specifically eliminate these tumor cells. Such elimination of degenerated cells occurs ubiquitously in various tissues of a healthy organism.
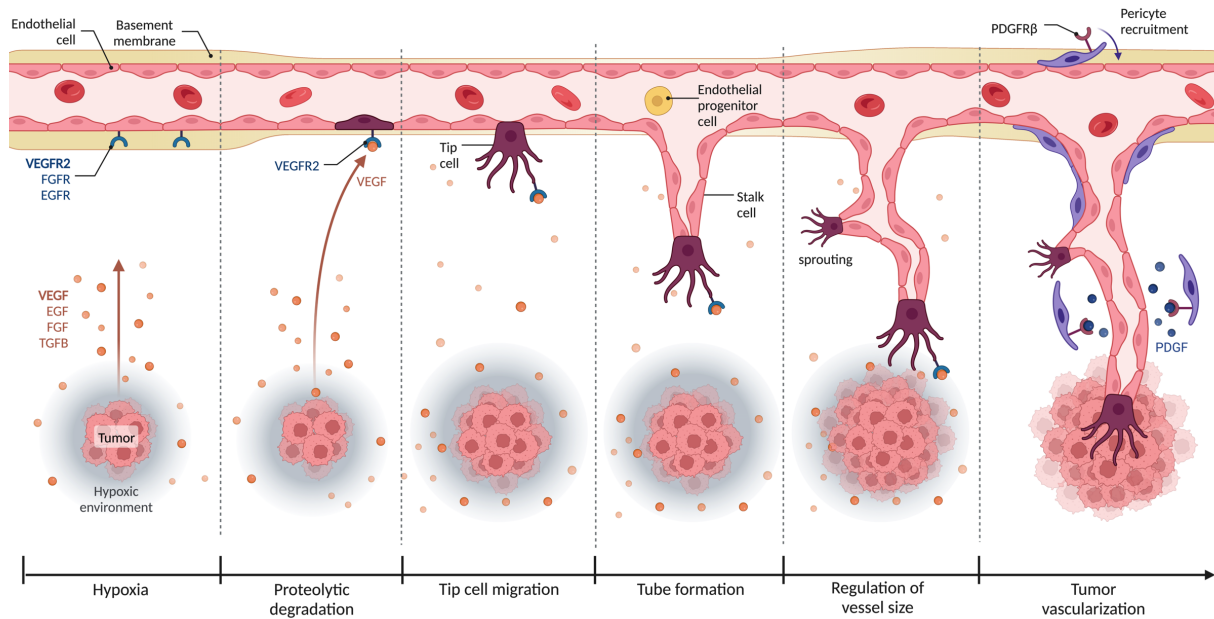
**Figure 1.1: Formation and vascularization of a solid tumor**

Formation of tumor cells can be induced by various factors such as carcinogens, radiation, viral infections, chronic inflammation or genetic mutations. When intrinsic and extrinsic tumor suppressor mechanisms are not sufficient to eliminate tumor cells, they accumulate and start to build a solid tumor. Tumor cell-derived cytokines such as VEGF induce the migration of tip cells leading to the formation of new blood vessels. Endothelial cells are stimulated to produce PDGF, recruiting pericytes providing structural support for vascularization. The progressive vascularization of the tumor ensures its development and progression by transporting nutrients and oxygen to the tumor cells. Created with BioRender.com.

However, if more tumor cells are generated in a tissue site than the immune system can eliminate, tumor cells accumulate and subsequently form a solid tumor (Figure 1.1). Tumor cells are characterized by a greatly increased metabolism and division rate, crucial for tumor development and progression (Hanahan and Weinberg 2011). Tumor cells secrete cytokines such as vascular endothelial growth factor (VEGF), epidermal growth factor (EGF), Hypoxia-inducible factor 1$\alpha$ (HIF-1$\alpha$), fibroblast growth factor (FGF) or transforming growth factor (TGF)-$\beta$, driving the formation of new blood vessels that continuously supply the tumor with nutrients and oxygen (Saman et al. 2020). VEGF binds to the VEGF receptor 2 (VEGFR2) of an endothelial cell, which is selected to be the tip cell leading the outward extension of the sprout. Neighboring endothelial cells remain attached to the tip cell and migrate behind it, forming a stalk (Chappell et al. 2011). Endothelial cells produce platelet-derived growth factors (PDGF) recruiting pericytes that provide structural support for vascularization (Thijssen et al. 2018).

### 1.1.2 The Tumor Microenvironment and cell types shaping its immune status

The accumulation of tumor cells leads to the formation of a solid tumor in the course of vascularization. Already at an early stage, a large number of immune cells of the innate and adaptive immune system migrate to the tumor site. If the immune system does not succeed in eliminating these tumor cells, the tumor establishes and forms an individual, highly heterogeneous environment, which is referred to as

Tumor Microenvironment (TME) (Whiteside 2008). The TME comprises the entirety of numerous cell types, including tumor cells, fibroblasts, endothelial cells and various immune cell types, their secreted mediators in addition to blood vessels and structure-giving extracellular matrix. The cytokines and chemokines secreted by tumor cells, host cells and immune cells contribute significantly to the modulation of the immune status of the TME (Lihong Li et al. 2020). Figure 1.2 schematically shows the composition of the TME.
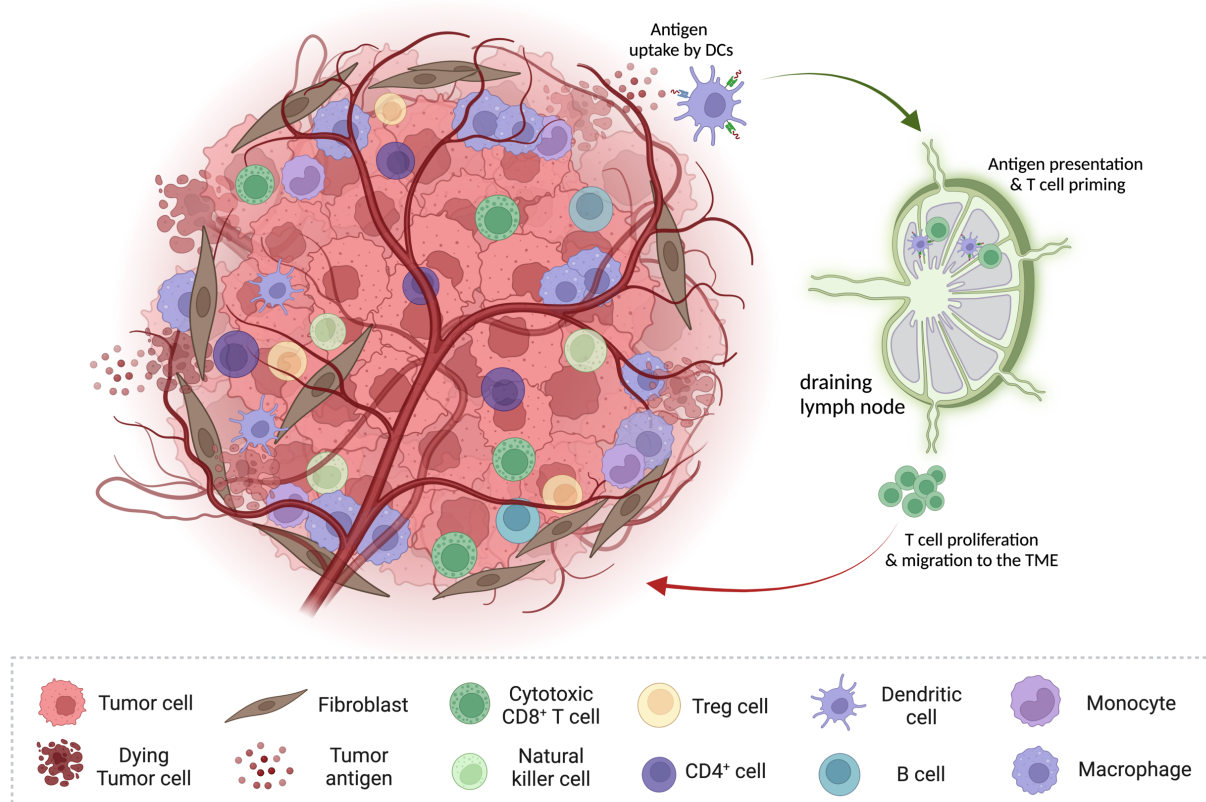


**Figure 1.2: The Tumor microenvironment**

The tumor microenvironment consists of numerous cell types, including tumor cells, fibroblasts, endothelial cells and various immune cell types, soluble components such as cytokines and chemokines and the structure-giving extracellular matrix. The tumor antigens released during elimination of tumor cells by cytotoxic cells are taken up by DCs. These migrate to draining lymph nodes and prime naïve T cells activating and stimulating them for proliferation. The chemokines produced in the TME form a gradient within the organism the activated T cells can migrate along to the tumor in order to eliminate tumor cells. DC = Dendritic cell; TME = Tumor microenvironment; Treg = regulatory T cell. Created with BioRender.com.

*Innate lymphoid cells*

One of the first barriers of anti-tumor immunity represents the family of innate lymphoid cells (ILC), which consists of NK cells, ILC1s, ILC2s and ILC3s (Jacquelot et al. 2022). In the context of TME mainly the NK cells and ILC1s show an anti-tumor function. NK cells provide one of the first barriers against the establishment of tumor cells. They are activated and stimulated to mature by cytokines such as type I interferons, Interleukin (IL)-12, IL-18 or IL-15 (Waldhauer and Steinle 2008). Activated NK cells are able to kill tumor cells directly in different ways. The best researched mechanism is the NKG2D-NKG2DL-mediated release of perforin- and granzyme-containing granules inducing apoptosis in tumor cells (Cheng et al. 2013). Upon activating signals, NK cells express the death ligands Fas antigen ligand

(FasL) or Tumor necrosis factor related apoptosis-inducing ligand (TRAIL), also inducing apoptosis in tumor cells (Rossin et al. 2019). In addition, activated NK cells produce IFN-$\gamma$, inducing cell cycle arrest in tumor cells which consequently prevents their proliferation (Ni and Lu 2018). Indirectly, NK cells can activate cytotoxic CD8^{+} T cells by producing IFN-$\gamma$ and thus also promote the differentiation of CD4^{+} T cells into T helper type 1 (Th1) cells, able to contribute to anti-tumor immunity by producing pro-inflammatory cytokines (Chiossone et al. 2018). The role of NK cells in anti-tumor immunity has been evaluated in various tumor models, where infiltration of the TME by NK cells contributed to tumor growth control (Guerra et al. 2008; Mishra et al. 2010; Smyth et al. 2005). This is supported by the fact that NKG2D knockout mice interbred with transgenic adenocarcinoma mouse prostate (TRAMP, spontaneous prostate cancer model) mice or E$\mu$-*myc* (lymphoma model) mice showed higher susceptibility to tumor development (Guerra et al. 2008). ILC1s are mainly activated by the cytokines IL-12, IL-15 and IL-18, leading to the production of the anti-tumor cytokines IFN-$\gamma$ and tumor necrosis factor (TNF)-$\alpha$ (Bernink et al. 2013; A. Fuchs et al. 2013; Klose et al. 2014). In this setting, IFN-$\gamma$ induces the upregulation of MHC I molecules on tumor cells, enabling them to be recognized and eliminated by T cells to a greater extent (Martini et al. 2010). Since IFN-$\gamma$ is associated with inhibiting tumor cell proliferation, promoting tumor cell apoptosis and inhibiting angiogenesis, ILC1s are able to contribute to anti-tumor immunity in the TME in an indirect way (Beatty and Paterson 2001; Ni and Lu 2018).

*Natural killer T cells*

Another innate immune cell type contributing to tumor control are Natural killer T (NKT) cells, which co-express T cell receptors (TCR) and NK lineage markers (Van Kaer 2007). There are 3 types of NKT cells, including type I NKT, type II NKT and NKT-like cells. Type I NKT cells are the most abundant and are also called invariant NKT (iNKT) cells due to their restricted TCR set (Godfrey et al. 2004). The TCR of NKT cells has an invariant TCR$\alpha$- and a semi-variant TCR$\beta$-chain and recognizes lipid antigens presented on the non-classical MHC class I molecule CD1d of antigen-presenting cells (APC) (Godfrey and Berzins 2007). Tumor cells expressing CD1d molecules can be eliminated directly by iNKT cells via Fas-FasL interaction, the release of granzyme- and perforin-containing granules or the expression of TRAIL (Díaz-Basabe et al. 2020). Upon activation, iNKT cells express cytokines, including IFN-$\gamma$, IL-2, IL-4, TNF-$\alpha$, Transforming growth factor (TGF) $\beta$ and Granulocyte Macrophage colony-stimulating factor (GM-CSF) affecting a wide range of anti-tumor immune cells making them to a linker between innate and adaptive immune response (Coquet et al. 2007, 2008). Such a linker function of iNKT cells is the expression of CD40 ligand (CD40L), which binds to CD40 on DCs inducing their maturation (Kitamura et al. 1999). As a result, DCs express co-stimulatory molecules such as CD80, CD86 and CD40 to a greater extent and produce IL-12, which in a positive feedback loop enhances IFN-$\gamma$ production by iNKT cells, NK cells and CD8^{+} T cells (Ma and Clark 2009; Taraban et al. 2008; Y.-F. Yang et al. 2000).

*Tumor-infiltrating monocyte-derived cells*

Monocytes are circulating mononuclear phagocytes able to migrate into various types of tissues as a response to inflammatory signals (Jakubzick et al. 2013). In mice, three types of monocytes have been described, including classical monocytes (Ly6C$^{hi}$ CD43$^{lo}$ CX3CR1$^{lo}$), non-classical monocytes (Ly6C$^{lo}$, CD43$^{hi}$, CX3CR1$^{hi}$) and intermediate monocytes (Ly6C$^{int}$, CD43$^{hi}$, CX3CR1$^{hi}$) (Ziegler-Heitbrock et al. 2010). In the bone marrow (BM) classical Ly6C$^{hi}$ monocytes arise from common monocyte progenitors (cMoP) and can differentiate into non-classical or intermediate monocytes after entering the circulating blood (Orozco et al. 2021; Sunderkötter et al. 2004; Yona et al. 2013). Classical monocytes require the CC chemokine receptor 2 (CCR2) to leave the bone marrow and migrate within the bloodstream along the gradient of CCR2 ligands such as Chemokine (C-C motif) ligand (CCL)2, CCL7 or CCL12 into tissues (Jakubzick et al. 2013; Serbina and Pamer 2006). The recruitment of classical monocytes to the tumor starts at an early tumor stage and proceeds during tumor progression (Franklin et al. 2014). For numerous tumor models, it has been described that this recruitment mainly takes place via the chemokine CCL2 (Chun et al. 2015; Franklin et al. 2014; Qian et al. 2011). Once in the TME, monocytes can differentiate as response to environmental stimuli into monocytic myeloid-derived suppressor cells (**M-MDSC**) and further into tumor-associated macrophages (**TAM**) or tumor-associated dendritic cells (**TADC**) (Lavin et al. 2017; Ugel et al. 2021; Veglia, Perego, and Gabrilovich 2018; Zilionis et al. 2019).

MDSCs are a very heterogeneous myeloid cell population, characterized by their immunosuppressive properties, favoring tumor progression. The accumulation of MDSCs depends on two groups of signals (Condamine and Gabrilovich 2011). The first group of signals is driven by tumor-derived factors and includes GM-CSF, G-CSF, M-CSF, Stem cell factor (SCF) and VEGF (Dolcetti et al. 2009; Umansky and Sevko 2013). The second group includes inflammatory signals such as IFN-$\gamma$, IL-1b, -4, -6, -13 or TNF-$\alpha$ (Veglia, Perego, and Gabrilovich 2018). CD11b$^{+}$ Ly6G$^{+}$ Ly6C$^{lo}$ polymorphonuclear-MDSCs (PMN-MDSCs) are distinguished from CD11b$^{+}$ Ly6G$^{-}$ Ly6C$^{hi}$ CCR2$^{+}$ M-MDSCs (Damuzzo et al. 2015; Lesokhin et al. 2012). M-MDSCs can be distinguished from TAMs since TAMs show a high F4/80 expression and a lower Ly6C expression compared to M-MDSC (D. I. Gabrilovich and Nagaraj 2009).

TAMs are the most abundant myeloid cell type in the TME and originate mostly from monocytes, as they can be recruited in large numbers from the blood (Ginhoux et al. 2016). Once in the TME, CCR2$^{+}$ monocytes can upregulate TAM-associated markers such as F4/80, CD11c, MHC class II or vascular cell adhesion molecule 1 (V-CAM1) within a few days. In the TME, these monocyte-derived TAMs show the ability to proliferate which even increases their number (Franklin et al. 2014). Another source of TAMs are tissue-resident macrophages (TRM), which arise from fetal-yolk sac or fetal-liver progenitors (Mass

et al. 2016). While TRMs are more related to tissue remodeling and wound healing, monocyte-derived TAMs are essentially considered to have a pro-tumor immunosuppressive function (Y. Zhu et al. 2017).

TADCs represent a smaller population in the TME, but with their ability to process and present antigens, they link the innate and adapted immune response and can thus contribute to immune control in the TME. DCs arise in the BM from macrophage/DC progenitors (MDP) and differentiate via intermediates into conventional DCs (type 1 (cDC1) and type 2 (cDC2)), the plasmacytoid DCs (pDCs) and the monocyte-derived DCs (moDC) (Broz et al. 2014). CDC1s are detectable by the surface markers CD8a, CD103 and XCR1 (Gardner et al. 2020). A central function of CDC1s in TME is the uptake of tumor antigen and cross-presentation to naive CD8$^+$ T cells in the tumor-draining lymph nodes (dLN). This activates T cells and stimulates them to proliferate, enabling elimination of tumor cells in an antigen-specific manner, thereby preventing tumor progression (Broz et al. 2014). This cross-presentation of tumor antigen to naive CD8$^+$ T cells can also be supported by monocyte-derived Ly6C$^+$ moDCs with a similar efficiency to cDCs (Diao et al. 2018). cDC2s are detectable by the surface markers CD11b and Sirp$\alpha$ (A. Gardner, de Mingo Pulido, and Ruffell 2020). In contrast to cDC1s, they contribute to anti-tumor immunity by activating and stimulating CD4$^+$ T cells to proliferate through MHC class II-mediated pathways (Guilliams et al. 2016). Priming and activation of CD4$^+$ and CD8$^+$ T cells by cDCs is enhanced by co-stimulatory molecules. In this regard, the interactions between DCs and T cells via CD80/86-CD28, CD70-CD27 or OX40L-OX40 induce enhanced T cell activation and thus anti-tumor immunity (Böttcher and Reis e Sousa 2018; Dannull et al. 2005; Kim et al. 2021). In addition, soluble factors such as cytokines and chemokines are essential for the activation and migration of cytotoxic cells to the TME. A central role is played by IL-12, which is produced by cDC1s and stimulates T cells and NK cells to migrate to the TME for eliminating tumor cells (C. W. Kim, Kim, and Lee 2021). Taken together, DCs as part of innate immunity exhibit a crucial role in TME by controlling the elimination of tumor cells by activating the adaptive immune response. In this regard, a high density of TADCs in patients is associated with improved overall survival and an enhanced anti-tumor T cell immune response which has been described for breast, lung or head and neck cancer (Broz et al. 2014; Dieu-Nosjean et al. 2008).

*Tumor-infiltrating T cells*
T cells play a central role in the TME, as they can contribute decisively to the elimination of tumor cells in addition to the cytotoxic cells of the innate immune system. In this respect, the infiltration of a tumor by T cells is of central importance for anti-tumor immunity and thus for the rejection of a tumor. Already at an early stage of tumor growth, tumor antigens get released when tumor cells are eliminated. The tumor antigens are taken up by cDC1s which migrate to the dLN (Figure 1.2) (Broz et

al. 2014). The CD8^{+} T cells activated by cDC1s via cross-presentation in the dLN proliferate and migrate along chemokine gradients to the tumor. The main interactions between chemokines secreted by the TME and chemokine receptors on T cells include CCL2-CCR2, CXCL9/10-CXCR3 and CCL3/4/5-CCR5 (Fridman et al. 2012; Harlin et al. 2009). When activated and primed CD8^{+} T cells enter the TME, they recognize tumor cells since they present tumor antigens via MHC I molecules on their surface. T cells bind with their antigen-specific TCR to the complex of MHC I molecule and antigen. This binding process activates TCR signaling initiating the T cell-driven elimination of the tumor cell (Figure 1.3).
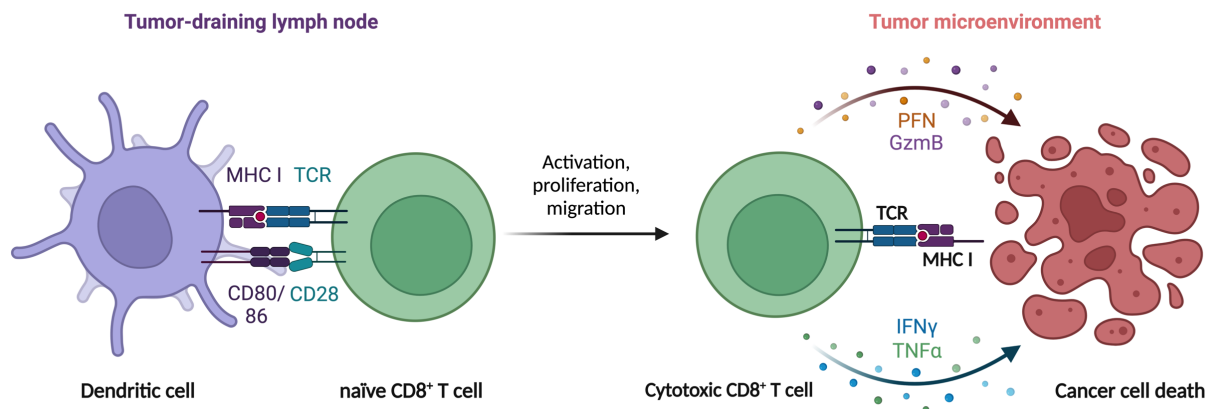


**Figure 1.3: Cytotoxic CD8^{+} T cells eliminate tumor cells in an antigen-specific manner**
DCs present tumor antigens that they have taken up in the TME to naïve T cells in the draining lymph nodes on MHC I molecules. During priming, co-stimulatory signals such as the binding of CD80/86 and CD28 lead to increased activation of T cells. These proliferate and migrate to the TME, where they induce apoptosis in the tumor cell via the release of perforins, granzymes, IFN-γ and TNF-α. Created with BioRender.com.

A key role in this T cell-driven elimination of tumor cells is played by IFN-γ, which is also produced by NK cells, NKT cells and ILCs (Shen et al. 2018). IFN-γ inhibits tumor cell proliferation by enhancing the expression of cell cycle inhibitors such as p27Kip, p16 or p21, which has been described for breast cancer (Kochupurakkal et al. 2015), colorectal cancer (L. Wang et al. 2015) and hepatocellular carcinoma (W. Li et al. 2012). Similar to NK and NKT cells, CD8^{+} T cells also induce apoptosis in tumor cells by the release of granzyme and perforin-containing granules (Voskoboinik et al. 2015). cDC2s take up tumor antigens in the TME and migrate to the draining lymph node in the same way as cDC1s (Guilliams et al. 2016). In the dLN, they prime naïve CD4^{+} T cells in an MHC II-dependent manner. During this process, cDC2s secrete IL-12, which triggers the CD4^{+} T cells to differentiate to Th1 cells. Once in the TME, as response to cytotoxic lymphocyte-derived IFN-γ, Th1 cells also produce IFN-γ and IL-2. These cytokines directly cause tumor cell elimination and indirectly recruit pro-inflammatory macrophages and activate CD8^{+} T cells, able to contribute to anti-tumor immunity (Saito et al. 2022). Another subtype of T cells are the CD4^{+} CD25^{+} forkhead box P3 (FoxP3)[+] regulatory T (Treg) cells (Hori et al. 2003; Sakaguchi et al. 1995). As mediators of self-tolerance, they inhibit an exuberant immune response in peripheral tissues and thus prevent autoimmune diseases. In the TME, however, they

suppress anti-tumor immunity via various mechanisms and thus promote tumor growth (Itahashi et al. 2022).

### 1.1.3 Immunosuppressive mechanisms driving cancer immune evasion

If innate and adaptive anti-tumor immune responses fail to eliminate a tumor, this is often due to immunosuppressive mechanisms within the TME. Mechanisms that directly promote tumor growth are distinguished from mechanisms that suppress anti-tumor immunity and thus prevent immune control, indirectly leading to tumor progression. The immune system not only contributes to tumor elimination but can also promote tumor progression. This process is called **cancer immuno editing** (Schreiber, Old, and Smyth 2011) (Figure 1.4).
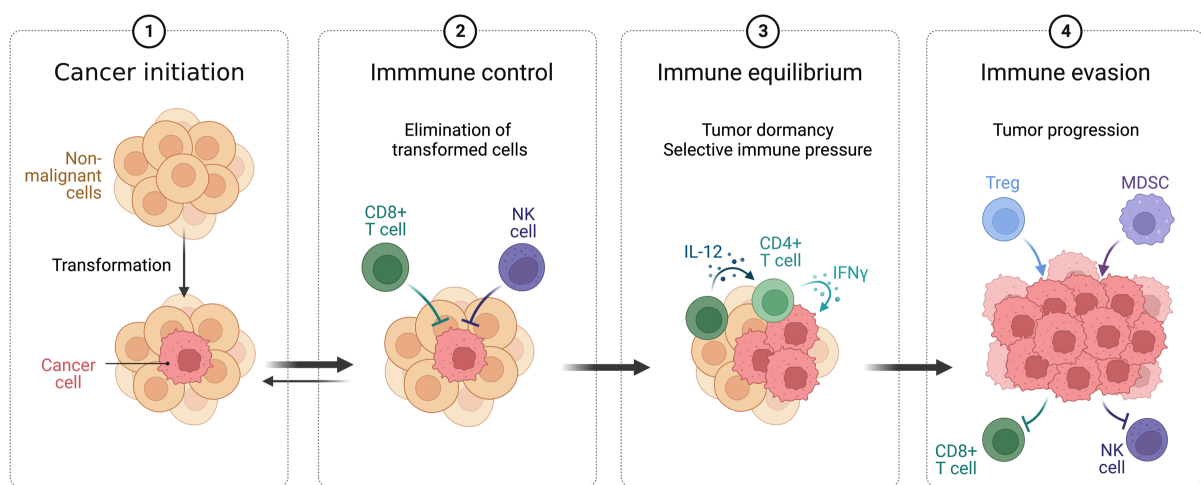


**Figure 1.4: Phases of cancer immuno editing**

Cancer immuno editing describes the process in which the immune system can both prevent and support the development of a tumor. After the initiation of a solid tumor, cancer immuno editing comprises three phases, immune control, immune equilibrium and immune evasion (Schreiber, Old, and Smyth 2011). Created with BioRender.com.

Cancer immuno editing comprises three phases. In the **immune control** (or elimination) phase, the immune system eliminates more tumor cells than proliferate, which in the best case leads to the complete disappearance of a tumor. However, if immunosuppressive mechanisms are going on in the TME, they inhibit the anti-tumor immunity leading to a reduced tumor cell elimination. The phase in which eliminated tumor cells correspond to proliferated tumor cells, is called **immune equilibrium**. This state is also called tumor dormancy and can last up to several years. If the immunosuppressive mechanisms inhibit the anti-tumor immunity to such an extent that more tumor cells proliferate than the immune system can eliminate, the phase of **immune evasion** (or immune escape) is reached. If a tumor was initially successfully rejected but then reappeared, it can enter the process of cancer immuno editing again. Depending on the intensity of the anti-tumor immunity and proliferation of tumor cells, the phases of immune control and equilibrium can also be skipped and the state of immune evasion is reached directly which is often associated with a rapid tumor growth and a poor

outcome for a patient (O'Donnell et al. 2019). In the following, we characterize immunosuppressive mechanisms that inhibit anti-tumor immunity and thus induce the transition to the state of immune evasion.

The infiltration of the TME by tumor-reactive T cells is of central importance for the successful elimination of tumor cells. In this context, mechanisms have been described that induce T cell exclusion, which Spranger and Gajewski refer to as innate evasion (Spranger and Gajewski 2018). Tumors in which the $\beta$-catenin pathway is activated produce CCL4 in a reduced form, whereby Batf3-lineage DCs in the TME are significantly reduced. However, pre-clinical mouse models showed Batf3-lineage CD103$^+$ DCs in the TME are essential for T cell infiltration. This shows that there is a clear link between the activation of $\beta$-catenin in tumor cells and the absence of T cells in the TME, which is associated with resistance to immunotherapy (Spranger et al. 2015). Another mechanism leading to a non-T-cell-inflamed TME is a loss-of-function mutation of phosphatase and tensin homolog (PTEN) in tumor cells (Peng et al. 2016). Tumors with reduced or no PTEN expression show reduced expression of the autophagy-related genes LC3I and LC3II. Autophagy contributes to the activation of APCs and cross-presentation of tumor antigens (Zhong et al. 2016). Thus, it is conceivable that the loss-of-function mutation of PTEN in tumor cells leads to reduced activation of DCs and macrophages, resulting in the absence of T cells and reduced anti-tumor immunity (Spranger and Gajewski 2018). Another reason for the exclusion of T cells can be tumor cell metabolism. This is characterized by hypoxia, which is triggered by rapid proliferation and inadequate angiogenesis (Vander Heiden et al. 2009). Hypoxia activates the HIF-1$\alpha$ signaling pathway, which results in the activation of VEGF and Cox genes, thereby reducing adhesion molecules. This is accompanied with increased FasL-mediated T cell death which even reduces the amount of T cells in the TME (Motz et al. 2014).

If infiltration of the TME by tumor-reactive T cells is not prohibited, numerous other mechanisms can take place in the TME preventing potent anti-tumor immunity and thus promote immune evasion. Pre-clinical models showed that strong selection pressure in the TME exerted by tumor-reactive T cells leads to an outgrowth of tumor cell variants that exhibit antigen-loss or reduced antigen expression (DuPage et al. 2012; Matsushita et al. 2012). In this regard, it has been described that reduced expression or complete loss of $\beta_2$-microglobulin expression in tumor cells leads to insufficient MHC I expression. As a result, less antigen is presented or antigen presentation is completely suppressed and CD8$^+$ T cells can recognize and eliminate the tumor cells less well or not at all (del Campo et al. 2014). In addition, mutations in the antigen processing machinery can lead to the situation that intact MHC I molecules cannot present antigens, as these are not or insufficiently processed. Tumor cells that do not present antigens or do present antigens that are not recognized by the T cells, thus experience a selection advantage and avoid elimination, which clearly supports ongoing tumor progression. Tumor

cells can also avoid elimination by losing sensitivity to effector molecules from cytotoxic lymphocytes. Janus kinases (JAK) are involved in the downstream signaling of IFN receptors (Castro et al. 2018). In this context, it is known that loss-of-function mutations in JAK-encoding genes lead to insensitivity of tumor cells to IFN-$\gamma$ (Zaretsky et al. 2016). As a result, IFN-$\gamma$ secreted by cytotoxic lymphocytes has no eliminating effect on the tumor cells thereby supporting tumor progression. However, it has also been shown that chronic IFN-$\gamma$ signaling in the tumor cells can lead to epigenetic changes and thereby induce the expression of immunosuppressive mediators such as PD-L1 or indoleamine 2,3-dioxygenase (IDO) (Benci 2016). This means that an exuberantly strong and long-lasting IFN-$\gamma$ production can lead in a negative feedback loop to suppression of cytotoxic T cells.

A strong influence that the TME exerts on the immune system is direct suppression of cytotoxic lymphocytes, especially T cells, prohibiting tumor cell elimination. In this regard, the immune checkpoints programmed cell death 1 (PD-1) and Cytotoxic T-lymphocyte protein 4 (CTLA-4) on the surface of T cells play an important role. PD-1 and CTLA-4 regulate exuberant immune reactions in order to prevent autoimmune reactions and tissue damage in the host (Le Mercier et al. 2015). The binding of the ligands PD-L1/PD-L2 to PD-1 or CD80/86 to CTLA-4 transmits inhibitory signals in T cells limiting their effector function. PD-1 expression of T cells is regulated by activation of TCR signaling. Thus, naïve T cells show a very low PD-1 expression, whereas after activation, T cells show a rapid increase in PD-1 expression (Agata et al. 1996). PD-1 expression increases when IL-12 and IL-6 act on the activated T cell during the activation process (Austin et al. 2014). This shows that the stronger the T cell activation, the stronger the PD-1 expression and thus the possibility that PD-L1^{+} cells can regulate the immune response of PD-1^{+} cells. PD-L1 is strongly expressed by tumor cells, but also by myeloid cells such as DCs, TAMs and inflammatory monocytes (Jiang et al. 2019). The regulation of CTLA-4 on the cell surface of T cells follows an analogous pattern. The stronger the T cell activation, the stronger the CTLA-4 expression and the possibility of an APC via CD80/86 to bind to CTLA-4 on the T cell and restrict its effector function (Oyewole-Said et al. 2020). However, a central problem in the TME is that activated T cells are continuously exposed to their antigen, as this is ubiquitous in the TME. This continuous antigen stimulation, together with inhibitory signals acting on the T cells, can put them into a state called exhaustion. T cell exhaustion leads to loss of effector function, upregulation of multiple inhibitory receptors, altered expression of key transcription factors, metabolic dysfunction and failed formation of responsive memory T cells (Doering et al. 2012; Wherry 2011). Sustained antigen stimulation induces increased expression of PD-1, CTLA-4 and the inhibitory molecules lymphocyte activation gene 3 (Lag3), T cell immunoglobulin domain and mucin domain-containing protein 3 (TIM3), T cell immunoreceptor with immunoglobulin and ITIM domains (Tigit), 2B4 and CD160. The higher the number of co-expressed inhibitory receptors, the stronger the state of exhaustion (Wherry and Kurachi

2015). Soluble mediators in the TME can also enhance the state of T cell exhaustion. These include, for example, the immunosuppressive cytokines IL-10 and TGF-$\beta$ as well as type I interferons, which can in turn induce the expression of IL-10, PD-L1 or indoleamine 2,3-dioxygenase (IDO) upon continuous exposure (Wherry 2011; Wherry and Kurachi 2015). Since Treg cells are also a source of IL-10, TGF-$\beta$ and IL-35, it is conceivable that they can also contribute to T cell exhaustion (Damo and Joshi 2019).

A large proportion of T cell inhibition in the TME is associated with myeloid cells. Their immuno-suppressive function is mainly due to MDSCs and TAMs. The immunosuppressive function of MDSCs mainly originates from arginase (ARG)1, inducible nitric oxide synthase (iNOS), TGF-$\beta$, IL-10, cyclooxygenase 2 (COX2), IDO and prostaglandin E2 (PGE2), mainly inhibiting the function of effector T cells within the TME (Gabrilovich et al. 2012; Tomić et al. 2019). This MDSC-mediated immuno-suppression is dynamically enhanced in the TME, as tumor-isolated M-MDSCs showed stronger suppressive activity than MDSCs isolated from the spleen, indicating a stronger suppressed tumor cell elimination by T cells in the TME (D. I. Gabrilovich, Ostrand-Rosenberg, and Bronte 2012). The CCR2/CCL2 axis plays a crucial role in the recruitment of monocytes as precursors for MDSCs to the TME. CCL2 is secreted by tumor cells, but also by MDSCs and TAMs, whereby these promote their accumulation in the TME in a positive feedback loop (Xu et al. 2021). Besides immunosuppressive functions, MDSCs and TAMs induce tumor progression by promoting angiogenesis through secretion of VEGF, thereby promoting nutrient supply and thus tumor progression which is referred to as angiogenic switch (Hanahan and Weinberg 2011; Riabov et al. 2014; Sorrentino et al. 2015). TAMs modulate the TME by inducing cancer cell invasion, immunosuppression and metastasis, which ultimately promotes tumor growth (Mantovani et al. 2017; Quail and Joyce 2013). TAMs express PD-L1/PD-L2 and CD80/86 binding to PD-1 and CTLA-4 on the surface of T cells, NK cells and NKT cells, inhibiting their effector function upon ligation (Belai et al. 2014). In addition, by secreting IL-10, TGF-$\beta$ and CCL22, TAMs inhibit the maturation of DCs and recruit Treg cells into the TME. This results in reduced antigen presentation and increased suppression of cytotoxic T cells (Curiel et al. 2004; Mantovani et al. 2017).

Immunosuppressive cytokines in the TME also inhibit the function of DCs, which indirectly promotes tumor progression by reducing T cell priming. IL-6, IL-10, VEGF and TGF-$\beta$ are known to inhibit DC function in the TME (Zong et al. 2016). Tumor-derived IL-6 inhibits DC maturation and migration and induces tolerogenic DC phenotypes (Alshamsan 2012; Chomarat et al. 2000; Pahne-Zeppenfeld et al. 2014). IL-10, which can be produced by MDSCs, TAMs and Treg cells, also inhibits the maturation of DCs and their ability to secrete IL-12, which is important for potent T cell priming (L.-Y. Huang et al.

2001; A. S. Yang and Lattime 2003). The maturation of DCs is also inhibited by VEGF and TGF-β (Brown et al. 2001; D. Gabrilovich et al. 1998).

Treg cells are another cell type that contributes significantly to the inhibition of T cell effector function and thus limits anti-tumor immunity. APCs express CD80/86 as co-stimulatory molecules, which bind to CD28 on the surface of T cells during priming. However, the affinity of CD80/86 to CD28 is weaker than that to CTLA-4. Treg cells express CTLA-4 and bind CD80/86 on APCs with a higher affinity thereby weakening the priming of T cells (Itahashi, Irie, and Nishikawa 2022). The cytokine IL-2 is essential for the activation and proliferation of T cells, especially of Treg cells. Since the IL-2 production of Treg cells is absent due to their FoxP3 expression, they consume the IL-2 produced by other immune cells in the TME. This means that the effector T cells have less IL-2 available, which inhibits their activation and proliferation (Spolski, Li, and Leonard 2018). Via the expression of CD39 and CD73, Treg cells induce the production of the immunosuppressive adenosine in the TME (Allard et al. 2017). Adenosine binds to the adenosine receptor A2A on effector T cells and induces inhibitory signals that lead to reduced anti-tumor immunity. Treg cells even increase this process by the release of huge amounts of ATP which is catalyzed by CD39 and CD73 to adenosine (Deaglio et al. 2007; Ohta et al. 2012; Stagg et al. 2011). In addition, Treg cells produce immunosuppressive cytokines such as IL-10, IL-35 and TGF-β, which inhibit the activity of APCs and effector T cells. Through the secretion of granzymes and perforins, they can even induce apoptosis in APCs and effector T cells (Jarnicki et al. 2006; Turnis et al. 2016).

## 1.2 Cancer Immunotherapy

The complex network of the TME represents a major obstacle to the elimination of a tumor by the immune system because of its great heterogeneity and multitude of immunosuppressive factors. In addition to conventional cancer therapy approaches such as radiotherapy or chemotherapy, cancer immunotherapy has been gaining importance for more than two decades now. Cancer immunotherapy describes the therapeutic approach aiming to enable the host´s immune system to eliminate tumor cells on its own. Since the beginning of cancer immunotherapy in the late 19th century by William B. Coley (McCarthy 2006) who successfully treated many bone and soft-tissue sarcoma patients with bacterial products, called Coley´s toxin, numerous other methods have been developed. In this regard, therapeutic approaches are needed that specifically sensitize the host immune system to the tumor, able to specifically address targets in the TME, that is mainly weakening the efficiency of immuno-therapeutic approaches.

### 1.2.1 Immune checkpoint blockade-mediated cancer immunotherapy

The function of effector T cells is controlled by various negative regulators known as checkpoint molecules. These have the task of preventing exuberant immune reactions that could lead to autoimmune reactions and host tissue damage. CTLA-4 and PD-1 are the most potent checkpoint molecules for T cell regulation. CTLA-4 primarily regulates T cell activation in the lymph node, while PD-1 regulates the function of already activated T cells at the site of inflammation, such as the TME (Fife and Bluestone 2008) (Figure 1.5).
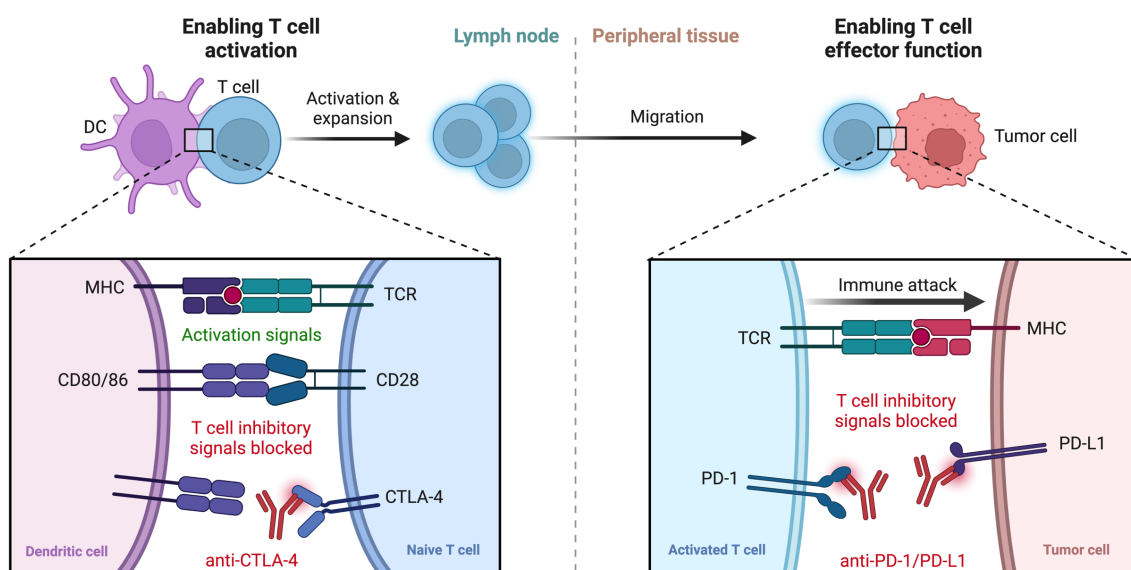


**Figure 1.5: Function of immune checkpoint blockade by anti-CTLA and anti-PD-1**
Activation of T cells in the lymph node is regulated by activating (CD28) and inhibitory (CTLA-4) receptors. Activated T cells migrate to peripheral tissues, such as the TME, to eliminate tumor cells. In the TME, PD-L1 expressing cells, such as tumor cells, can inhibit the function of effector T cells by PD-1 ligation. Anti-CTLA-4 and anti-PD-1 aim to prevent this inhibition to enable anti-tumor immunity. Adapted from Akiko Iwasaki and Ribas 2012. Created with BioRender.com.

CTLA-4 is a member of the immunoglobulin (Ig) superfamily and bears a high similarity to the surface protein CD28 on T cells, which mediates co-stimulation in T cell activation (Brunet et al. 1987; Harper et al. 1991). CTLA-4 is expressed by naïve T cells at a basal level and is strongly upregulated upon antigen contact, whereas $CD4^+$ $CD25^+$ Treg cells constitutively express CTLA-4. The co-stimulatory molecules CD80/86 on the surface of APCs bind to CD28 on the T cell upon antigen presentation, which triggers an activating signaling pathway. However, CD80/86 binds CTLA-4 with a higher affinity compared to CTLA-4. APCs therefore bind via CD80/86 to CTLA-4 of already activated T cells, triggering an inhibitory signal in these T cells (Linsley et al. 1994). This results in reduced T cell activation and proliferation (Krummel and Allison 1995). CTLA-4 expressing Treg cells have an immunoregulatory effect by binding to CD80/86 via CTLA-4 and thus limiting the activation of effector T cells (Jain et al. 2010). Allison and colleagues were the first to use a neutralizing anti-CTLA-4 antibody to enhance anti-tumor immunity against transplanted colon carcinoma and fibrosarcoma (Leach, Krummel and Allison 1996). The first approved anti-CTLA-4 antibody was Ipilimumab in 2011, which was effective in stage III/IV melanoma and prolonged short-term and long-term survival (Hodi et al. 2010; Schadendorf et al. 2015). However, clinical studies on the effect of ipilimumab in renal cell carcinoma, small-cell and non-small-cell lung cancer and prostate cancer showed less strong effects (Kwon et al. 2014; Lynch et al. 2012; Reck et al. 2013; J. C. Yang et al. 2007).

Analogous to CTLA-4, PD-1 inhibits exuberant effector function of T cells in peripheral tissues to prevent autoimmune reactions and tissue damage (Le Mercier, Lines, and Noelle 2015). However, in the TME ligation of PD-1 leads to suppression of the effector function of T cells thereby favoring tumor progression. Ligation of PD-1 by its ligands PD-L1 and PD-L2 induces phosphorylation of the immuno-receptor tyrosine-based switch motifs (ITSM) and immunoreceptor tyrosine-based inhibitory motifs (ITIM), leading to recruitment of the phosphatases SHP1 and SHP2. These dephosphorylate several key proteins downstream of the TCR, suppressing signaling pathways such as PI3K/AKT, Ras, MAPK, ERK and ultimately inhibiting the T cell cycle, cytokine production and therefore T cell proliferation and differentiation. Consequently, this leads to loss of immune function (Hui et al. 2017; Patsoukis et al. 2012; Sharpe and Pauken 2018). Due to the role of PD-1 in the negative regulation of the effector function of T cells, research has focused on whether blocking the PD-1 axis can be used for immunotherapy. Neutralizing anti-PD-1 antibodies made it possible to prevent tumor cell-mediated suppression of T cells via PD-1 ligation and to enable anti-tumor immunity (Hirano et al. 2005; Iwai et al. 2002). In mouse models, anti-PD-1 was also shown to limit the formation of metastases in B16 melanoma and CT26 colon carcinoma (Iwai et al. 2005). In 2014, the first anti-PD1 antibodies pembrolizumab and nivolumab were approved for the treatment of unresectable melanoma (Gong et al. 2018). In advanced melanoma studies, pembrolizumab showed an improvement over CTLA-4

blockade by ipilimumab (Robert et al. 2015), which was also shown in further studies for head and neck squamous cell carcinoma, Hodgkin lymphoma, urothelial carcinoma and gastric/gastro-oesophageal junction cancer (Bellmunt et al. 2017; Cohen et al. 2019; C. S. Fuchs et al. 2018; Moskowitz et al. 2016). The effect of nivolumab has so far been demonstrated for renal cell carcinoma, head and neck squamous cell carcinoma, urothelial carcinoma, hepatocellular carcinoma and Hodgkin lymphoma (Ansell et al. 2015; El-Khoueiry et al. 2017; Ferris et al. 2016; Motzer et al. 2015; Sharma et al. 2017). Despite the promising studies, the response rates of patients to single immune checkpoint blockade (ICB) vary dramatically, ranging from almost nonexistent in pancreatic cancer or microsatellite-stable colonic adenocarcinoma, to 15-30 % in most other tumor types, to 50-80 % in melanoma, Hodgkin lymphoma, squamous-cell skin carcinoma and Merkel cell carcinoma (Esfahani et al. 2020). Besides response rates, immune-related adverse events (irAEs) are a central problem of ICB. Anti-CTLA-4 is more likely to cause toxic adverse events affecting the gastrointestinal tract and brain, while anti-PD1-based ICB carries a higher risk of hypothyroidism, hepatoxicity and pneumonitis (Kumar et al. 2017). In addition, anti-CTLA-4-based ICB is more often associated with an increased risk of autoimmune complications (Bertrand et al. 2015; P.-F. Wang et al. 2017).

### 1.2.2 Adoptive cell transfer-mediated cancer immunotherapy

Adoptive cell transfer is another cancer immunotherapy method. Therefore, autologous or allogeneic hematopoietic stem cells (HSC) or immune cells are infused into patients. Hematopoietic stem cell transplantation (HSCT) is mainly used for lymphomas, leukemia, multiple myelomas and myelo-proliferative neoplasms but also for treating solid tumors such as neuroblastomas (Tuthill and Hatzimichael 2010). Since HSCs have the ability to self-renew and differentiate into all mature blood lineages, HSCT aims to replace the defective HSCs and reconstitute the entire hematopoietic system (Ogonek et al. 2016). For the first adoptive transfer of T cells, tumor-infiltrating leukocytes (TIL) isolated from tumor biopsies were expanded with the T cell-stimulating cytokine IL-2 and then injected intravenously into melanoma patients together with IL-2. This resulted in a response rate of about 30 %, but the median response duration was limited. Lymphodepletion prior to adoptive T cell therapy of metastatic melanoma patients resulted in an increase in the response rate and enabled complete tumor regression in over 20 % of patients (Rosenberg et al. 1988, 1994 and 2011). Chimeric antigen receptor (CAR) T cells represent a further development of this method. To produce CAR T cells, T cells isolated from a patient or a donor are modified *in vitro* to express TCRs that recognize antigens on the surface of malignant cells to eliminate them (Sadelain et al. 2013). When modifying the TCR, activating domains such as CD28 or CD40L are incorporated to enhance T cell activation and thus tumor cell elimination (Kuhn et al. 2019; Maher et al. 2002). However, the development of CAR T cells is problematic due to the fact that a suitable tumor antigen must be characterized. Therefore, CAR T cell

therapy has so far shown the most promising results in the treatment of B cell-associated tumors such as chronic lymphocytic leukemia or B cell acute lymphoblastic leukemia, as these show stable CD19 expression (Brentjens et al. 2013; Porter et al. 2011). Side effects associated with CAR T cell therapy are neurotoxicity and the frequently occurring cytokine release syndrome, which induces flu-like symptoms with varying intensity (Neelapu et al. 2018). Further disadvantages of CAR T cell therapy are that antigens have to be characterized patient-specific and the production process of CAR T cells is currently still very complex and especially very cost-intensive.

### 1.2.3 Vaccination-mediated cancer immunotherapy

Another field of research in cancer immunotherapy which is gaining popularity is cancer vaccination. Within the last decades, numerous methods have been developed aiming to enhance the activation of cellular specific anti-tumor immune responses to enable the immune system for eliminating tumor cells in a targeted manner.

### 1.2.3.1 Prophylactic cancer vaccination

For the prevention of numerous viral infectious diseases, multiple vaccines have been developed with great success (van Panhuis et al. 2013). With regard to cancer vaccination, this enabled the development of prophylactic cancer vaccines against the cancer-causing hepatitis B virus (HBV) and human papilloma virus (HPV) (Crews et al. 2021). The enormous success of vaccines against infectious diseases, including the cancer-causing viral diseases HBV and HPV, is attributed to the fact that most of the causative structures are known and recognized by the immune system as "non-self". In contrast, tumor cells developing in host tissues primarily express "self" antigens which are more likely to be tolerated by the immune system (Donninger et al. 2021). Therefore, a central part of the research and development of therapeutic anti-tumor vaccines involves the identification of tumor-associated antigens (TAA) enabling a targeted response against tumor cells.

### 1.2.3.2 Whole-cell- and peptide-based vaccination

Cancer vaccination focuses on priming and expanding T cells with TAAs in order to generate potent tumor-reactive T cells. In this process, DCs are of central importance, as they can take up TAAs and mediate the priming of naïve T cells in the tumor-dLN. This process is exploited with so-called whole-cell vaccines. DCs are loaded with TAAs and administered to a patient. This causes the generation of TAA-specific T cells. The first and so far only Food and Drug Association (FDA)-approved cancer vaccine Sipuleucel T (Provenge®) is such a whole-cell vaccine, which is used to treat metastatic castration-resistant prostate cancer patients. Autologous DCs are isolated from the patient and loaded with prostatic acid phosphatase (PAP) antigen fused with GM-CSF. This aims to generate CD8^{+} T cells that

can specifically recognize and eliminate PAP-expressing prostate tumor cells (Gardner et al. 2012). In a clinical study, a small but significant benefit in overall survival was observed with Sipuleucel T (Kantoff et al. 2010). However, this method also has the disadvantages of very complex production combined with high costs. Peptide-based vaccines offer an alternative to whole-cell-based vaccines. In this case, the TAAs are administered directly, aiming to be taken up by APCs to prime naïve T cells. The selection of a TAA is crucial in order to generate potent anti-tumor immunity. Peptides used for development and studies include cancer/testis antigen 1B (CTAG1B), MAGE family member A3 (MAGE-A3) or Wilm's tumor 1 (WT1) (Baumgaertner et al. 2016; Brayer et al. 2015; Vansteenkiste et al. 2016). However, none of the studies have been able to demonstrate a significant benefit, which is why there are currently no FDA-approved peptide-based cancer vaccines in use.

### 1.2.3.3 DNA- and mRNA-based cancer vaccination

DNA and mRNA vaccines are another possibility for administering Tumor antigen to enable specific T cell priming for anti-tumor immunity. The tumor antigen-encoding gene sequence is administered in the form of closed circular DNA plasmids or mRNA molecules (Lopes et al. 2019; Pardi et al. 2018). This offers the possibility of administering the coding gene sequence for adjuvants, such as Toll-like receptor (TLR)-activating substances or chemokines that target specific DC subsets or recruit T cells. DNA and RNA vaccines are internalized after intramuscular injection. The coding DNA needs to translocate to the nucleus, where it is transcribed into mRNA (Bai et al. 2017). RNA vaccines have the advantage that the mRNA does not have to translocate into the nucleus, as it can be translated into proteins directly after entering the cytoplasm. During translation, the tumor antigens and, depending on the vaccine composition, the adjuvants in form of TLR-activating substances or chemokines are expressed. The tumor antigens are processed and presented on the cell surface via MHC I and MHC II molecules, which enables a $CD8^+$ and $CD4^+$ T cell response (Lei Li and Petrovsky 2016). In addition, the adjuvants are expressed, which enhances the vaccination. In pre-clinical tumor models, DNA vaccines have been shown to provide potent anti-tumor immunity characterized by a $CD4^+$ and $CD8^+$ T cell immune response (Duperret et al. 2019). In clinical trials, however, DNA cancer vaccines have shown minor progress so far, which was mainly attributed to the insufficient immunogenicity (Suschak et al. 2017). In contrast, various mRNA vaccines have achieved promising results in clinical trials for the treatment of aggressive metastatic solid tumors. The mRNA vaccines TriMix and BNT111 showed potent $CD4^+$ and $CD8^+$ T cell responses in patients with melanoma and ICB-resistant metastatic melanoma, respectively (De Keersmaecker et al. 2020; Sahin et al. 2020). Somatic mutations in transformed host cells include gene mutations and gene rearrangements and promote oncogenesis (Hanahan and Weinberg 2011). If changes occur in the protein sequence due to these mutations, they are referred to as neoantigens. Compared to TAAs, which can also be expressed on host cells,

neoantigens are rather considered by the immune system to be "non-self" and are therefore better recognized by T cells (M. J. Lin et al. 2022). The identification of such neoantigens by next-generation sequencing and bioinformatic analyses is the basis for personalized vaccines. mRNA vaccines encoding multiple personalized neoantigens are showing promising results in ongoing clinical trials for the treatment of various solid tumors and underpin progress in this field (Cafri et al. 2020; Sahin et al. 2017; Zhan et al. 2020). However, regardless of the vaccination method, the identification of suitable tumor neoantigens will be a key aspect of cancer vaccine research.

### 1.2.3.4 Transcutaneous immunization

Transcutaneous immunization (TCI) is a non-invasive needle-free drug delivery system that allows targeting of APC subsets localized in skin tissue to generate an antigen-specific potent T cell immune response. This aims to overcome the limitations of conventional vaccination methods in terms of inadequate cellular immune responses. In contrast to conventional vaccination methods, the vaccine is applied directly onto or into the skin, which was first conducted in 1998 by Glenn and colleagues (Glenn et al. 1998). The skin is made up of a large number of different immune cell types that built the skin associated lymphoid tissue (SALT), making the skin to an ideal tissue for vaccination (Figure 1.6).
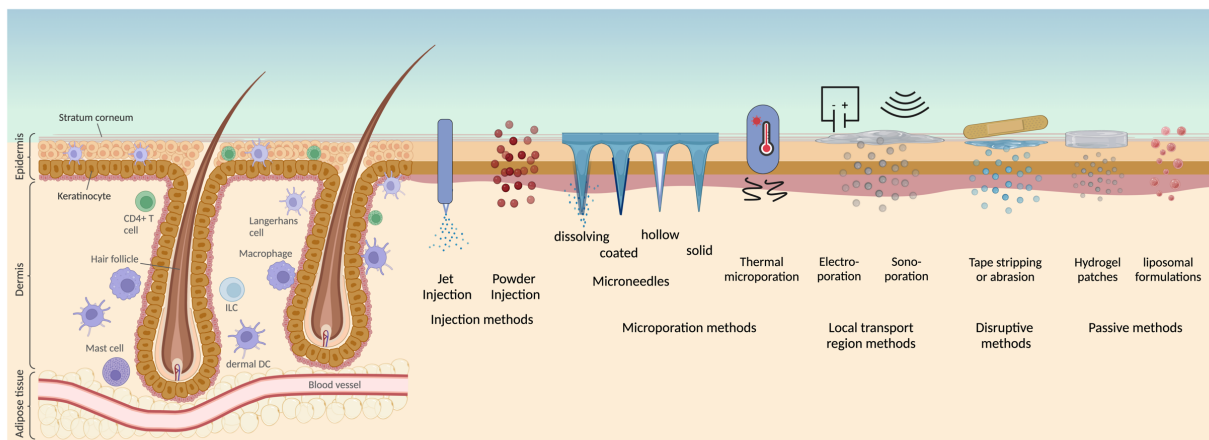


**Figure 1.6: Composition of the skin and transcutaneous drug delivery methods**

The Epidermis is largely populated by Keratinocytes, Langerhans cells and CD8^{+} T cells. Instead in the Dermis occur mainly CD4^{+} T cells, Mast cells, dermal DCs, Macrophages and ILCs. The Subcutis which is located under the Dermis consists primarily of adipose and connective tissue as well as blood vessels running through (adapted from Pasparakis et al. 2014). Furthermore, various transcutaneous drug delivery methods are described. These include injection methods (jet injection and powder injection), microporation methods (microneedles or thermal microporation), local transport region methods (electroporation or sonoporation), disruptive methods (tape stripping or abrasion) and passive methods (hydrogel patches or liposomal formulations) (adapted from Engelke et al. 2015). Created with BioRender.com.

The stratum corneum, as the outermost layer of the skin, plays a decisive role, as it represents a penetration barrier and must be overcome by the vaccine components. Various techniques have been developed to overcome this skin layer. These include injection techniques (jet injection or powder injection), microneedle-based systems (dissolving, coated, hollow or solid microneedles), thermal microporation, electroporation, sonoporation, disruptive approaches (waxing, tape stripping) or

passive delivery approaches (hydrogel patches or liposomal formulations) (Engelke et al. 2015). When the antigens contained in the vaccine have crossed the stratum corneum and arrived in the other epidermal layers or the dermis underneath, they can be taken up by APC subtypes such as dermal DCs (dDCs) or Langerhans cells (LC). The dDCs and LCs migrate to the draining LN and present the antigens to naïve T cells, which activates and stimulates them to proliferate. The antigens contained in the vaccine thus represent exogenous antigens presented by DCs to naïve CD4$^+$ T cells. However, through the process of cross-presentation, DCs and LCs can also present exogenous antigens to CD8$^+$ T cells (Stoitzner et al. 2006), which significantly expands the repertoire of the generated T cell immune response.

In addition to generating a strong cellular immune response, the TCI method offers further advantages. There are no medical professionals needed to vaccinate patients and there is no direct contact with the patient's bloodstream during vaccination, which additionally to needle-free application, drastically reduces the risk of infection. In this regard, the World Health Organization (WHO) estimates that about 40 % of the 16 billion injections per year worldwide are performed with re-used injection equipment (World Health Organization 2015), resulting in over 300,000 HCV infections and over 1,6 million HBV infections in 2010 (Pépin et al. 2014). In addition, needle phobia is avoided in patients due to needle-free application. The focus in the field of TCI is on the development of microneedle-based drug delivery systems, which have shown promising immune responses in pre-clinical models (Alimardani et al. 2021). For some non-cancer diseases, different microneedle-based systems have also been tested in clinical trials or some are still in ongoing clinical trials (Dongdong Li et al. 2021). However, transcutaneous immunization methods for cancer immunotherapy have not yet been tested in clinical trials. Thus, the use of TCI by various dermal drug delivery methods is mainly limited to pre-clinical research, which is why no approved TCI-based vaccine is available on the market today. Compared to drug delivery platforms such as DNA or RNA vaccines, TCI-based platforms such as microneedles offer the further advantages of cheap and easy production and increased thermostability to avoid cold chains. This proved to be an obstacle to global vaccine supply, especially in pandemic situations, such as the ongoing COVID-19 pandemic (O'Shea et al. 2021).

1.2.3.5 Dithranol- and Imiquimod-based transcutaneous immunization for cancer immunotherapy

The TCI method developed in 2005 by Rechtsteiner and colleagues involved the passive delivery of ovalbumin-derived antigenic peptides together with the Toll-Like Receptor 7 agonist imiquimod (Rechtsteiner et al. 2005). Imiquimod in the form of the commercially available cream formulation Aldara® was applied onto the intact back skin of mice. This induced the formation of antigen-specific CD8+ T cells. However, this method failed to induce a memory T cell response due to TLR-7-independent effects that induced expansion of inhibitory MDSCs and Treg cells. In order to induce a memory T cell response, the imiquimod-containing freeze-dried nano-emulsion IMI-Sol was developed in cooperation with the research group of Prof. Dr. Peter Langguth (Gogoll et al. 2016). IMI-Sol contains the same imiquimod concentration of 5 %, but generated an increased CD8+ T cell response compared to the Aldara®-based TCI. However, administration of IMI-Sol alone also failed to induce a memory T cell response. Only the combined administration with the ICI anti-CTLA-4, which prevented inhibitory Signals and enhanced the T cell response, led to the formation of a memory T cell response (Rausch et al. 2017). Likewise, this could be achieved by co-stimulation through CD40 ligation (Bialojan et al. 2019). Both methods enhanced the immune response and enabled prolonged protective immunity in the B16-OVA tumor model. However, the therapeutic rejection of solid tumors could not be achieved by these methods. Furthermore, the administration of the additional agents required intraperitoneal injection, which contradicted the needle-free handling of TCI. This necessitated the development and characterization of a skin-responsive adjuvant that could induce a potent primary and memory T cell response. The combination of the anti-psoriatic dihydroxyanthrone dithranol with IMI-Sol-based TCI (**D**ithranol/**I**MQ-based transcutaneous **va**ccination (**DIVA**)) enhanced the vaccination efficiency and for the first time induced a memory T cell immune response. The T cell immune response was characterized by superior cytolytic CD8+ T cells and CD4+ T cells with a Th1 cytokine profile (Sohl et al. 2022). Since the ear skin of the mice was used as immunization area, the method also reduced the required immunization area threefold compared to the previously immunized area on the back skin. Dithranol induced an inflammatory environment in the immunized skin tissue that recruited monocytes to the skin tissue and enhanced TLR-7-dependent activation of DCs and macrophages. This resulted in significantly increased T cell priming, which enabled protection against vaccinia virus. The significantly enhanced primary and memory T cell immune response makes DIVA a promising method for use as a therapeutic cancer vaccine. Figure 7 schematically illustrates the strategy of using DIVA to generate tumor antigen-specific T cells. Dithranol is applied to the skin, which recruits diverse immune cells, primarily monocytic cells, to the immunized tissue. Imiquimod in the form of Imi-Sol and ovalbumin-derived peptides are applied onto the skin 24 h later. This allows the inflammatory environment induced by dithranol to be used for optimal activation of APCs and to induce their antigen uptake.
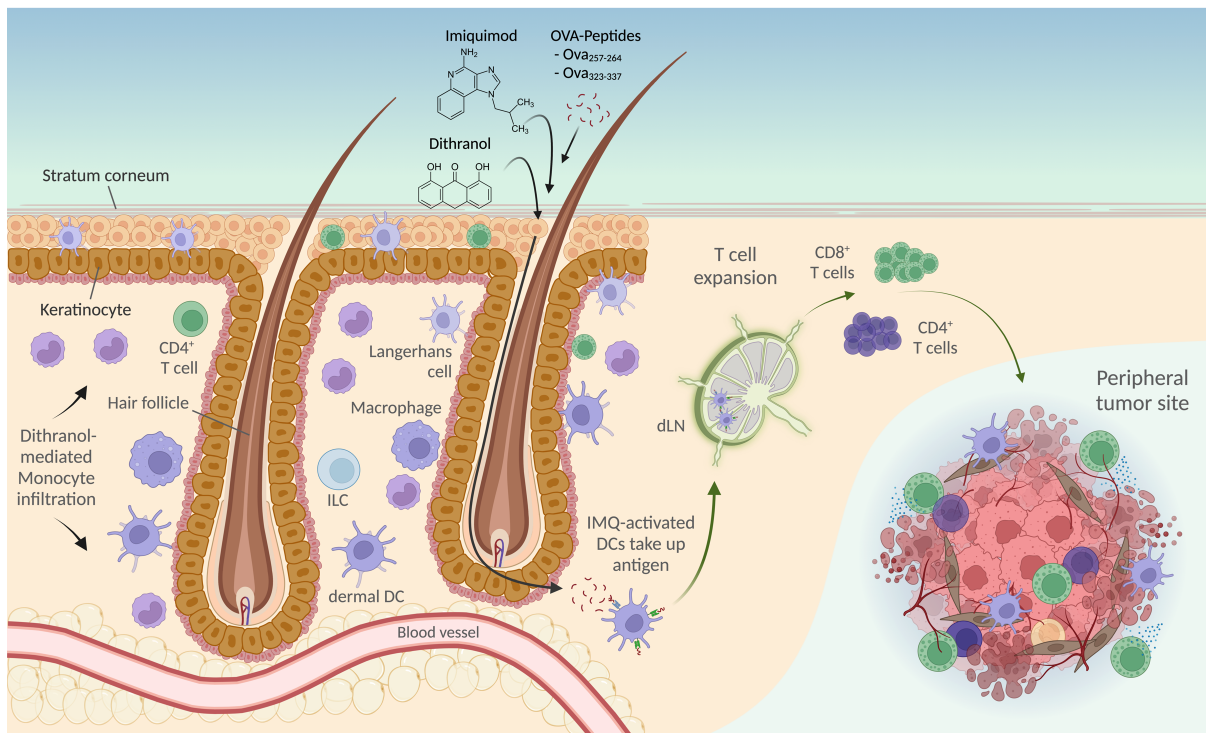
**Figure 1.7: The immunological strategy to generate tumor-reactive T cells with DIVA**

Schematic view of the immunological mechanisms occurring during the transcutaneous immunization based on the adjuvants Dithranol and imiquimod. Adjuvants are administered onto the skin surface together with OVA-derived Peptides. These enter the dermis via hair follicles and activate APCs that take up the Antigens an migrate to draining lymph nodes to prime naïve T cells. Activated T cells are stimulated to proliferate and migrate to the TME to eliminate tumor cells. Created with BioRender.com.

In this process, the adjuvants and peptides diffuse primarily through hair follicles to reach the dermis. APCs are activated by imiquimod in a TLR-7-dependent manner, take up the MHC I and II-restricted ovalbumin-derived peptides and migrate to the dLNs. Once in the dLNs they present the peptides to naïve CD4$^+$ and CD8$^+$ T cells, which are activated and stimulated to expand. The activated and expanded T cells migrate along chemokine gradients to the TME to recognize and eliminate tumor cells that present ovalbumin-derived peptides via MHC I molecules.

## 1.3   Aim of the project

The Imiquimod-based TCI methods developed in the research group of Prof. Dr. Markus Radsak enabled the generation of a potent primary immune response, characterized by activation of antigen-specific CTLs. However, induction of a memory T cell immune response and protection against injected tumor cells was only possible with help of intraperitoneally injected enhancers such as the ICI anti-CTLA-4 or additional co-stimulation through CD40-ligation. Consequently, therapeutic rejection of solid tumors could not be achieved by these methods. Combining imiquimod with the anti-psoriatic dihydroxyanthrone dithranol induced for the first time the generation of a memory T cell immune response.

The TME, with its complex heterogeneous structure consisting of a variety of immunosuppressive cell types and soluble factors, reflects the main obstacle for successful cancer immunotherapy to treat solid tumors. On the one hand, these factors in the TME directly promote the proliferation of tumor cells and on the other hand, they inhibit immunological anti-tumor mechanisms for tumor cell elimination. Therefore, it is essential to characterize the immunosuppressive mechanisms in the TME in order to understand how immunizations must be adapted to control tumor growth in a therapeutic setting.

In the present work, the first aim was to optimize the amount of memory T cells generated by the dithranol-imiquimod-based TCI method in order to observe a tumor-controlling effect. Further on, the focus of the work was to identify the cellular composition of the TME after optimized therapeutic dithranol-imiquimod-based TCI. In this context, a precise phenotypic characterization of the individual cell types in the TME should provide information about immunosuppressive mechanisms in the TME and to which extent they prevent successful anti-tumor immunity. Immunosuppressive effects of the cell types detected in the TME characterization should be functionally demonstrated in depletion experiments to identify specific targets that can be used to inhibit immunosuppression for successful immunotherapy.

## 2 Material

### 2.1 Laboratory Equipment

**Table 2.1: Laboratory Equipment**

| Device | Company |
| --- | --- |
| Analysis scale | Sartorius CP64 (Göttingen, Germany) |
| BD Rhapsody™ single cell analysis system | BD Bioscience (Franklin Lakes, USA) |
| Cell counter (Vet Animal blood counter) | Scil veterinary excellence (Viernheim, Germany) |
| $CO_2$ incubator | Sanyo (München, Germany) |
| Cooling centrifuge | Hereaus (Hanau, Germany) |
| Digital caliper | Thermo Fisher Scientific (Darmstadt, Germany) |
| Electric shaver | B. Braun (Melsungen, Germany) |
| ELISpot reader AiD iSpot (ELR08IFL) | AiD Diagnostika GmbH (Straßberg, Germany) |
| Flow cytometer (FACS Canto, Symphony) | BD Bioscience (Franklin Lakes, USA) |
| Freezer (-20 °C, -80 °C) | Liebherr (Biberach an der Riß, Germany) |
| Fridgerator (4 °C) | Liebherr (Biberach an der Riß, Germany) |
| Incubation waterbath (Aqualine AL12) | Lauda (Königshofen, Germany) |
| Infrared lamp (INFRARED-H95E) | Philips (Hamburg, Germany) |
| Injection cage | Kent Scientific (Torrington, USA) |
| Laminar flow workbench | Heraeus (Hanau, Germany) |
| MACS seperator | Miltenyi Biotec (Bergisch-Gladbach, Germany) |
| Mini centrifuge (MCF-2360) | LMS (Tokyo, Japan) |
| Multichannel pipette | Eppendorf (Hamburg, Germany) |
| Neubauer counting chamber | Roth (Karlsruhe, Germany) |
| Oxygen concentrator | Respironics (Herrsching, Germany) |
| Pipetboy comfort | INTEGRA bioscience (Fernwald, Germany) |
| Pipettes | Eppendorf (Hamburg, Germany) |
| Platform shaker (Titramax 100) | Heidolph (Schwabach, Germany) |
| Thermal mixer | Thermo Fisher Scientific (Darmstadt, Germany) |
| UniVet anesthesia Induction chamber | Groppler Medizintechnik (Deggendorf, Germany) |
| UniVet Porta anesthesia machine | Groppler Medizintechnik (Deggendorf, Germany) |
| Vortex mixer | VWR (Leuven, Belgium) |

## 2.2 Chemicals and consumable materials

### 2.2.1 Consumables

**Table 2.2: Consumables**

| Consumable | Company |
|---|---|
| Autoclavable bags | Roth (Karlsruhe, Germany) |
| C-Chip Counting Chamber | Nanoentek (Waltham, USA) |
| Cell culture flask (25 cm$^2$, 75 cm$^2$, 175 cm$^2$) | Greiner (Frickenhausen, Germany) |
| Cell strainer (40 µm, 70 µm) | Greiner (Frickenhausen, Germany) |
| Centrifuge tubes (15 ml, 50 ml) | Greiner (Frickenhausen, Germany) |
| ELISpot plates | Merck Millipore (Darmstadt, Germany) |
| Latex and nitril gloves | Starlab (Hamburg, Germany) |
| Multi-well plates (F-, U- or V-bottom) | Greiner (Frickenhausen, Germany) |
| Petri dishes | Sigma-Aldrich (Steinheim, Germany) |
| Reagent reservoir | Corning incorporated (New York, USA) |
| Reagent tubes (0,5 ml, 1,5 ml, 2 ml) | Eppendorf (Hamburg, Germany) |
| Reagent tubes for Flow Cytometry | Greiner (Frickenhausen, Germany) |
| Scale dishes | VWR (Leuven, Belgium) |
| Scalpels | Dahlhausen (Halberstadt, Germany) |
| Syringes (1 ml, 30 ml) | B. Braun (Melsungen, Germany) |

### 2.2.2 Kits and staining dyes

**Table 2.3: Kits and dyes**

| Kit | Company |
|---|---|
| BD Rhapsody Cartridge Kit | BD Bioscience (Franklin Lakes, USA) |
| BD Rhapsody Cartridge Reagent Kit | |
| BD Rhapsody cDNA Kit | |
| BD Rhapsody WTA Amplification Kit | |
| BD Rhapsody Sample Buffer | |
| Calcein AM | Thermo Fisher Scientific (Waltham, USA) |
| DRAQ7 | BD Bioscience (Franklin Lakes, USA) |
| eBioscience FoxP3 / Transcription Factor Staining Buffer Set | Thermo Fisher Scientific (Waltham, USA) |
| Fixable Viability Dye eFluor$^{TM}$ 780 | Thermo Fisher Scientific (Waltham, USA) |

## 2.2.3 Reagents

**Table 2.4: Reagents**

| Reagent | Company |
|---|---|
| 3-Amino-9-ethyl-carbazole (AEC) | Sigma-Aldrich (Steinheim, Germany) |
| Ammonium chloride | Roth (Karlsruhe, Germany) |
| BSA | PAN Biotech (Aidenbach, Germany) |
| CFSE | Thermo Fisher Scientific (Waltham, USA) |
| Collagenase-4 | Worthington Biochemical Corporation (New Jersey, USA) |
| Dithranol | Sigma-Aldrich (Steinheim, Germany) |
| DMSO | Sigma-Aldrich (Steinheim, Germany) |
| DNase-I | Sigma-Aldrich (Steinheim, Germany) |
| EDTA | Sigma-Aldrich (Steinheim, Germany) |
| Ethanol (96 %) | Merck (Darmstadt, Germany) |
| FCS | Gibco (Darmstadt, Germany) |
| Hydrogen peroxide (30 %) | Merck (Darmstadt, Germany) |
| Ketamine hydrochloride (2 ml) | Inresa (Freiburg, Germany) |
| L-Glutamine | Roth (Karlsruhe, Germany) |
| - OVA$_{257-264}$ (SIINFEKL)<br>- OVA$_{323-337}$ (ISQAVHAAHAEINEAGR) | Peptides & elephants (Henningsdorf, Germany) |
| Penicillin/Streptomycin | Serva (Tübingen, Germany) |
| Rompun 2 % (Xylazin hydrochloride) | Bayer (Leverkusen, Germany) |
| RPMI | Gibco (Darmstadt, Germany) |
| Sodium pyruvate | Serva (Tübingen, Germany) |
| Trypan blue solution | Calbiochem (Darmstadt, Germany) |
| Tween-20 | Roth (Karlsruhe, Germany) |
| Vectastain ABC-Kit | Maravai Life Sciences (San Diego, USA) |

2.2.4    Buffers and media

**Table 2.5: Buffers and media**

| Buffers/media | Composition |
|---|---|
| ACK buffer | • 8,02 g/l Ammonium chloride<br>• 0,1 g/l Potassium hydrogen carbonate<br>• 0,037 g/l Ethylenediaminetetraacetic acid (EDTA) |
| AEC complex solution (50 ml) | • 1 3-Amino-9-ethylcarbazole (AEC) tablet<br>• 2,5 ml Dimethyl formamide<br>• In Sodium acetate buffer filled up to 50 ml and sterile filtrated |
| EDTA blood buffer | • 30 mM Ethylenediaminetetraacetic acid (EDTA)<br>• 0,01 % Sodium azide<br>• dissolved in 1x Phosphate buffered saline (PBS) |
| FACS buffer | • 0,5 % Bovine serum albumin (BSA, 0,2 µm)<br>• 5 mM EDTA dissolved 1x in PBS |
| FCS | • the FCS was ordered from Gibco. Before the usage the FCS was heat inactivated in the waterbath for 45 min at 56 °C and centrifuged at 600 *g* |
| Gey's lysis buffer | • 150 mM Ammonium chloride<br>• 1 mM Potassium hydrogen carbonate<br>• 1 mM EDTA<br>• dissolved in desalted Water, adjusted on pH 7,3 and sterile filtrated (0,2 µm) |
| IMDM5/IMDM10 (5 %/10 % FCS) | • 5 %/10 % FCS<br>• 1 % Sodium pyruvate<br>• 1 % Glutamine<br>• dissolved in IMDM (Iscove`s Modified Dulbecco`s Medium (Sigma))<br>• 1:1000 Penicillin/Streptomycin |
| MACS buffer | • 0,5 % BSA (0,2 µm)<br>• 5 mM EDTA (pH 7,2)<br>• dissolved in 1x PBS and degased before usage |

| Buffers/media | Composition |
|---|---|
| MEM | • 10,58 g/l MEM dry powder<br><br>• 4,77 g/l HEPES buffer<br><br>• 1 % Penicillin/Streptomycin<br><br>• 1 % β-Mercaptoethanol<br><br>• dissolved in desalted water and sterile filtrated (0,2 μm) |
| Phosphate buffered saline (1x PBS) | • 8,18 g/l Sodium chloride<br><br>• 1,56 g/l Sodium hydrogen phosphate dihydrate<br><br>• dissolved in desalted Water, adjusted on pH 7,3 and sterile filtrated (0,2 μm) |
| Physiological Trypanblue solution | • 0,2 % Trypan blue in desalted water<br><br>• 4,25 % Sodium chloride in desalted water<br><br>• Mixing in a ratio of 1:5 |

### 2.2.5    Antibodies

**Table 2.6: Antibodies**

| Antibody | Conjugate | Clone | Company | Dilution | Usage |
|---|---|---|---|---|---|
| αCD3 | PE-Cy5 | 17A2 | BioLegend | 1:500 | |
| αCD8 | PB | 53-6.7 | BioLegend | 1:500 | |
| αCD8 | BV785 | 53-6.7 | BioLegend | 1:500 | |
| αCD11b | BV605 | M1/70 | BioLegend | 1:500 | |
| αCD11c | APC-R700 | N418 | BioLegend | 1:500 | |
| αCD11c | PE-Cy7 | N418 | BioLegend | 1:500 | |
| αCD16/32 | - | 2.4G2 | BD | 1:100 | |
| αCD19 | PE-Cy5 | 6D5 | BioLegend | 1:500 | |
| αCD44 | APC | IM7 | BioLegend | 1:400 | |
| αCD45pan | BV785 | 30-F11 | BioLegend | 1:500 | |
| αCD45pan | BUV805 | 30-F11 | BD | 1:1000 | |
| αCD62L | FITC | MEL-14 | BioLegend | 1:1000 | FACS |
| αCD64 | BUV737 | X54-5/7.1 | BD | 1:500 | |
| αCD90.2 | biotinylated | 30-H12 | BD | 1:400 | |
| αCD103 | BV711 | M290 | BD | 1:100 | |
| αCCR2 | PE | SA203G11 | BioLegend | 1:200 | |
| αCTLA-4 | biotinylated | MC10-4B9 | eBioscience | 1:200 | |

| Antibody | Conjugate | Clone | Company | Dilution | Usage |
|---|---|---|---|---|---|
| αF4/80 | BB790 | T45-2342 | BD | 1:500 | FACS |
| αFoxP3 | FITC | FJK-16s | eBioscience | 1:200 | |
| αGr-1 | FITC | RB6-8C5 | BioLegend | 1:100 | |
| αGranzym B | PE-Cy7 | QA16A02 | BioLegend | 1:200 | |
| αLag-3 | PerCP eFluor™ 710 | eBioC9B7W | eBioscience | 1:200 | |
| αLy6C | BV570 | HK1.4 | BioLegend | 1:500 | |
| αLy6G | BV750 | 1A8 | BD | 1:500 | |
| αMHC-II | BV786 | M5/114.15.2 | BioLegend | 1:500 | |
| αNK1.1 | PE-Cy5 | PK136 | BioLegend | 1:500 | |
| αKLRG1 | BV421 | 2F1 | BioLegend | 1:200 | |
| αPD-1 | APC | RMP1-30 | BioLegend | 1:200 | |
| αSirp1α | PE-Cy7 | P84 | BioLegend | 1:500 | |
| αTim-3 | PE-Dazzle 594 | B8.2C12 | BioLegend | 1:200 | |
| αXCR1 | BV650 | ZET | BioLegend | 1:500 | |
| αVβ5.1/5.2 | APC | MR9-4 | BioLegend | 1:200 | |
| SIINFEKL-H2K$^b$ | PE | 25.D1.16 | own product | 1:125 | |
| Streptavidin | BV605 | - | BD | 1:1000 | |
| αCD8a | magnetically labeled | - | Miltenyi | 1:10 | MACS |
| αCD45 | magnetically labeled | - | Miltenyi | 1:10 | |
| αIFN-γ | biotinylated | R4-6A2 | Mabtech | 1:500 | ELISpot-Assay |
| αIFN-γ | purified | AN-18 | Mabtech | 1:100 | |

## 2.3    Mouse strains

**Table 2.7: Mouse strains**

| Mouse Strain | Origin | Description |
|---|---|---|
| C57BL/6 | Own breeding | Inbred wildtype mouse strain |
| C57BL/6JOlaHsd | Envigo | Inbred wildtype mouse strain |
| C57BL/6-Tg(TcraTcrb)1100Mjb/Crl (OT-I) | Charles River | The mice exhibit the inserts for the murine T cell receptor (TCR) $\alpha$-V2 and TCR$\beta$-V5 genes. The expressed transgenic T cell receptor (TCR) is specific for the Ovalbumin$_{257\text{-}264}$ epitope (SIINFEKL) (Clarke et al. 2000; Hogquist et al. 1994). |

## 2.4    Cell lines

**Table 2.8: Cell lines**

| Cell line | Description |
|---|---|
| MC38 | The cell line MC38 was isolated from a colon carcinoma in a C57BL/6-Mouse after a long period exposition to the carcinogen DMH (Tan, Holyoke, and Goldrosen 1976). Tumors that arise from MC38 cells are immunogenic and capable for the *in vivo* investigation of adjuvant immunotherapies (Belnap et al. 1979). |
| MC38mOVA | The cell line MC38mOVA was transduced with a pIRES (internal ribosome entry site) vector containing the sequences coding the membrane standing form of the Ovalbumin protein and eGFP. This has the advantage that the cells can be proved to be positive for the membrane bound Ovalbumin by flow cytometry (kindly provided by Dr. Danielle Arnold-Schild, Institute for Immunology, University Medical Center Mainz, Germany (Stickdorn et al. 2022)). |

## 2.5    Software

**Table 2.9: Software**

| Software | Company |
|---|---|
| AiD ELISpot 8.0 | AiD Diagnostika GmbH (Straßberg, Germany) |
| Flow Jo v10 | BD Bioscience (Franklin Lakes, USA) |
| GraphPad Prism 9.5.0 | GraphPad Software (La Jolla, USA) |
| MS Office 2016 (Word, Excel, Powerpoint) | Microsoft Corporation (Redmond, USA) |
| R, R Studio, Bioconductor package, iSEE package | Open source software |

# 3 Methods

## 3.1 In vivo experiments

### 3.1.1 Adjuvants and peptides used for the Dithranol-Imiquimod-based TCI called DIVA

#### 3.1.1.1 Dithranol vaseline

The dithranol vaseline was prepared by the pharmacy of the University medical center of the Johannes Gutenberg-University Mainz under standardized protocols. For the antioxidation and stabilization the creme formulation contains 0,1 % ascorbyl-6-palmitate and is filled in an aluminum tube. In this work dithranol concentrations of 600, 300, 150 and 75 ng/mg vaseline were used. For the usage within DIVA the dithranol vaseline was stored at RT.

#### 3.1.1.2 The imiquimod containing solid nanoemulsion IMI-Sol

The imiquimod-containing solid nanoemulsion IMI-Sol (P. A. Lopez et al. 2017) was produced under standardized conditions within a cooperation by the research group of Prof. Dr. Peter Langguth (Biopharmaceutics and Pharmaceutical Technology, Institute of Pharmaceutical and Biomedical Sciences of the Johannes Gutenberg-University Mainz). Purified water, sucrose fatty acid ester S-1670 and imiquimod were combined with 25 g of zirconium oxide grinding bowls (Ø 1 mm) in a 45 ml Fritsch$^{TM}$ zirconium grinding bucket and grinded with a Fritsch$^{TM}$ Pluverisette 6 planet mill at 650 $g$ for two cycles á 20 min with 10 min pause in between. After the separation of the grinding bowls from the suspension the formulation was homogenized under usage of an Avestin Emulsiflex C3 high pressure homogenizer for four cycles at 500 bar and eight cycles at 1000 bar. The oil component, composed of Squalen:Tocopherol 6:4 (m/m), was added to the suspension and preemulgated with a Ultra Turrax® at 8000 $g$ for 5 min. For the production of a nanoemulsion the dispersion was homogenized at high pressure for four cycles at 500, 1000 and 1500 bar, respectively. Afterwards the nanoemulsion was frozen at -85 °C for 15 min with a height of the sample dish of around 5 mm. The 24 h primary drying process of the frozen nanoemulsion was conducted with a Christ alpha 1-4 freeze dryer at -21 °C and a maximum vacuum of 0,055 mbar. For the usage within TCI the solid nanoemulsion was stored at -20 °C.

#### 3.1.1.3 Basic creme DAC for peptide administration

To administer the ovalbumin peptides OVA$_{257-264}$ and OVA$_{323-337}$ onto the ear skin of mice, 10 µl of each of the peptides dissolved in dimethyl sulfoxide (DMSO) (10 mg/ml) were stirred into basic creme (according to the German Phamaceutics Codex (DAC)).

### 3.1.2 Application pattern of DIVA and DIVA[2]

For immunization procedures the Mice were injected *intraperitoneally* (*i.p.*) with a Ketamin (7,14 mg/ml in 1x PBS) and Xylazin (1,14 mg/ml in 1x PBS) solution in a dose of 100 µl/10 g body weight. The order of the administered adjuvants and peptides is schematically shown in Figure 3.1.

**a)** **DIVA**
- Dithranol (600 ng/mg)
- IMI-Sol (5% Imiquimod)
- Peptides OVA$_{257-264 / 323-337}$

Ova$_{257-264}$-H2K$^b$-Tetramer assay

IFN-$\gamma$ ELISpot assay

day 0/1          day 7/35          day 8/35

**b)** **1$^{st}$ DIVA**
- Dithranol (300 ng/mg)
- IMI-Sol (5% Imiquimod)
- Peptides OVA$_{257-264 / 323-337}$

**2$^{nd}$ DIVA**
- Dithranol (300 ng/mg)
- IMI-Sol (5% Imiquimod)
- Peptides OVA$_{257-264 / 323-337}$

- Ova$_{257-264}$-H2K$^b$-Tetramer assay
- ear thickness measuring
- IFN-$\gamma$ ELISpot assay

day 0/1          day 6/7          day 14-49

**Figure 3.1: Application pattern for DIVA in immunization experiments**
For DIVA the application pattern in **a)** and for DIVA[2] the application pattern in **b)** were performed. To analyze the quality and quantity of the antigen-specific T cells Tetramer FACS assay and IFN-$\gamma$ ELISpot assay were conducted at indicated timepoints.

### 3.1.3 Blood collection for the proof of antigen-specific CD8$^+$ T cells

For the proof of DIVA induced antigen-specific CD8$^+$ T cells *in vivo*, blood from immunized mice was collected in 1x PBS + 30 mM EDTA after tail vein incision. After an erythrocyte lysing step for 10 min by adding 3 ml ACK buffer to each blood sample, the cells were centrifuged (1700 rpm, 3 min) and the pellets, containing the lymphocytes, were resuspended in FACS buffer. Staining of the lymphocytes was performed with anti-mouse Fluorescence-labeled Antibodies as indicated in Table 2.6 for 30 min at 4 °C in a total volume of 50 µl in FACS buffer. H-2K$^b$-OVA$_{257-264}$-specific T cells were detected by PE-coupled H2-K$^b$ tetramer in Flow cytometry analysis.

### 3.1.4 Measurement of the ear thickness

In order to measure the ear thickness of mice a mechanical measuring gauge with an uncertainty of the measurement of 0,003 mm was used. Therefore, the mice were anesthetized with 5 % isofluran gas in an anesthesia chamber for a short anesthesia of around 10-15 sec. In this time the thickness of the ears was measured.

### 3.1.5    Inoculation of tumor cells and measuring of the tumor volume

Due to the homogeneous constitution of the skin only female mice in the age of 8-12 weeks were used for tumor experiments. After Ketamin-Xylazin based anesthesia as indicated in 3.1.2 the fur of the mice was shaved at the right flank to uncover the skin for *subcutaneous* (*s.c.*) injection of 100 µl of tumor cell suspension (in 1x PBS) of various concentration. The tumor of every mouse was measured with a digital caliper three times per week. When the tumor volume exceeded 600 $mm^3$ or an ulzeration of the tumor was observed the mouse was sacrificed with $CO_2$. The tumor volume was calculated based on the following equation:

$$\text{tumor volume } [\text{mm}^3] = (\text{lower dimension } [\text{mm}])^2 * \text{larger dimension } [\text{mm}] * 0,5$$

### 3.1.6    Application pattern of prophylactic and therapeutical tumor experiments

For prophylactic and therapeutic tumor experiments different application pattern were conducted that are schematically shown in Figure 3.2. In case of therapeutic tumor experiments, the mice were evenly distributed to different groups based on the measured tumor volume when the tumor were measurable for the first time. Afterwards DIVA was performed as indicated.
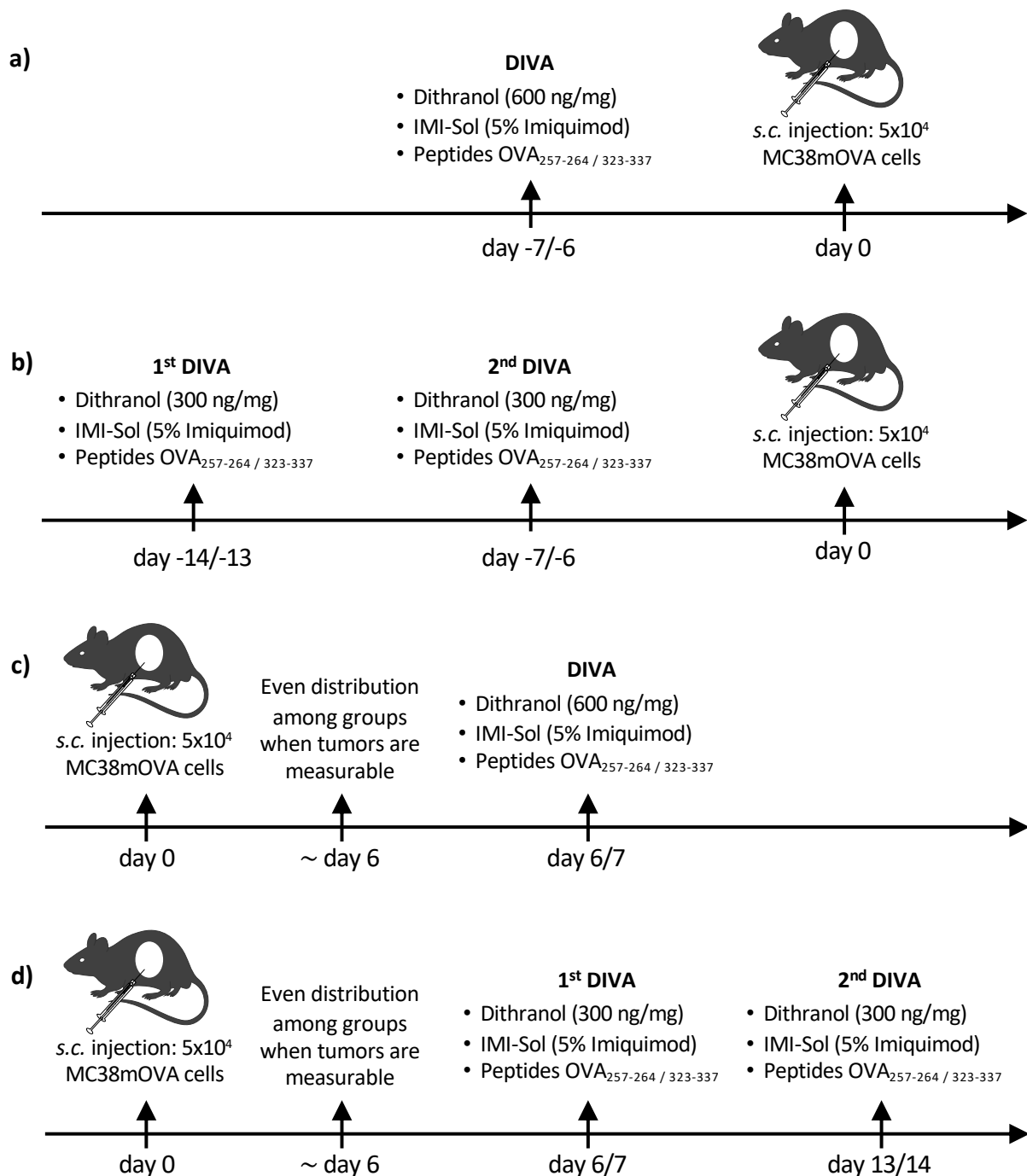
**Figure 3.2: Application pattern for DIVA in prophylactic and therapeutic tumor experiments**

Shown are the application pattern for prophylactic tumor experiments with DIVA in **a)** and DIVA[2] in **b)** and therapeutic tumor experiments with DIVA in **c)** and DIVA[2] in **d)**. The tumor cells were inoculated *s.c.* at the shaved right flank of the mice and the tumor volume of every mouse was measured three times per week with a digital caliper.

3.1.7    Injection of depleting and blocking antibodies in tumor experiments

The anti-CCR2 antibody MC-21 (Mack et al. 2001) (kindly provided by Prof. Dr. Matthias Mack, University Regensburg, Germany) was administered intravenously (*i.v.*) to C57BL6/J mice for depletion of CCR2$^+$ monocytes during tumor experiments from day 15-19 after tumor cell inoculation at a dose of 20 µg/mouse (dissolved in 100 µl 1x PBS) daily. The anti-PD-1 antibody RMP1-14 was administered

to C57BL6/J mice for blocking the ligation of PD-1 on the T cell surface by PD-L1 expressing cells during tumor experiments. Therefore, mice were injected 5x between day 6 and day 20 after tumor cell inoculation at a dose of 250 µg/mouse (dissolved in 100 µl 1x PBS).

## 3.2    Isolation of murine cell populations

### 3.2.1    Splenocyte preparation

For the preparation of splenocytes the mice were sacrificed with $CO_2$ and cut open on the left flank with preparation scissors. The peritoneum was opened and the spleen was separated from the surrounding tissue. Afterwards the spleen was grinded with a syringe plunger on a 70 µm cell strainer, previously wetted with 5 ml 1x PBS and rinsed with another 5 ml 1x PBS. The cell suspension was collected in a 50 ml tube and centrifuged (675 $g$, 3 min), whereupon the cell pellet was lysed for 1 min with 1 ml Gey´s Lysis buffer per spleen. After the incubation time the lysis was stopped by filling the tube up to 25 ml with 1x PBS and the suspension was washed twice with RPMI complete media (675 $g$, 3 min).

### 3.2.2    Tumor cell preparation

For isolation of tumor cells from solid tumors the mice were sacrificed with $CO_2$ and the skin was cut open on the ventral side of the body with preparation scissors. The skin was opened in the direction to the right flank and the tumor was cut out from the inside with a scalpel and transferred to a GentleMACS® C tube, prefilled with 3 ml of RPMI complete media with 800 U/ml Collagenase IV and 100 µg/ml DNAse I. Afterwards the tumor was cut into pieces with a diameter of around 1 mm. The tubes were set onto a Miltenyi GentleMACS® Octo Dissociator to run the preinstalled digestion program "37C_m_TDK1". To obtain a pure single cell suspension the cells were first pipetted onto a 70 µm, in a second step onto a 40 µm cell strainer and washed twice with RPMI complete media (675 $g$, 3 min).

### 3.2.3    Magnetic cell purification of Tumor Infiltrating Leukocytes

To receive CD45+ tumor infiltrating leukocytes (TIL) for single-cell RNA-sequencing (scRNA-seq), the tumor cell suspension was purified by magnetic separation using the CD45 (TIL) MicroBeads and the MACS hardware from Miltenyi Biotec. For this procedure, the cell suspension was centrifuged (675 $g$, 3 min) and the pellet resuspended in 90 µl of MACS buffer per $10^7$ cells. 10 µl of CD45 (TIL) MicroBeads per $10^7$ cells were added and the suspension was incubated for 15 min in the dark at 4 °C. During the incubation the Miltenyi LS Columns were equilibrated with 3 ml MACS buffer. Afterwards the cell suspension was pipetted onto the column whereby the CD45+ cells in the cell suspension are

magnetically bound within the column material of the LS column, which was placed in the magnetic field of the magnetic cell separator. Removed from the magnetic cell separator the cells were eluted from the column by flushing 3 ml of MACS buffer through the column with a syringe into another 15 ml tube, collecting the CD45$^+$ cell population.

## 3.3 Cell culture and determination of the living cell count

The *in vitro* cell cultivation was conducted under sterile conditions in a sterile laminar flow working bench and incubators at 37 °C and 5 % $CO_2$. For the determination of the living cell count, 10 µl of a cell suspension were diluted with Trypan blue (1:10/1:100), depending on the supposed cell number. 10 µl of the diluted cell suspension were pipetted into a Neubauer cell counting chamber and four quadrants were counted. Afterwards the cell number was calculated based on the following equation:

$$\text{cell number} = \frac{\text{n counted cells}}{\text{n Quadrants}} \text{ x Vol. cell suspension } [\mu l] \text{ x } 10^4 \text{ x overall Vol. } [ml]$$

Thereby the multiplier of $10^4$ constitutes the calculation factor of the chamber. The cell concentration was adjusted with the required volume of 1x PBS or media.

## 3.4 Flow cytometry

The method of Flow cytometry enables the analysis of fluorophore-labeled cells. Thereby, a cell suspension is soaked into the needle of a flow cytometer, accelerated in a thin single cell fluid stream and leaded past laser beams with various wavelengths. When the light of a laser hits a cell from the front the forward scatter light (FSC) is measured. Its intensity is a mass for the refraction of the light in the flat angle and depends on the volume of the cell. By contrast the intensity of the side scatter light (SSC) is a mass for the refraction of the light in the right angle and gives information about the granularity of the cell. When the surface molecules of a cell are labeled with fluorophore-coupled antibodies it comes to the excitation of the fluorophores by the laser beams, whereby light in a certain wavelength is emitted. The emitted light is detected by the Photomultiplier tubes of the cytometer and gets calculated into electronic signals. Because the emission spectra of various fluorophores can overlap, a compensation, in which the overlap intensity of the fluorophores is determined, has to be done prior to the measuring procedure. The overlap intensity is integrated into the calculation of the fluorescence intensity of the fluorophores. In this work the flow cytometry analysis was conducted with the cytometers FACS Canto and FACS Symphony and the software FACS-DIVA (BD Biosciences). Afterwards the data was post-analyzed with the software FlowJo (BD Biosciences) and visualized by GraphPad Prism (GraphPad Software).

### 3.4.1    Staining of cell surface epitopes

Surface molecules on cells give much information about the cell type, the subset they belong to as well as their biological function. After washing a cell suspension in a 96-well plate twice with 150 µl FACS buffer per sample (675 $g$, 3 min), the surface molecules of the cells were stained with the FACS antibodies under the conditions as indicated in Table 2.6 in a total volume of 50 µl in FACS buffer per sample for 30 min at 4 °C. To determine the viability of a cell the additional staining with the eBioscience™ Fixable Viability Dye efluor™ 780 was conducted. To ensure that only Antigen-specific binding is going on during the staining procedure, the murine Fc blocking reagent ($\alpha$CD16/$\alpha$CD32) was used. In this way the Fc receptors on the surface of monocytes, macrophages, DCs and B cells are saturated and false positive results are impeded. For this step a fixation of the cells is not necessary. Afterwards the cells were washed twice with 150 µl FACS buffer per sample (675 $g$, 3 min) and transferred to a 1 ml FACS tube for further Flow Cytometry analysis.

### 3.4.2    Staining of intracellular epitopes

The intracellular staining of cells can be conducted after the extracellular staining (as indicated in 3.4.1) and the fixation and permeabilization with the eBioscience™ FoxP3/Transcription Factor Fixation/Permeabilization Kit. Therefore, the cells were resuspended in the fixation/permeabilization solution (ratio of concentrate/diluent of 1:4) for at least 20 min at 4 °C and washed twice with Fix Perm buffer (1:10 with $_d$H$_2$O, 675 $g$, 3 min). The staining with intracellular FACS antibodies was conducted in a total volume of 50 µl in Fix Perm Buffer. After two washing steps with FACS buffer (675 $g$, 3 min) the cells were transferred to 1 ml FACS tubes for further Flow cytometry.

### 3.4.3    Staining of intracellular cytokines

If the production of cytokines has to be analyzed, cells need to be restimulated in prior of staining to increase the TCR signaling intensity. By adding monensine solution to the restimulation the transport of the proteins from the endoplasmic reticulum to the golgi apparatus is prohibited, which enables the enrichment of the produced cytokines in the cytosol of the cells. Therefore, the cells were washed with 1x PBS (675 $g$, 3 min), resuspended in restimulation media containing 50 ng/ml PMA, 1 µg/ml ionomycin and the monensine solution (1:1000) and incubated for 4 h at 37 °C.

## 3.5   Enzyme linked Immuno Spot assay (ELISpot)

The ELISpot assay was performed to prove the antigen-specific IFN-$\gamma$ production of T cells after restimulation with the ovalbumin peptides OVA$_{257-264}$ and OVA$_{323-337}$. The preparation of the ELISpot plate was started with the prewetting of the membrane by adding 20 µl of 35 % EtOH to each well, followed by three washing steps with 1x PBS. All washing steps in this protocol were conducted with a 12-channel plate washing head. Afterwards the membrane was coated with the primary antibody anti-IFN-$\gamma$ (1 µg/µl) in a dilution of 1:1000 with 1x PBS ($\triangleq$ 10 µg/ml) and incubated in the dark for 24 h at 4 °C. For the usage of the plate at the next day it was washed three times with 1x PBS whereupon 100 µl of IMDM10 were added to each well for the blocking of possible binding sites for 1 h at 37 °C to avoid unspecific binding. The IFN-$\gamma$ production was analyzed for splenocytes from immunized mice as wells as for *ex vivo* tumor cells. Single cell suspensions of these populations were performed as indicated in 3.2.1 and 3.2.2 and adjusted to a concentration of 5x10$^5$ cells/50 µl in IMDM10. Furthermore, 50 µl of the cell suspension were pipetted into each well of the ELISpot Plate. In case of the restimulated samples, 50 µl of IMDM10 with OVA$_{257-264}$ or OVA$_{323-337}$ peptides ($\triangleq$ end concentration of 1 µg/µl) were added, however in case of the unstimulated samples 50 µl IMDM10 were added. After the incubation of 20 h at 37 °C in the dark the plate was washed three times with 1x PBS + 0,05 % Tween and for the detection of the IFN-$\gamma$ the secondary biotinylated antibody anti-IFN-$\gamma$ (1 µg/µl) was pipetted onto the membrane (diluted 1:500 in 1x PBS + 0,5 % BSA, $\triangleq$ end concentration of 2 µg/ml). After another incubation of 2 h at 37 °C the plate was washed again three times with 1x PBS + 0,05 % Tween. For the detection of membrane-bound IFN-$\gamma$ the Vectastain Kit (Vector Laboratories) was used. Therefore, an Avidin-Biotin enzyme complex (ABC complex) is used, which reacts with the 3-Amino-9-ethylcarbazole solution (AEC solution, Sigma Aldrich) to a red dye. Per well 70 µl of the ABC complex were pipetted onto the membrane and incubated for 1 h at RT in the dark. Subsequently, 5 µl of 30 % H$_2$O$_2$, that acts as a radical starter, were added to 10 ml AEC complex. To ensure the correct procedure of the substrate enzyme reaction, 30 µl of the ABC complex and 30 µl of the AEC solution (with added H$_2$O$_2$) were pipetted together in a 1,5 ml tube. Only if the solution became red the protocol was continued with three washing steps with 1x PBS + 0,05 % Tween and another three steps with 1x PBS, respectively. Thereupon, 70 µl of the AEC complex (with H$_2$O$_2$) were pipetted onto the membrane and incubated for around 10-15 min, depending on the staining intensity. Terminally, the plate was washed 10 times with water to stop the staining reaction. The plastic layer underneath the membrane of the ELISpot plate was removed and the plate dried overnight. IFN-$\gamma$ produced by cells is visible on the membrane as a red spot. Thus, the number of the red spotforming units (SFU), counted with an ELISpot reader (AiD Diagnostika GmbH, AiD ELISpot 8.0) is a relative mass for the number of IFN-$\gamma$ producing cells.

## 3.6 Proliferation assay of OT-I T cells

To analyze the antigen presentation of the OVA$_{257-264}$ epitope on MHC-I molecules on the surface of MC38 and MC38OVAmb cells *ex vivo* at various time points in the tumor cell growth chart, *in vitro* proliferation assays with OT-I T cells were performed. Therefore, splenocytes from OT-I mice were prepared as indicated in 3.2.1 and labeled with 5 µM CFSE in 1x PBS for 4 min at 37 °C in a waterbath. After a washing step with FCS, the cells were counted in RPMI media and resuspended in RPMI + 10 % FCS + 50 µM β-Mercaptoethanol to get a concentration of 1x10$^7$ cells/ml. Tumor cells were prepared as indicated in 3.2.2 and adjusted to a concentration of 1x10$^7$ cells/ml. The pipetting schemes for the coincubation of the splenocytes and the Tumor cells are shown in Table 3.1 and Table 3.2. After 48 h of coincubation the cells were harvested and stained extracellular as indicated in 3.4.1 with FACS antibodies for the epitopes CD45, CD8, CD90.2 and Vβ5.1/5.2 for flow cytometry analysis of proliferated T cells.

**Table 3.1: Pipetting scheme for *in vitro* proliferation assay with *in vitro* Tumor cells**

The coincubation of OT-I splenocytes and MC38(mOVA) tumor cells was conducted at 37 °C for 48h in 48-Well plate with a total volume of 500 µl/well. After 24 h 500 µl/well of media were added, in case of coincubation samples with peptide restimulation, the added 500 µl contained OVA$_{257-264}$ (SIINFEKL) (10 ng/µl, in DMSO). For analysis of the proliferation of the T cells within the OT-I splenocytes, flow cytometry was performed.

| Pipetting scheme for 48-Well | coincubation | | | | | | | | | | | |
|---|---|---|---|---|---|---|---|---|---|---|---|---|
| | OT-I + MC38OVA *in vitro* | | | | OT-I + MC38 *in vitro* | | | | OT-I + MC38 *in vitro* + SIIN | | | |
| E:T-Ratio | 4,5:1 | 13,5:1 | 40,5:1 | 121,5:1 | 4,5:1 | 13,5:1 | 40,5:1 | 121,5:1 | 4,5:1 | 13,5:1 | 40,5:1 | 121,5:1 |
| MC38OVA cells [10x10$^6$/ml] *in vitro* | 33,3 | 11,1 | 3,7 | 1,2 | | | | | | | | |
| MC38 cells [10x10$^6$/ml] *in vitro* | | | | | 33,3 | 11,1 | 3,7 | 1,2 | 33,3 | 11,1 | 3,7 | 1,2 |
| OT-I cells [10x10$^6$/ml] | 116,7 | 138,9 | 146,3 | 148,8 | 116,7 | 138,9 | 146,3 | 148,8 | 116,7 | 138,9 | 146,3 | 148,8 |
| RPMI + SIINFEKL [1 µg/ml] | | | | | | | | | 5 | 5 | 5 | 5 |
| RPMI (10 % FCS, 50 µM β-Mercapto-EtOH) | 350 | 350 | 350 | 350 | 350 | 350 | 350 | 350 | 345 | 345 | 345 | 345 |
| total Volume | 500 | 500 | 500 | 500 | 500 | 500 | 500 | 500 | 500 | 500 | 500 | 500 |

**Table 3.2: Pipetting scheme for *in vitro* proliferation assay with *ex vivo* Tumor cells**

The coincubation of OT-I splenocytes and MC38(mOVA) tumor cells was conducted at 37 °C for 48h in 48-Well plate with a total volume of 500 µl/well. After 24 h 500 µl/well of media were added, in case of coincubation samples with peptide restimulation, the added 500 µl contained OVA$_{257-264}$ (SIINFEKL) (10 ng/µl, in DMSO). For analysis of the proliferation of the T cells within the OT-I splenocytes, flow cytometry was performed.

| Pipetting scheme for 48-Well | coincubation | | | | | | | | | OT-I control | |
|---|---|---|---|---|---|---|---|---|---|---|---|
| | OT-I + MC38OVA *ex vivo* | | | OT-I + MC38 *ex vivo* | | | OT-I + MC38 *ex vivo* + SIIN | | | OT-I + SIIN | OT-I |
| E:T-Ratio | 4,5:1 | 13,5:1 | 40,5:1 | 4,5:1 | 13,5:1 | 40,5:1 | 4,5:1 | 13,5:1 | 40,5:1 | | |
| MC38OVA cells [10x10$^6$/ml] *ex vivo* | 33,3 | 11,1 | 3,7 | | | | | | | | |
| MC38 cells [10x10$^6$/ml] *ex vivo* | | | | 33,3 | 11,1 | 3,7 | 33,3 | 11,1 | 3,7 | | |
| OT-I splenocytes [10x10$^6$/ml] | 116,7 | 138,9 | 146,3 | 116,7 | 138,9 | 146,3 | 116,7 | 138,9 | 146,3 | 150 | 150 |
| RPMI + SIINFEKL [1 µg/ml] | | | | | | | 5 | 5 | 5 | 5 | |
| RPMI (10 % FCS, 50 µM β-Mercapto-EtOH) | 350 | 350 | 350 | 350 | 350 | 350 | 345 | 345 | 345 | 345 | 350 |
| total Volume | 500 | 500 | 500 | 500 | 500 | 500 | 500 | 500 | 500 | 500 | 500 |

## 3.7   Single-cell RNA-sequencing

### 3.7.1   scRNA-seq sample preparation of TILs

For characterizing the immune cells within the TME scRNA-seq of CD45$^+$ TILs was performed. CD45$^+$ TILs were prepared *ex vivo* from MC38mOVA tumor cell suspensions as indicated in 3.2.3. For scRNA-seq sample preparation the cell concentration was adjusted to $1 \times 10^6$ cells/ml in BD sample buffer. Cells were stained in BD sample buffer 1:1000 with calcein AM (BD Biosciences) and 1:1000 DRAQ7 (BD Biosciences) for 10 min at 37 °C. Afterwards, 10 µl of the stained cell suspension were pipetted into the counting chamber of a C-Chip (Nanoentek, Waltham, USA) and the viability frequence was analyzed with a BD Rhapsody$^{TM}$ scanner. When the viability frequence was ≥ 80 %, the sample preparation was continued. Each sample was tagged with a unique sample tag allowing multiplexing of samples on the same single cell capturing cartridge. DNA libraries for Whole Transcriptome Analysis (WTA) and Sample Tags were created, following the BD Rhapsody System mRNA whole Transcriptome Analysis (WTA) and Sample Tag Library Preparation protocol with the BD WTA Amplification Kit (BD Biosciences, Franklin Lakes, USA). The sample preparation was performed in cooperation with the Research Center for Immunotherapy (FZI) Core Facility Next Generation Sequencing (NGS) of the University Medical Center of the Johannes Gutenberg-University Mainz.

### 3.7.2   DNA sequencing and raw data processing

The sequencing of the WTA DNA library and Sample Tag DNA library was performed by Novogene Co., Ltd. (Cambridge, UK). Raw data processing was conducted by uploading the obtained fastq-files to the BD Rhapsody WTA analysis pipeline (BD biosciences, Franklin Lakes, USA). For each biological replicate of a scRNA-seq experiment one csv-file in form of a "molecules_per_cell"-file was generated by the processing pipeline and was downloaded afterwards. These csv-files did serve as input files for bioinformatic analysis platforms.

## 3.8    Bioinformatic Analysis of scRNA-seq Data

### 3.8.1    Analysis with R studio and the R packages Bioconductor and iSEE

The scRNA-seq data was analyzed with R studio within a cooperation by Federico Marini (Institute for Medical Biostatistics, Epidemiology and Informatics (IMBEI) of the University Medical Center of the Johannes Gutenberg-University, Mainz). After importing the pre-processed BD Rhapsody data in form of csv-files (3.7.2) the analysis steps were performed in the following order:

1. Gene level annotation to set up the cell type annotation
2. Performing quality control and processing steps on every samples:
    a. Formatting row and table data
    b. Exclusion of cells with high mitochondrial count
    c. Exclusion of cells with low library size
    d. Exclusion of cells with low feature count
    e. Exclusion of doublet cells
3. Calculation of dimensionality reduced visualization methods (PCA, t-SNE, UMAP)
4. Performing prediction of immune cell types among samples
5. Integrating the datasets of every sample to obtain one data set (incl. accounting for technical sources of variation)
6. Performing clustering calculation based on different algorithms
7. Visualization of the integrated uncorrected data set by t-SNE plots
8. Continuation of the cell type annotation among the whole data set
9. Storing the results for interactive data exploration as rds-file
10. Differential expression and abundance analysis to compare conditions

### 3.8.2    Data visualization with the interactive Summarized Experiment Explorer

The scRNA-seq data that was processed as indicated in 3.8.1 can be visualized and explored with the interactive Summarized Experiment Explorer (iSEE) (Rue-Albrecht et al. 2018). For this purpose, the Bioconductor package and the iSEE package were installed in R studio. Afterwards the exploration session was started in R studio as following:

```
> "name_of_rdsfile" <- readRDS("thread_of_rdsfile")
> library(iSEE)
> iSEE("name_of_rdsfile")
```

## 3.9   Statistical analysis

The visualized data in this work are means ± SD, when not indicated otherwise. The stated p values were calculated by unpaired Student´s t test or 2-way ANOVA with Bonferroni´s post-hoc test with Graphpad Prism 9.0. The significance niveau was determined as a p value $\leq 0,05$. Multiple comparisons between more than two groups were performed by two-way ANOVA with Sidak's multiple comparisons test and one-way ANOVA with Kruskal-Wallis test, when sample numbers were different. Comparisons of two groups were performed by unpaired Mann-Whitney test and unpaired t test with Welch´s correction, when sample numbers were different. Comparisons of survival curves were performed by Log-rank (Mantel-Cox) test. The significance level was determined as a p value $\leq 0,05$. The statistical analysis was performed using GraphPad Prism (version 9.4.1 for Mac OS, GraphPad Software, San Diego California, USA).

# 4    Results

In 2007, Warger and colleagues already used imiquimod-based TCI to generate antigen-specific anti-tumor immunity. This approach could be enhanced by combination with UV exposure (Stein et al. 2011), immune checkpoint blockade by anti-CTLA-4 (Rausch et al. 2017) or co-stimulation by CD-40 ligation (Bialojan et al. 2019), but in none of the cases was the generated immune response sufficient to reject a solid tumor. In this context, there is an increased interest in the study of the Tumor microenvironment (TME), which provides with its complexity a multitude of potentially immunosuppressive immunological mechanisms that stand in the way of a successful anti-tumor immunity. The detailed characterization of these immunosuppressive mechanisms is necessary to understand how TCI needs to be modulated to generate a potent anti-tumor immunity. To address this question, we first chose a suitable tumor model and analyzed the influence of DIVA on the growth of MC38mOVA tumor cells *in vivo*. We investigated different application patterns of DIVA and first analyzed the influence on the TME by flow cytometry. We figured out that immune evasion occurs after transient immune control and investigated whether this is due to antigen loss on the surface of MC38mOVA tumor cells. To obtain more in-depth information about the immune cells within the TME, we performed scRNA-seq analyses of tumor infiltrating leukocytes which showed that immunosuppressive monocytes were absent during immune control and appeared until immune evasion. Hence, we evaluated their immunosuppressive capacity and influence on the growth of MC38mOVA tumors by depleting CCR2$^+$ peripheral blood monocytes to prevent their migration to the tumor site. To assess the biological capacity of DIVA$^2$ we compared DIVA$^2$ with immune checkpoint blockade by anti-PD-1.

## 4.1    Therapeutic DIVA fails to control the growth of MC38mOVA solid tumors

### 4.1.1    MC38mOVA tumor cells induce proliferation of OT-I T cells

The MC38 model is an established and accepted tumor model for optimizing immunotherapeutic approaches to prime tumor-reactive cytotoxic T cells (Hos et al. 2020). We decided to use the tumor model MC38 transfected with membranous Ovalbumin (MC38mOVA (Stickdorn et al. 2022), kindly provided by Dr. Danielle Arnold-Schild, Institute for Immunology, Mainz, Germany) to test the biological efficacy of DIVA in a tumor setting. In this context, it was first necessary to prove that the MC38mOVA cells are antigenic and can serve as a target for antigen-specific T cells. The intracellular antigen processing of ovalbumin in this MC38 cell line leads to presentation of ovalbumin-derived peptides on MCH molecules on the surface of the tumor cells. Since we use the MHC class I and II-restricted OVA$_{257-264/323-337}$ peptides as model antigens in our DIVA protocol, the MC38mOVA tumor cells should be suitable as an *in vivo* target for DIVA-induced antigen-specific CD8$^+$ T cells (Figure 4.1a).

We proved the antigenicity of MC38mOVA cells by co-culturing them with CFSE-labelled splenocytes of transgenic OT-I mice and performing of an *in vitro* proliferation assay (Figure 4.1b). The T cells of OT-I mice exhibit the inserts for the murine T cell receptor (TCR) $\alpha$-V2 and TCR$\beta$-V5 genes. Their expressed transgenic TCR is specific for the $Ova_{257-264}$ epitope (SIINFEKL) (Clarke et al. 2000; Hogquist et al. 1994). After Co-culturing with MC38mOVA cells, but not with MC38 cells, we observed proliferation of V$\beta$5.1/5.2$^+$ CD8$^+$ T cells within CFSE-labeled OT-I splenocytes of up to 85 %. We observed this T cell proliferation to a similar extent of up to 90 % in the peptide control with the $OVA_{257-264}$ peptide, demonstrating its antigenicity and suitability for testing DIVA with ovalbumin-derived peptides in an *in vivo* tumor setting.
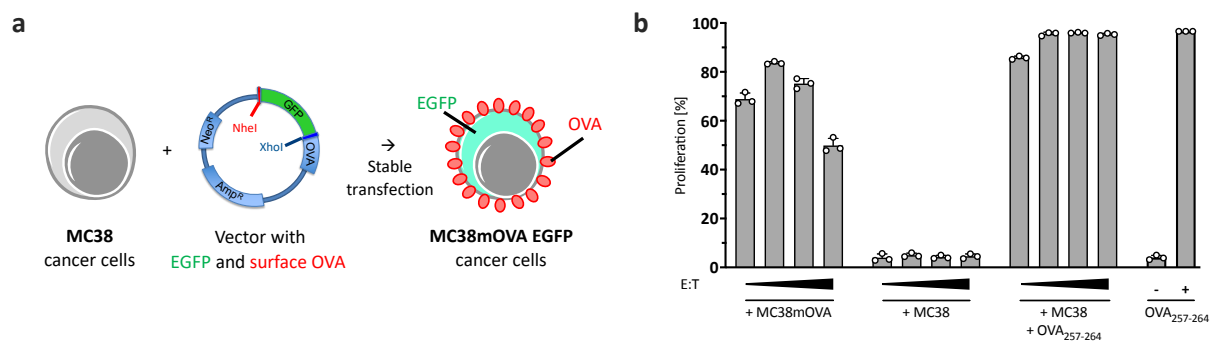


**Figure 4.1: MC38mOVA tumor cells induce proliferation of V$\beta$5.1/5.2$^+$ CD8$^+$ T cells from OT-I mice**

**a)** Schematic overview of the transfection strategy of MC38 cells to generate MC38mOVA cells. Figure adapted from Stickdorn et al. 2022. **b)** *In vitro* proliferation assay of CFSE-labelled OT-I splenocytes. Proliferation of TCRV$\beta$5.1/5.2$^+$ T cells was determined after 48 h co-culture by flow cytometry. Effector:Target (E:T) ratios of OT-I splenocytes to tumor cell suspension were 4,5:1; 13,5:1; 40,5:1. Peptide control samples were cultured with a $OVA_{257-264}$ concentration of 10 ng/ml. Shown are individual values of separate *in vitro* co-cultures, mean and SD.

### 4.1.2 DIVA fails to control growth of MC38mOVA solid tumors

To examine the impact of DIVA on the growth of tumor cells *in vivo*, we applied DIVA in a therapeutic tumor setting with MC38mOVA cells. We inoculated $5\times10^4$ MC38mOVA cells *s.c.* in the flank of C57BL/6J mice. When tumors were palpable, we performed DIVA (Figure 4.2a). Until day 10 after inoculation, the tumors developed in case of DIVA-treated mice a volume of around 30-50 mm$^3$ (Figure 4.2b), whereas in case of the untreated mice tumor volumes differed between 10 and 100 mm$^3$ (Figure 4.2c). From day 10 we observed a faster growth of the tumors, independent from the treatment. After a plateau in the growth chart of untreated mice between day 16 and 18 the tumors of treated and untreated mice started to grow more rapidly. Overall, we observed no impact of therapeutic DIVA on the growth of MC38mOVA tumors, indicating the need of adapting the immunization strategy.
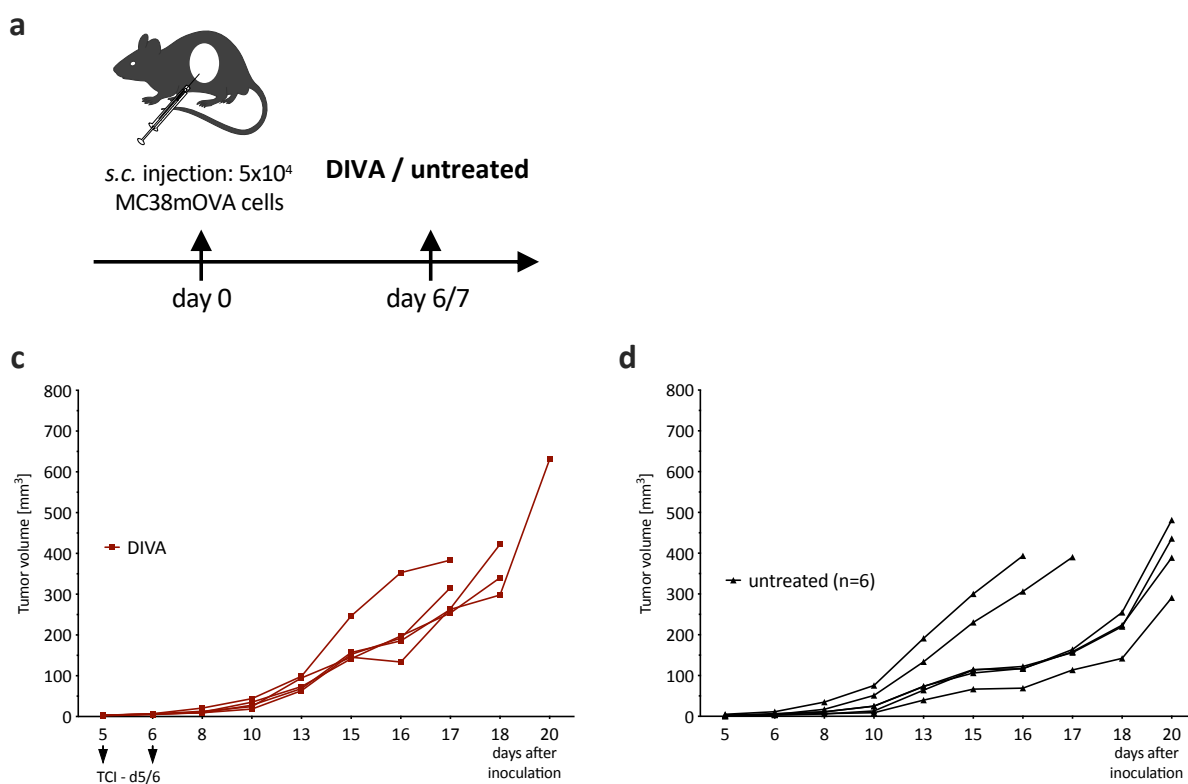


**Figure 4.2: Therapeutic DIVA has no impact on the growth of MC38mOVA tumors**

**a)** Schematic overview of the application pattern for DIVA in a therapeutic tumor setting with MC38mOVA cells. **b)** and **c)** Tumor volumes were assessed three times per week. Visualized are single curves of individual mice (n=5-6).

## 4.2 Multiple DIVA strongly enhances T cell response eliminating tumor cells in a prophylactic setup

After showing that DIVA had no impact on the growth of MC38mOVA tumors after single application with dithranol concentration of 600 ng/mg in the therapeutic setting, the application pattern of DIVA had to be adapted to generate a stronger CTL frequency at an earlier stage. A promising method to increase T cell frequency is boost vaccination. The first findings on boost vaccination with DIVA were obtained by Dr. Julian Sohl and colleagues (Sohl 2021). DIVA was carried out three times with a lower dithranol concentration of 75 ng/mg. The dithranol concentration of 600 ng/mg, which we used in our previous work (Sohl et al. 2022) is only applicable once, due to the intensity of the induced skin inflammation. The primary immune response induced by this threefold approach was very strong with about 30 % antigen-specific CD8$^+$ T cells, but it takes three weeks until the peak CTL frequency is reached and the memory immune response is strongly reduced with about 5-10 %, when compared to the primary response. Hence, we needed a further adaptation of the multiple DIVA vaccination protocol that reduces side effects but reaches its peak CTL frequency earlier than the threefold application with a dithranol concentration of 75 ng/mg.

### 4.2.1 Multiple DIVA strongly enhances the generation of highly functional antigen-specific CTLs

To optimize the efficacy of DIVA, we tested boosting approaches with different application pattern and dithranol concentrations (Figure 4.3a). Vaccination with lower dithranol concentrations (150 and 75 ng/mg) was performed threefold, whereas dithranol in a concentration of 300 ng/mg is only applicable twice, due to the intensity of the induced skin inflammation. Surprisingly, we observed the highest increase of specific CD8$^+$ T cells after applying 2x DIVA (300 ng/mg dithranol), yielding up to 60 % circulating antigen-specific CD8$^+$ T cells in the primary phase after 14 days. Applying 3x DIVA with a lower dithranol concentration (150 or 75 ng/mg) resulted in maximum frequencies after 14 days of 30 % and 8 %, respectively. IMQ-TCI alone showed similar results to 3x DIVA (75 ng/mg). These data indicate that the frequency of antigen-specific CD8$^+$ T cells correlates with dithranol concentration in multiple DIVA approaches. We quantified the circulating antigen-specific CD8$^+$ T cells until day 49 to determine the durability of the induced T cell response. Accordingly, we observed the highest frequency of antigen-specific CD8$^+$ T cells after applying 2x DIVA (300 ng/mg), whereas applying 3x DIVA (150 or 75 ng/mg) resulted in frequencies like IMQ-TCI (Figure 4.3b, c). Consequently, we received the highest specific IFN-$\gamma$ production of CD8$^+$ T cells after 2x DIVA (300 ng/mg) by an IFN-$\gamma$ ELISpot assay upon splenocyte restimulation with the OVA$_{257\text{-}264}$ peptide, reflecting their highly activated and functional effector state. Furthermore, we detected antigen-specific IFN-$\gamma$ production of CD4$^+$ T cells after restimulation of the splenocytes with OVA$_{323\text{-}337}$, which was induced after 2x DIVA (300 ng/mg) and 3x DIVA (150 ng/mg), indicative of a Th1 cell phenotype (Figure 4.3d).
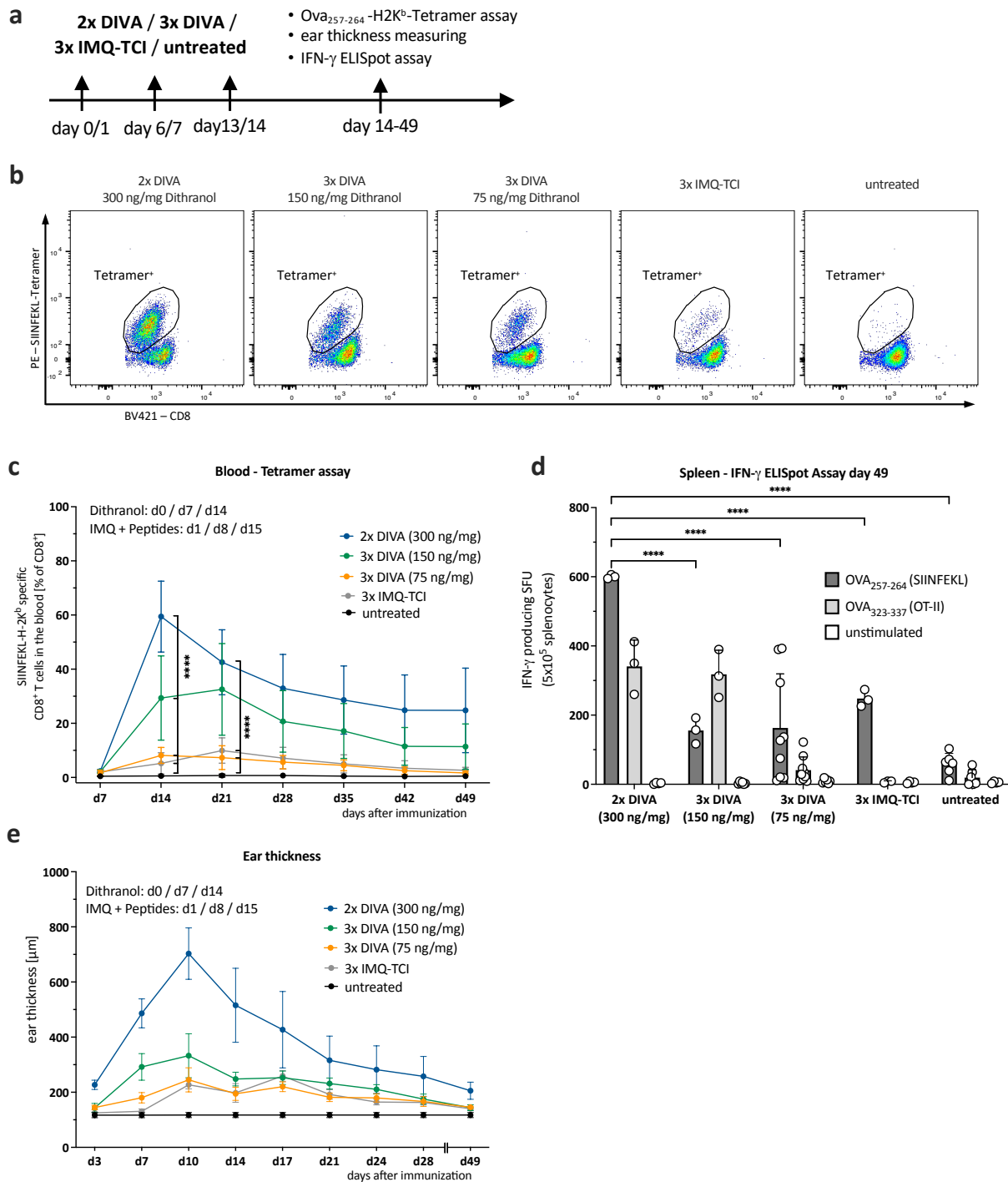
**Figure 4.3: Multiple DIVA strongly enhances the generation of highly-functional antigen-specific CD8+ T cells**

**a)** Schematic overview of the application pattern for multiple DIVA. Mice were immunized on both ears with dithranol in vaseline (concentrations as indicated [% w/w], day 0) and Imi-Sol (5% Imiquimod [w/w]) together with $OVA_{257-264}$ and $OVA_{323-337}$ (stirred into cremor basalis, day 1), treated only with IMQ together with $OVA_{257-264}$ and $OVA_{323-337}$ peptides or left untreated. **b)** Representative flow cytometry dot plots of CD8+ tetramer-positive T cells after different DIVA protocols. **c)** After seven days, tetramer staining was performed once a week until memory phase (day 49) (n=5). **d)** Splenocytes were restimulated at day 49 in an ELISpot assay to assess specific IFN-γ production. Bars represent mean and SD (n=3-9). **e)** Ear thickness was determined twice per week until day 28 and additionally on day 49 (n=10 ears of 5 mice). *p < 0.05 by 2Way Anova with Sidak's multiple comparisons test and one-way ANOVA with Kruskal-Wallis test, when sample numbers were different.

Previously, we showed the DIVA-induced side effects of inflammation and swelling of the ear skin, mainly due to dithranol, mediated by local monocyte recruitment (Sohl et al. 2022). As expected, we observed a dithranol concentration-dependent increase in ear swelling. Especially, 2x DIVA (300 ng/mg) led to a massive increase with its maximum after 10 days. However, the inflammation and swelling recovered until the memory phase, since the ear thickness nearly reached the level of IMQ-TCI at day 49 (Figure 4.3e). Taken together, these data indicate that multiple administration of DIVA leads to a stronger skin inflammation, but significantly increases the generated antigen-specific CD8^{+} T cells. We have shown that these cells can be detected in the primary but also in the memory phase, highly functional in specific IFN-$\gamma$ production. Two applications of DIVA with a dithranol concentration of 300 ng/mg elicited the strongest immune response. From now on, we will refer to this immunization protocol as "**DIVA²**".

### 4.2.2 DIVA² enables complete protection against MC38mOVA tumor cells in a prophylactic setting

We wanted to evaluate the biological efficacy of DIVA² in a prophylactic setting. Therefore, C57BL/6 mice were immunized prior to subcutaneous injection of 5x10⁴ MC38mOVA tumor cells (Figure 4.4a).
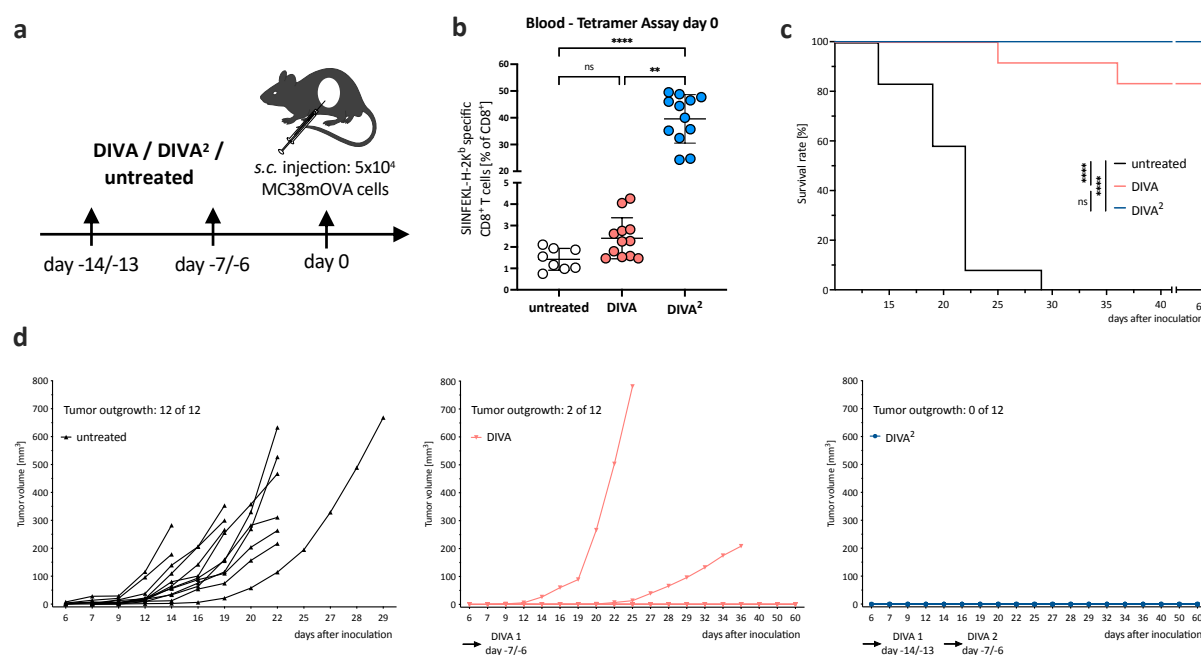


**Figure 4.4: DIVA² enables complete protection against MC38mOVA tumor cells in a prophylactic setup**
**a)** Schematic overview of the application pattern for Boost DIVA in a prophylactic tumor setting. At day 0 5x10⁴ MC38mOVA tumor cells were inoculated subcutaneously. **b)** Tetramer staining of pre-immunized mice at the day of tumor cell inoculation (=day 0; n=12). **c)** Kaplan-Meier survival curve. **d)** Tumor volumes were assessed three times per week. Every curve represents the tumor volume of one individual mouse (n=12). *p < 0.05 by 2Way Anova with Sidak's multiple comparisons test and one-way ANOVA with Kruskal-Wallis test, when sample numbers were different. Comparisons of survival curves were performed by Log-rank (Mantel-Cox) test.

On the day of inoculation, we quantified circulating ovalbumin-specific T cells by $OVA_{257-264}$-$H2K^b$ tetramers. Application of DIVA induced an averaged CTL frequency of 2,5 % of $CD8^+$ T cells, whereas $DIVA^2$ boosted the immune response to a CTL frequency of about 40 % (Figure 4.4b). Both DIVA and $DIVA^2$ significantly prolonged the survival of the injected mice (Figure 4.4c) with a protection rate of 83 % upon single treatment with DIVA. However, after performing $DIVA^2$ we did not observe outgrowing tumors corresponding to a protection rate of 100 % (Figure 4.4d) and highlighting that complete clearing of tumor cells in a prophylactic setting requires $DIVA^2$.

## 4.3 $DIVA^2$ induces strong CTL infiltration enabling transient tumor immune control accompanied with an altered myeloid compartment of the TME

After adapting our DIVA protocol towards an effective boost strategy, we wanted to evaluate its biologic efficacy in a therapeutic tumor model. To address this task, we injected C57BL6/J mice subcutaneously with MC38mOVA cells and observed tumor growth. At different time points, we isolated in two consecutive experiments tumor-infiltrating leukocytes by magnetic bead sorting and analyzed their phenotype by flow cytometry. To characterize distinct populations, we performed in an unbiased approach clustering of myeloid populations using t-distributed Stochastic Neighbor Embedding (t-SNE) algorithms based on high-dimensional flow cytometry data and predicted immune cell types of the clustered populations using the FlowSOM algorithm.

### 4.3.1 Therapeutic $DIVA^2$ induces transient tumor control that turns into immune evasion

We injected C57BL/6 mice *s.c.* with $5x10^4$ MC38mOVA tumor cells and performed $DIVA^2$ when tumors were palpable (Figure 4.5a). $DIVA^2$ significantly reduced the tumor volume, resulting in an immune control that was maintained for over two weeks (Figure 4.5b). At the timepoint of the strongest immune control on day 16 after inoculation of the tumor cells, the averaged tumor volume after $DIVA^2$ was reduced eightfold (about 25 $mm^3$), compared to the untreated mice (over 200 $mm^3$) (Figure 4.5c). This immune control characterized by decreasing tumor volumes, transitioned to an immune equilibrium that lasted about 4 days and then entered the state of immune evasion (Figure 4.5d), characterized by a sharp relapse of tumor growth. On day 22 after inoculating the tumor cells, the averaged tumor volume of the $DIVA^2$-treated mice was no longer significantly different from that of the untreated mice (Figure 4.5e). To clarify the reasons of the tumor regrowth after initial immune control, we examined the tumor infiltrating leukocytes (TILs) by high-dimensional flow cytometry.
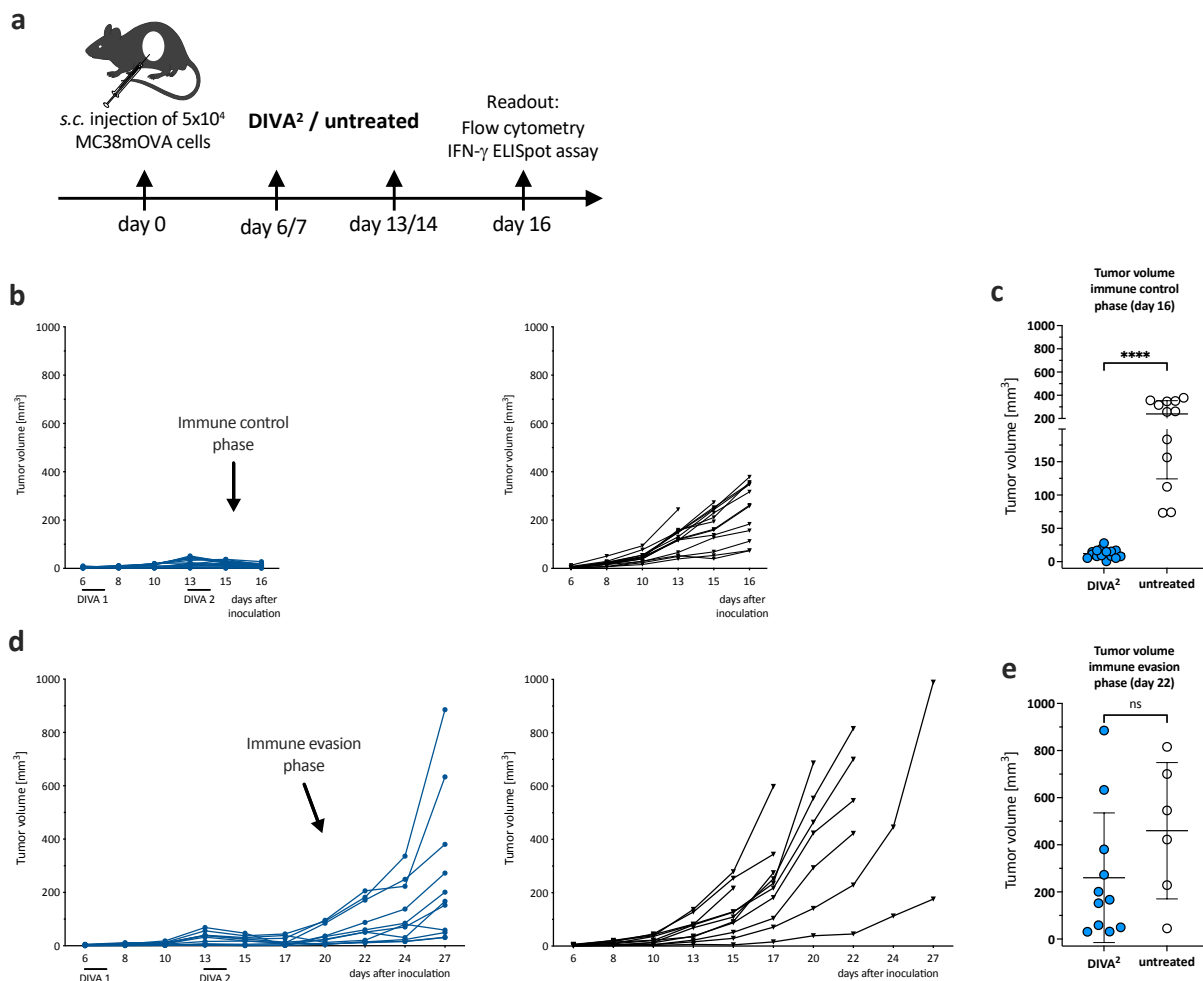
**Figure 4.5: Therapeutic DIVA² induces transient tumor control that turns into immune evasion**

**a)** Schematic overview of the application pattern for DIVA² in a therapeutic tumor setting. **b)** and **d)** Tumor volumes were assessed three times per week. Every curve represents the tumor volume of one individual animal (n=11-15). **c)** and **e)** Tumor volumes during immune control (day 16) and immune evasion (day 22). Visualized are individual data points, mean and SD. *p < 0.05 by two-way ANOVA with Sidak's multiple comparisons test and 1Way Anova with Kruskal-Wallis test, when sample numbers were different. *p< 0.05 by one-way ANOVA with Kruskal-Wallis test.

### 4.3.2 DIVA²-induced tumor-reactive cytotoxic lymphocytes infiltrate the tumor microenvironment

We examined the TILs by high-dimensional Flow cytometry during immune control (day 16) and the latest possible timepoint during immune evasion (day 22/27) to gain more detailed information about the TME. We observed an increase in the number of CD8+ T cells and in particular antigen-specific CD8+ T cells after DIVA². Surprisingly, the number of antigen-specific CD8+ T cells was higher during immune evasion than during immune control. Since PD-1 is an activation marker of CD8+ T cells in the TME (Gros et al. 2014; Inozume et al. 2010), but in line with the expression of CTLA-4 and Lag3 suggests an exhausted phenotype (Pauken and Wherry 2015), we analyzed the expression of these markers of antigen-specific CD8+ T cells. DIVA²-induced antigen-specific CD8+ T cells expressed about 90 % PD-1, but only about 10-15 % CTLA-4 and about 5 % Lag3 during both immune control and immune evasion (Figure 4.6a). This suggests a highly activated but not exhausted phenotype of these cells during both

immune control and immune evasion. To analyze their functional phenotype, we performed an IFN-γ ELISpot assay. This revealed an analogous phenotypic pattern. Splenocytes from DIVA[2]-treated mice showed significantly increased IFN-γ production after restimulation with the $OVA_{257-264}$ peptide, when compared to untreated mice (Figure 4.6b). This difference became apparent during immune evasion. In conclusion, these data show that DIVA[2] leads to the infiltration of highly activated, non-exhausted antigen-specific CD8^{+} T cells into the TME. The fact that immune evasion still occurs despite these potentially tumor-reactive T cells suggests that immune evasion mechanisms are operating within the TME.
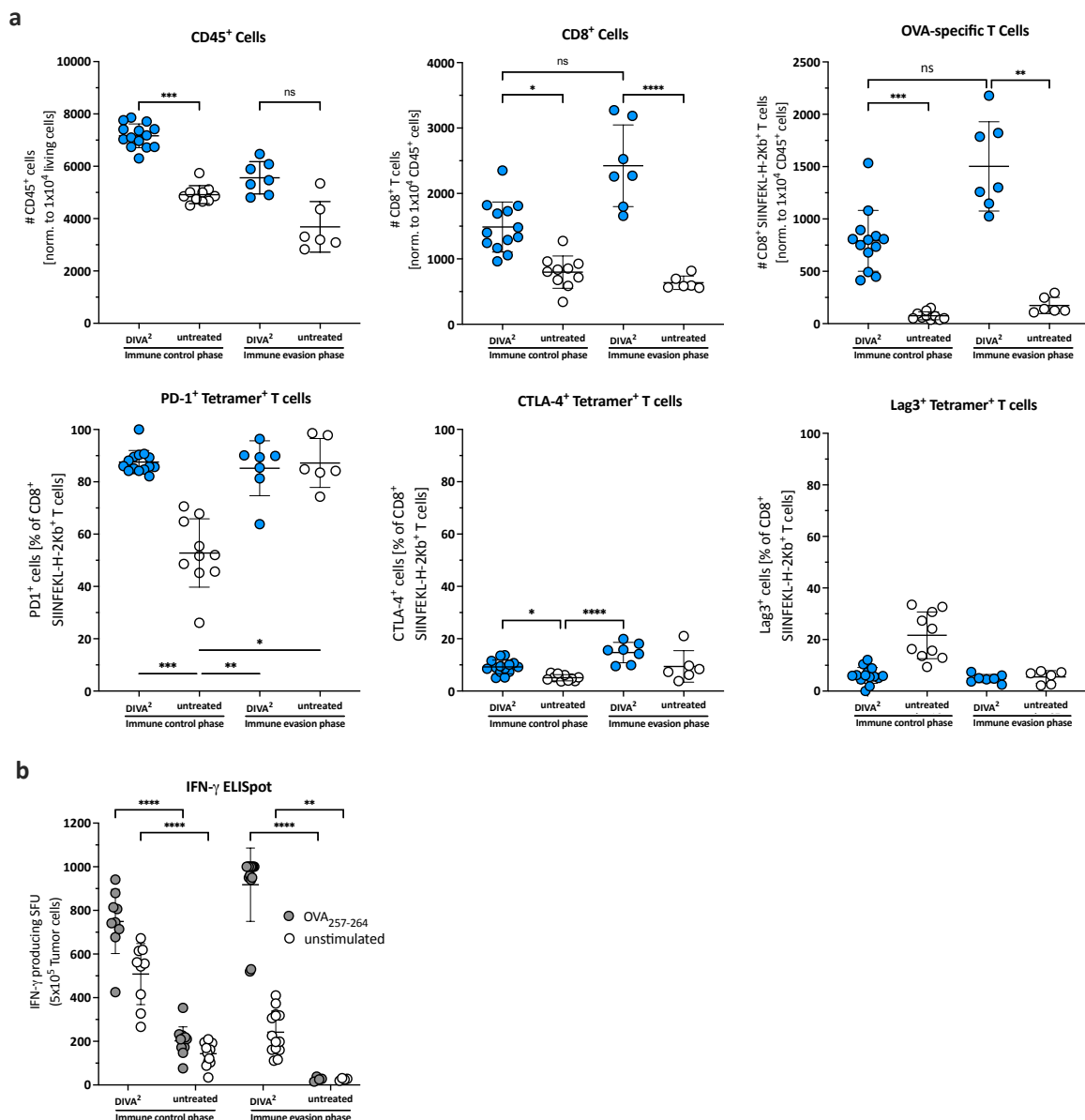


**Figure 4.6: Therapeutic DIVA[2] induces infiltration of highly activated OVA-specific T cells into the TME**

**a)** Cell counts of tumor infiltrating CD45^{+} cells, CD8^{+} T cells, antigen-specific CD8^{+} T cells and frequencies of their PD-1, CLTA-4 and Lag3 expression were assessed by flow cytometry during immune control (day 16) and immune evasion (day22) (n=11-15). Visualized are individual data points, mean and SD. **b)** *Ex vivo* tumor cell suspensions were restimulated with $OVA_{257-264}$ or left unstimulated and IFN-γ production was determined by ELISpot assay. *p< 0.05 by one-way ANOVA with Kruskal-Wallis test.

### 4.3.3 Myeloid cells in the tumor microenvironment differ greatly during DIVA[2]-induced immune control

Since anti-inflammatory myeloid cells within the TME, such as mononuclear phagocytes (Kubli et al. 2021), myeloid derived suppressor cells (MDSCs) (Gonda et al. 2017) or anti-inflammatory macrophages (H. Yang et al. 2020) are one of the most common inducers of immunosuppression which can result in immune evasion, we examined the myeloid compartment of the TME more detailed. Therefore, we calculated and visualized myeloid populations based on high-dimensional flow cytometry data using FlowSOM and t-SNE algorithms (Figure 4.7).
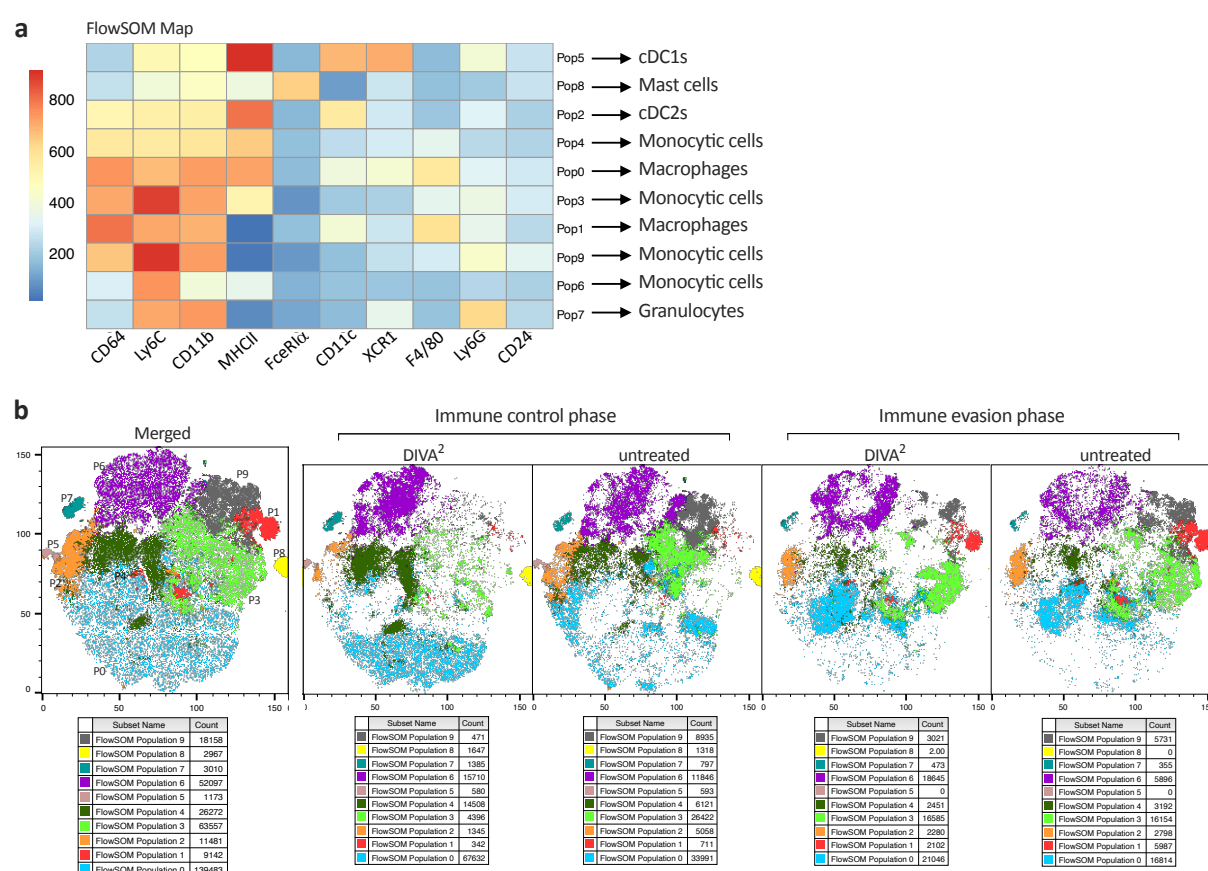


**Figure 4.7: The myeloid compartment of the TME differs greatly during DIVA[2]-induced immune control**

**a)** FlowSOM Map of CD45+ tumor infiltrating immune cells and their predicted cell types. Cells were pre-gated on living cells, single cells, Lineage- cells and CD45+ cells. Expression intensities were relatively set by the FlowSOM algorithm. **b)** t-SNE plots of CD45+ tumor infiltrating immune cells, merged per condition (immune control phase: n=15 for DIVA[2], n=12 for untreated; immune evasion phase: n=11 for DIVA[2], n=6 for untreated). FACS Markers included in the t-SNE calculation are analogous to markers in a). Coloring was set by applying the predicted FlowSOM populations onto the t-SNE plots.

Based on the fluorescence intensity of the myeloid FACS markers in the FlowSOM heatmap, we assigned the predicted populations to their possible cell types (Figure 4.7a). Strikingly, we found four different monocyte populations (P3, P4, P6 and P9) and two different macrophage populations (P0 and P1), in each case of various differentiation stadiums, indicated by their different MHCII and Ly6C expression intensities. While the t-SNE clustering during immune evasion was very similar between DIVA[2] and untreated, the analogous t-SNE plots during immune control differ greatly. These

differences mainly relate to the monocytic populations P3 and P9 and the macrophage population P0 (Figure 4.7b). However, based on the limited number of FACS markers in this analysis we were not able to derive further functional phenotypes of these myeloid populations.

Taken together, these data suggest that the DIVA[2]-induced immune response enables tumor immune control which is maintained for over two weeks. We highlighted the anti-tumoral character of antigen-specific CD8^{+} T cells and characterized the myeloid compartment where we found mainly differences in the clustering of monocytic cells and macrophages during immune control. Certainly, flow cytometry is limited when it comes to a more detailed characterization of these myeloid cells and especially their functional phenotype. To gain more information about these cells we decided to perform scRNA-seq of the TILs in an analogous experimental setup. Another question that arises at this point is whether the MC38mOVA tumor cells lose their antigen on the surface during the course of the experiment, thus initiating immune evasion. In order to detect their antigenicity and thus exclude antigen loss as a possibility for the initiation of immune evasion, we performed an *in vitro* proliferation assay of OT-I T cells after co-culturing with *ex vivo* MC38mOVA cells from DIVA[2]-treated and untreated mice at different time points during the course of the experiment.

## 4.4 DIVA[2] does not induce antigen loss on MC38mOVA tumor cells

Tumor cells can develop a wide variety of molecular mechanisms to circumvent elimination by pro-inflammatory immune cells. A common way how tumor cells drive immune evasion is the loss or decrease of antigen that gets presented to T cells via MHC class I molecules on the surface of tumor cells. This occurs by downregulating proteins involved in the antigen processing or presentation machinery (Spranger and Gajewski 2018) and can be increased by the selection pressure that is exerted by antigen-specific tumor infiltrating CD8^{+} T cells. Therefore, we investigated if there is a decrease or loss of the $OVA_{257-264}$ epitope on the surface of MC38mOVA cells during Diva[2]-induced immune control that could cause immune evasion. We performed DIVA[2] in a therapeutic tumor setting and prepared *ex vivo* tumor cells during immune control or evasion for 48 h co-culture with CFSE-labeled splenocytes from OT-I mice (Figure 4.8a). DIVA[2]-induced tumor infiltrating CD8^{+} T cells were over 40 % antigen-specific and highly activated, indicated by a CD44^{+} CD62L^{-} phenotype (Figure 4.8b, c). To detect antigen presentation on the surface of the tumor cells we measured the proliferation of $V\beta5.1/5.2^+$ CD8^{+} T cells within splenocytes of OT-I mice (Clarke et al. 2000; Hogquist et al. 1994). In order to demonstrate their response to the $OVA_{257-264}$ peptide, we exposed splenocytes from C57BL/6 mice or from OT-I mice to different concentrations of $OVA_{257-264}$ peptide *in vitro*. The CD8^{+} T cells within the B6 splenocytes did not proliferate, whereas those of the OT-I splenocytes were stimulated to proliferate (Figure 4.8d).
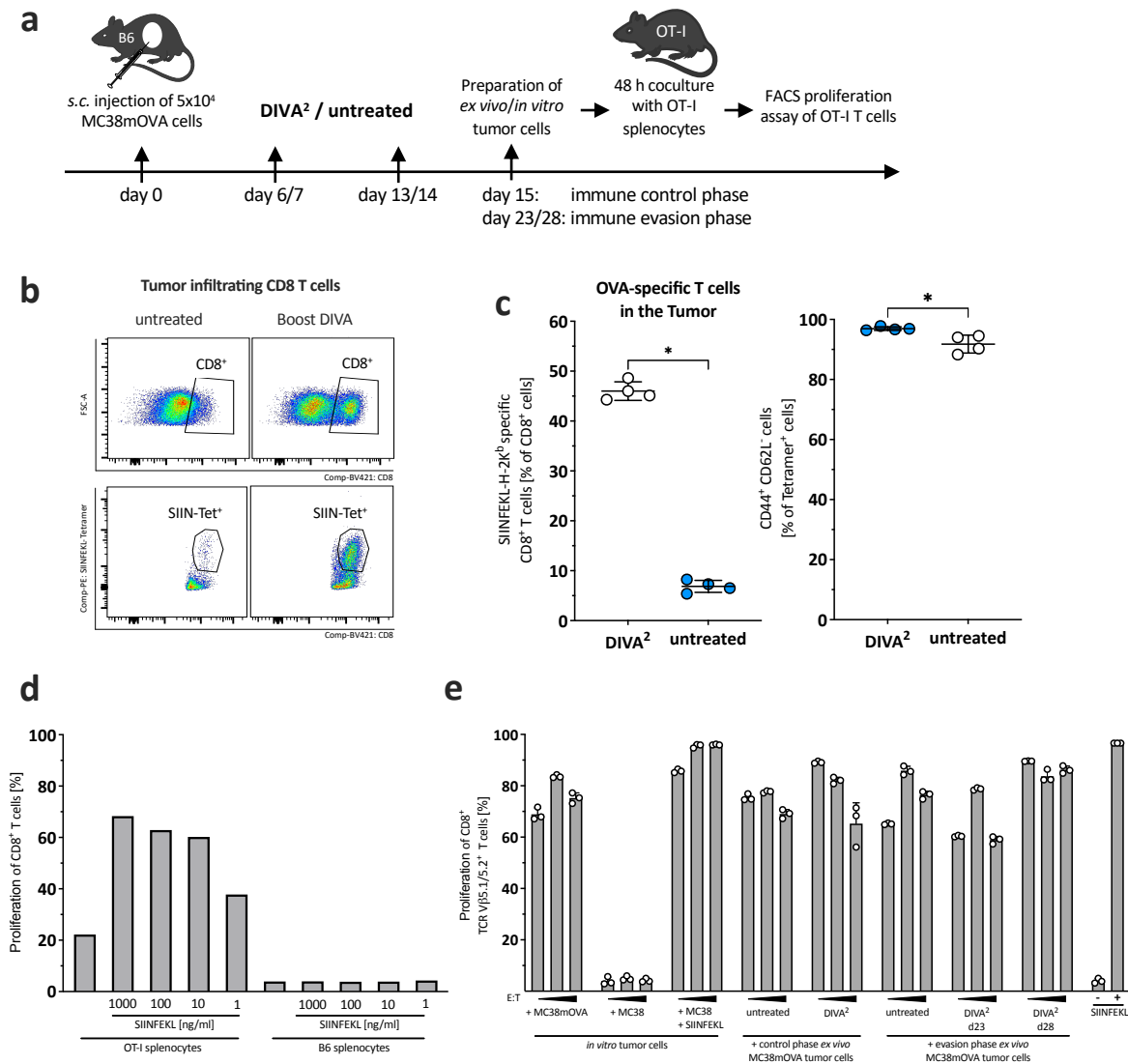
**Figure 4.8: DIVA²-induced antigen-specific T cells do not cause antigen loss on MC38mOVA tumor cells**

**a)** Schematic overview of the application pattern for DIVA² in a therapeutic tumor setting. *Ex vivo* tumor cell suspensions were prepared by MACS separation of CD45⁺ cells at day 15 (immune control phase), day 22 or day 28 (both immune evasion phase). *Ex vivo* and *in vitro* tumor cell suspensions were co-cultured for 48 h with CFSE-labeled OT-I splenocytes. T cell proliferation was assessed by flow cytometry. **b)** Representative flow cytometry dot plots of tumor-infiltrating CD8⁺ and antigen-specific CD8⁺ T cells of untreated and DIVA² treated mice. **c)** Antigen-specific CD8⁺ T cells and their activation state were determined by flow cytometry at day 23. **d)** *In vitro* proliferation assay of CFSE-labeled OT-I splenocytes. Proliferation of TCRVβ5.1/5.2⁺ T cells was determined after 48 h Co-culture by Flow cytometry. Effector:Target (E:T)-ratios of OT-I splenocytes to tumor cell suspension were 4,5:1; 13,5:1; 40,5:1. Peptide Control samples were cultured with a OVA₂₅₇₋₂₆₄ peptide (SIINFEKL) concentration of 10 ng/ml. Shown are individual values of separate *in vitro* co-cultures, mean and SD.

We observed a high proliferation of transgenic OT-I CD8⁺ T cells after co-culture with *in vitro* MC38mOVA tumor cells, but not with MC38 control cells, indicating the immunogenicity of MC38mOVA tumor cells. Surprisingly, OT-I T cells also proliferated after co-culture with *ex vivo* MC38mOVA cells, regardless of whether the mice were immunized or left untreated and whether tumor cells were isolated during immune control or immune evasion (Figure 4.8e). Taken together, these results indicate that the selection pressure exerted by DIVA²-induced antigen-specific CD8⁺ T cells on MC38mOVA tumor cells in the TME does not result in reduced antigen presentation on the surface of the tumor cells, why we can exclude antigen loss as a possible reason for immune evasion.

## 4.5 Single-cell RNA-sequencing reveals absence of immunosuppressive monocytes in the TME during DIVA$^2$-induced immune control

In the FACS-based characterization of the TME, we observed that DIVA$^2$ induces a significantly enhanced T cell immune response, but also substantially modulates the myeloid compartment of the TME, when compared to untreated. These discrepancies were detectable during immune control, but not during immune evasion. In the *in vitro* proliferation assay, we observed that there is no antigen loss on the surface of MC38mOVA tumor cells in the TME suggesting that it cannot be the reason for the development of immune evasion. Hence, we hypothesized that immunosuppression originates from myeloid cells, which showed a large discrepancy in their clustering during immune control. To obtain more information about these myeloid cells, we performed scRNA-seq of TILs. In the scRNA-seq approach that we performed, the mRNA of individual cells gets sequenced and bioinformatically analyzed. Distinct cell populations can be detected and their phenotype characterized in more detail which can give crucial information about immunological mechanisms that are operating within the TME.

### 4.5.1 DIVA$^2$-induced immune control is associated with a distinctly different TME

To gain more detailed information about the TME after DIVA$^2$ we set out to perform scRNA-seq of the TILs. For this purpose, we performed DIVA$^2$ in a therapeutic tumor setting and isolated TILs by magnetic bead sorting of CD45$^+$ cells during immune control and evasion from DIVA$^2$-treated and untreated mice (Figure 4.9a). The tumor volumes of the DIVA$^2$-treated and untreated mice exhibited the characteristic course shown in the FACS-based TME analysis (Figure 4.9b). We stopped the tumor experiment during the immune control phase at day 16, at which time the averaged tumor volume after DIVA$^2$ was about 5 mm$^3$, while that of the untreated mice was significantly different with about 155 mm$^3$. We stopped a separate tumor experiment in the immune evasion phase. Therefore, we chose a time point at which the tumors of the DIVA$^2$-treated mice had already reached the immune evasion phase, but the untreated mice had not yet reached the termination criteria. To accommodate this, we terminated the experiment on day 20 when the averaged tumor volume of the DIVA$^2$ treated mice was about 110 mm$^3$ and that of the untreated mice was about 400 mm$^3$. We prepared single cell suspensions from each of the mice and isolated the CD45$^+$ cells. The quality control results of the mRNA isolation and the metrics summary of the sequencing raw data are summarized in appendix 7.4.
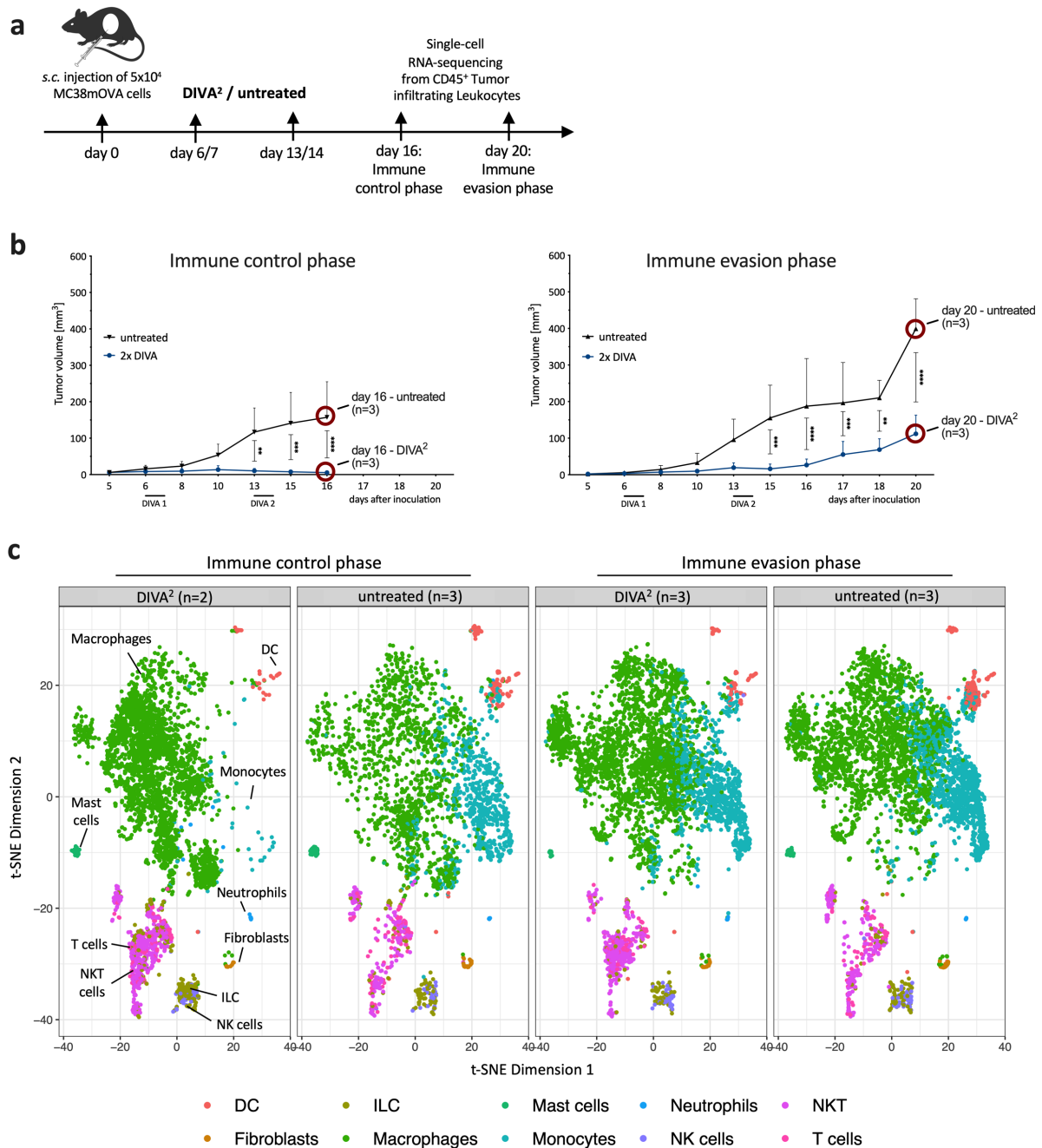
**Figure 4.9: scRNA-seq analysis reveals monocytes to be absent during DIVA$^2$-induced immune control**

**a)** Schematic overview of the application pattern for DIVA$^2$ in a therapeutic tumor setting. Tumor cell suspensions were prepared during immune control (day 16) or immune evasion (day 20), n=3/condition. Tumor infiltrating leukocytes were prepared by MACS isolation of CD45$^+$ cells. **b)** Tumor volumes during immune control (day 16) and immune evasion (day 22). Visualized are mean and SD. *p < 0.05 by two-way ANOVA with Sidak's multiple comparisons test. **c)** scRNA-seq-based t-SNE plots of TILs, merged per condition (n=2-3). Cell types were predicted based on the immgen database annotation immgen main.

In the processing of the scRNA-seq data, we assigned in an unbiased approach the sequenced single cells to immune cell types based on the immgen database annotation *immgen main* (status: 12/2022). To represent an overview of the diversity of the TILs across conditions, we calculated t-SNE plots (Figure 4.9c). During immune control, TILs clustered differently across conditions. Most strikingly, we detected almost no monocytes after DIVA$^2$, but a more strongly represented macrophage population.

This was accompanied by a stronger population of T cells and NKT cells. In contrast, TILs clustered very similarly during immune evasion, which is generally consistent with the results of the FACS-based t-SNE plots (Figure 4.7).

For better comparability we plotted the frequencies of the immune cell types relative to CD45$^+$ cells (Figure 4.10a). During immune control we detected after DIVA$^2$ around 1,2 % monocytes but in the untreated group around 27 %. However, this monocyte population appeared in DIVA$^2$-treated mice until immune evasion on day 20 and clustered to a very similar extent as the analogous monocyte population of the untreated group. The macrophages were with 73 % more present during immune control after DIVA$^2$ compared to untreated with 51 %. This discrepancy tended to neutralize until immune evasion. We also observed that after DIVA$^2$ a weaker DC population was represented during both immune control and immune evasion. Similar to the FACS-based characterization of the TME, we also observed that after DIVA$^2$ cytotoxic lymphocytes, such as T cells, NK cells, NKT cells and ILCs, were more abundant in total during immune control, reflecting around 21 % of the CD45$^+$ cells within the TME. The significant discrepancy in the total number of cytotoxic lymphocytes during immune control decreased until immune evasion, but we still detected with around 13 % a higher frequency after DIVA$^2$ during immune evasion when compared to untreated.

Seperated quantification of cytotoxic lymphocyte subtypes revealed that CD8$^+$ T cells were approximately twice as abundant compared to untreated. This discrepancy increased up to immune evasion, as the CD8$^+$ T cell frequency in the TME of untreated mice decreased (Figure 4.10b). In contrast, the frequency of CD4$^+$ T cells decreased after DIVA$^2$ slightly from immune control to immune evasion but increased to over 2 % in case of untreated mice. Within these CD4$^+$ T cells, we detected during immune control approximately half as many FoxP3$^+$ Treg cells after DIVA$^2$ compared to untreated. Until immune evasion, this frequency remained after DIVA$^2$ the same, whereas the frequency in the untreated mice increased to about 1,6 %. Furthermore, the analysis revealed that approximately twice as many NKT cells were detected during immune control compared to immune evasion, regardless of treatment. We observed a slightly smaller increase in NK cells, which was 1 % in the untreated group but increased to 1,5 % after DIVA$^2$. However, during immune evasion, the rate of DIVA$^2$-treated mice decreased again to 0,9 %, while that of untreated mice remained about the same at 1,2 %. Surprisingly, we detected about 7 % ILCs after DIVA$^2$ during immune control whereas in untreated mice this frequency was about 3 %. This discrepancy disappeared completely by the time of immune evasion and we detected about 2 % ILCs in each case. These data confirm the results of the FACS-based analysis of tumor-infiltrating CD8$^+$ T cells and also show which subtypes of cytotoxic lymphocytes were represented in the TME.

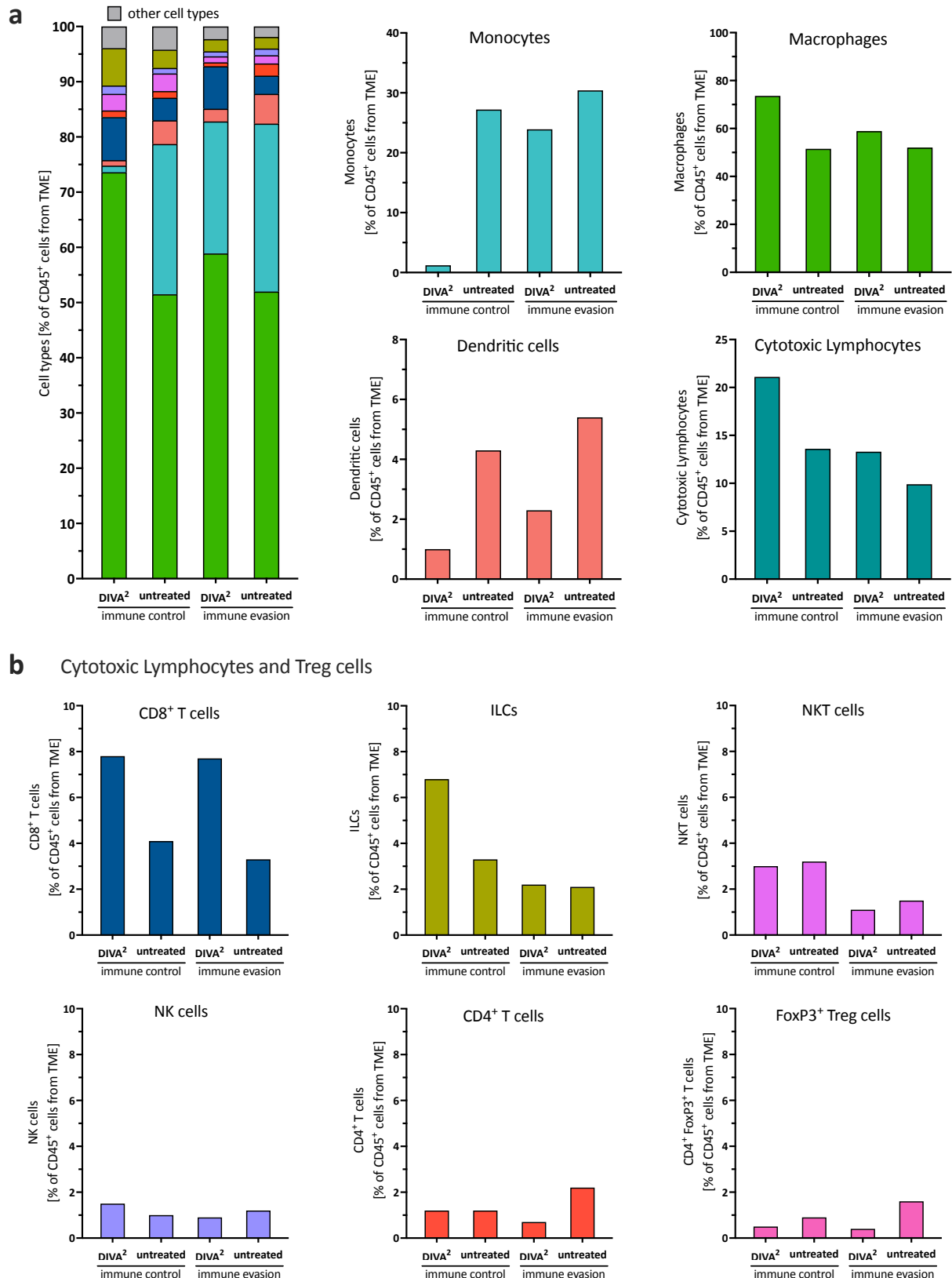**Figure 4.10: DIVA$^2$ induces a strong infiltration of the TME by cytotoxic lymphocytes**

**a)** scRNA-seq based quantitative distribution of TIL celltypes in the TME. Celltype prediction was performed based on the database immgen main, number of samples as indicated in Fig. 4.5.1. **b)** Quantitative distribution of cytotoxic lymphocytes that include T cells, NKT cells, ILCs and NK cells. Samples are merged per condition (n=2-3).

In summary, we conclude from the overview and the quantification of the scRNA-seq-based TME analysis that DIVA$^2$ led to a strong modulation of the immune cells within the TME. The discrepancy between the TILs of DIVA$^2$-treated and untreated mice was mainly detectable during immune control and largely decreased until immune evasion. During immune control, we mainly figured out that monocytes were almost absent after DIVA$^2$, however these cells appeared until immune evasion. This was accompanied by a strong influx of cytotoxic lymphocytes into the TME, whose frequency decreased from immune control until immune evasion, thus favoring tumor progression. Within the cytotoxic Lymphocytes, mainly the CD8$^+$ T cells were after DIVA$^2$ much more represented during both immune control and immune evasion, whereas the ILCs were only more represented during immune control. Since the scRNA-seq analysis allows a very precise assignment of cells to immune cell types due to the high number of marker genes, we thus not only confirmed the results of the FACS-based TME analysis, but specified them beyond that. To understand which immunological mechanisms enable the immune control and which immune evasion mechanisms in the TME of MC38mOVA tumors prevent an ongoing immune control, we needed to characterize the phenotype of the differentially distributed cell types more precisely. Therefore, we focused on analyzing marker gene expression of the cytotoxic lymphocyte subtypes that were strongly increased by DIVA$^2$ and the monocytes that appeared in the TME until immune evasion.

### 4.5.2 DIVA$^2$-induced cytotoxicity is mainly mediated by CD8$^+$ T cells and ILCs

After we had quantitatively identified which cytotoxic lymphocytes were represented in the TME after DIVA$^2$, it was necessary to characterize them phenotypically in more detail. For this purpose, we analyzed the different subsets of cytotoxic lymphocytes regarding the expression of a cytotoxic gene signature based on the scRNA-seq data (Figure 4.11). The merged view of the t-SNE plot showed that the expression of cytotoxic marker genes is essentially restricted to T cells, NKT cells, NK cells and ILCs in relation to all TIL populations (Figure 4.11a). In the t-SNE plots split by condition, we observed that DIVA$^2$ induced especially a larger population of T cells expressing the cytotoxic gene signature compared to untreated during both immune control and immune evasion. To highlight the differences in lymphocytes expressing the cytotoxic gene signature, we analyzed the expression intensities for each cytotoxic lymphocyte subtype separately and visualized them in violin plots (Figure 4.11b). The expression analysis of the cytotoxic gene signature showed that the DIVA$^2$-induced CD8$^+$ T cells detected in the quantitative analysis also largely expressed the cytotoxic gene signature. Like the results of the FACS-based TME analysis and the IFN-$\gamma$ ELISpot of the tumor cell suspensions (Figure 4.6), the cytotoxicity of these CD8$^+$ T cells increased from immune control to immune evasion, as the averaged signature score increased from about 10 to 15.

**a** Cytotoxic gene signature

**b**

**Figure 4.11: DIVA²-induced CD8⁺ T cells express cytotoxic marker genes**
**a)** t-SNE plots of TILs showing their signature score for cytotoxic marker genes that are listed. Merged and split by condition (samples merged per condition, n=2-3). **b)** Signature scores for cytotoxic marker genes separated per subtype of cytotoxic lymphocytes, split by condition (samples merged per condition, n=2-3).

This confirms that CD8⁺ T cells exhibit a cytotoxic phenotype during both immune control and immune evasion. The ILCs, detected in greater numbers during immune control, also expressed the cytotoxic marker genes to a large extent, suggesting an ILC type 1 phenotype which means that they could also contribute to immune control (Jacquelot et al. 2022). However, this effect was limited in time, as they were present in much lower cell numbers during immune evasion, suggesting that the ILCs could

contribute to the elimination of tumor cells to a much lesser extent from the onset of immune evasion. In the quantitative analysis, we detected an equal frequency of NKT cells regardless of treatment during immune control. However, these showed a slightly increased signature score after DIVA[2], indicating a slightly stronger cytotoxic phenotype. Although the NKT cells in both conditions also expressed cytotoxic marker genes during immune evasion, the number of these cells was reduced by half during this phase, suggesting that they were able to contribute to the elimination of tumor cells to a lesser extent at the development of immune evasion. In the case of CD4+ T cells, we observed in the expression analysis that the signature score was similar in both conditions and time points, but the number of cells had increased in the untreated mice until immune evasion. However, the lower average signature score suggests a lower cytotoxic contribution of the CD4+ T cells. The NK cells were represented in the lowest cell number of cytotoxic lymphocytes. However, these had the highest averaged signature score in the expression analysis, indicating these may have also contributed to the elimination of tumor cells. In summary, these observations show that the CD8+ T cells and ILCs highlighted in the quantitative analysis were also for the most part the cells that expressed the cytotoxic marker genes, while the NKT cells, NK cells and CD4+ T cells were less able or unable to contribute to cytotoxicity. Furthermore, we observed a marked decrease in the total cell number of cytotoxic lymphocytes from immune control to immune evasion, generally associated with a slightly lower expression of cytotoxic marker genes, with the exception of the CD8+ T cells. These observations may indicate the favoring of tumor progression and thus the switch from immune control to immune evasion.

### 4.5.3    DIVA[2]-induced CD8+ T cells partly express exhaustion marker genes

In the gene expression analysis of the cytotoxic gene signature, CD8+ T cells and ILCs in particular showed a cytotoxic phenotype within the cytotoxic lymphocytes. While the cell count of CD8+ T cells remained stable until immune evasion, the number of other cytotoxic lymphocyte subtypes decreased, favoring tumor growth. Besides a decreasing number of cytotoxic lymphocytes, another reason for tumor progression is T cell exhaustion. In parallel to the expression of cytotoxic marker genes, T cells can also express exhaustion marker genes. These are a sign of reduced to completely suppressed effector T cell function. To investigate this, we performed a gene expression analysis with the exhaustion marker genes PD-1, CTLA-4, Lag3, Tim-3 and Tigit (Wherry and Kurachi 2015) (Figure 4.12). This showed that PD-1 expression increased from immune control to immune evasion in the DIVA[2]-treated group, suggesting a continued antigen contact and activation state of these T cells. In the flow cytometry analysis, we observed that the expression of CTLA-4 and Lag3 was very low at about 15 and below 10 %, respectively. In contrast, the CD8+ T cells of all conditions showed higher values of 35-45 % in the scRNA-seq-based analysis.
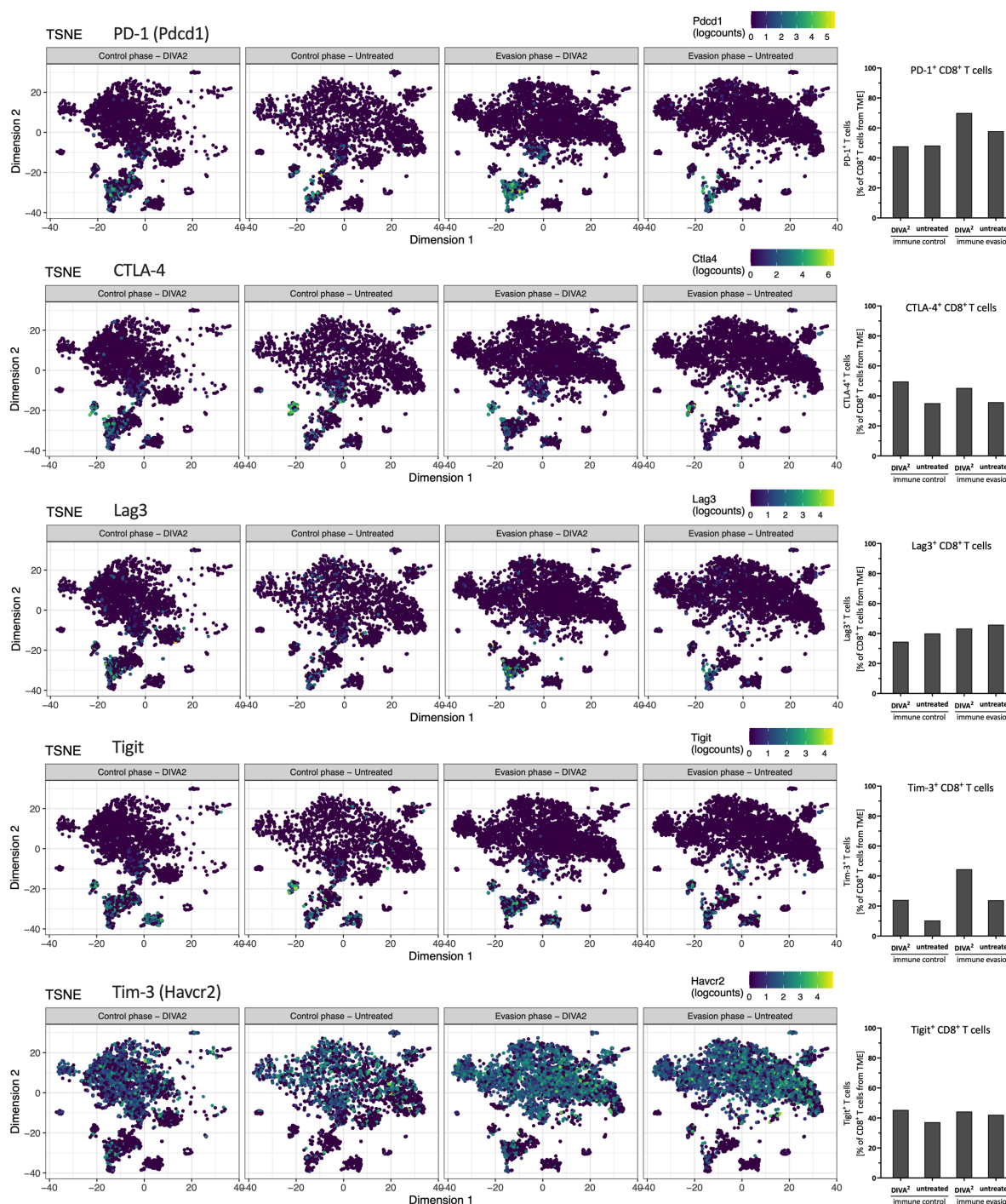
**Figure 4.12: CD8^{+} T cells partly express exhaustion marker genes**

t-SNE plots of TILs showing their expression of indicated exhaustion marker genes. Merged and split by condition (samples merged per condition, n=2-3). Plots in the right represent the frequency of CD8^{+} T cells expressing indicated exhaustion marker (samples merged per condition, n=2-3).

These values were also observed for Tigit in addition to CTLA-4 and Lag3. Only Tim-3 expression was lower, but increased to over 40 % in the DIVA[2]-treated group until immune evasion. These data indicate that some of the CD8^{+} T cells in the TME express exhausted marker genes and therefore it can be assumed that this results in reduced effector T cell function. In addition to the decreasing total number of cytotoxic lymphocytes at the time of immune evasion compared to immune control, this represents a further starting point for increased tumor growth after initial tumor immune control.

## 4.5.4    Monocytes show an immunosuppressive phenotype in immune evasion

In the expression analysis of the cytotoxic lymphocyte subtypes, we figured out that they expressed cytotoxic marker genes and that CD8^{+} T cells and ILCs were the main producers of cytotoxic cytokines. However, excepting CD8^{+} T cells, we also observed a decrease in the total cell number of cytotoxic lymphocytes from immune control until immune evasion. Furthermore, the CD8^{+} T cells partly expressed T cell exhaustion marker genes. Since there was a steady tumor growth in the TME despite the consistently high number of cytotoxic CD8^{+} T cells from immune control until immune evasion, it suggests that suppression of these cells in the TME might occur, causing T cell exhaustion. In the quantitative analysis of TILs, we also observed that monocytes were almost absent during immune control and appeared until immune evasion. To characterize the phenotype of these monocytes more precisely and to find out whether they contribute to the suppression of cytotoxic lymphocytes when entering the TME, we performed an expression analysis of immunosuppressive marker genes (Figure 4.13).
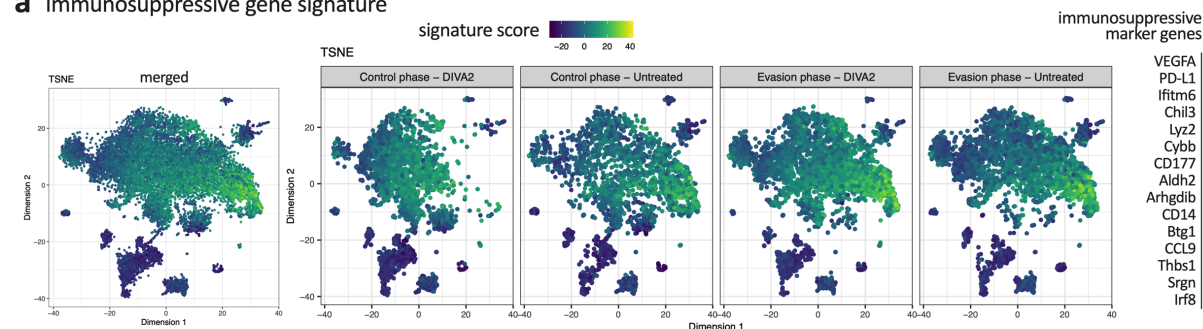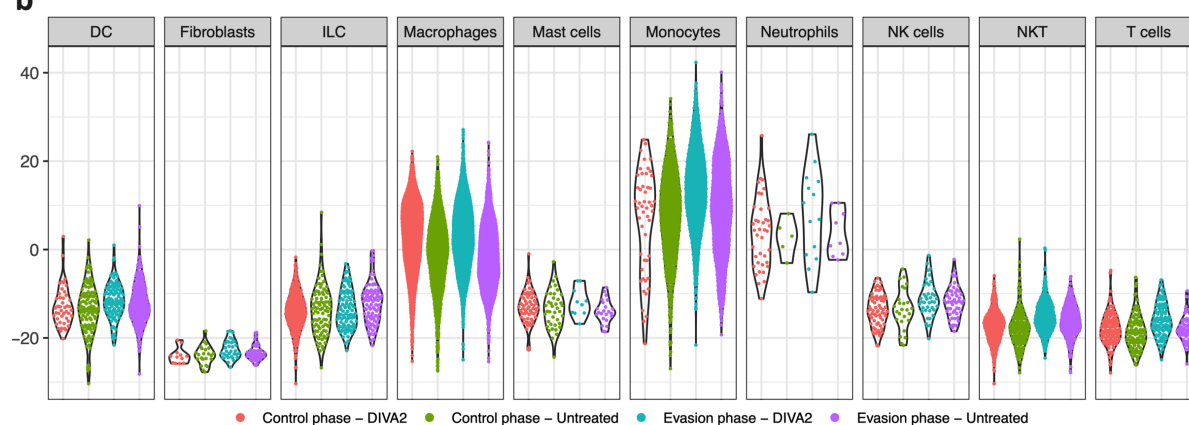


**Figure 4.13: Monocytes appearing in the TME until immune evasion in DIVA$^2$-treated mice express immunosuppressive marker genes**

**a)** t-SNE plots visualizing the expression score of immunosuppressive marker genes in merged view and split by condition. Analyzed immunosuppressive marker genes are listed. Samples are merged per condition (n=2-3) **b)** Violin plot visualizing the expression score of the immunosuppressive gene signature, split by condition (n=2-3) and cell type.

The merged view of the t-SNE plot showed that the anti-inflammatory marker genes are not exclusively but most strongly expressed by monocytes (Figure 4.13a). Consequently, in the t-SNE plots split by condition, we observed that the absence of monocytes during DIVA$^2$-induced immune control meant

that a significant proportion of TILs expressing the immunosuppressive marker genes were not represented in the TME. To further examine the extent to which the expression of the immunosuppressive marker genes relates to the monocytes, we plotted the expression intensity split by cell type (Figure 4.13b). As already indicated in the t-SNE plots, macrophages also expressed the immunosuppressive marker genes, but at a significantly lower signature score than monocytes. Only the neutrophil granulocytes had a signature score similar to that of the monocytes, but these were only represented in a very small number of cells. These data indicate that the monocytes that infiltrate the TME after the immune control phase exhibit an immunosuppressive phenotype and can thus contribute significantly to the immunosuppression of pro-inflammatory immune cells within the TME, for example by causing T cell exhaustion in a portion of CD8^{+} T cells.

To verify the immunosuppressive effect of these monocytes in an *in vivo* experiment, we examined the monocytes for a potential target that we can use to deplete them in a tumor setting. The CCL2/CCR2 axis plays a crucial role in the recruitment of monocytic cells to the tumor site. The chemokine CCL2 can be expressed in the TME by stroma cells, endothelial cells, tumor cells or leukocytes (Soria and Ben-Baruch 2008), forming a CCL2 gradient within the organism. Cells expressing the CCL2-receptor CCR2 on their cell surface can migrate along a systemic CCL2 gradient to the peripheral tumor site. Once in the TME, these cells can contribute to the suppression of pro-inflammatory cells. The t-SNE plot split by conditions showed that besides macrophages, mainly monocytes expressed CCR2 (Figure 4.14). Because monocytes were almost absent after DIVA[2], we consequently observed during immune control a strong reduced amount of CCR2^{+} cells in general. Furthermore, we observed that mainly myeloid cells expressed CCL2, including monocytes and macrophages (Figure 4.14). CCL2 expression was stronger in the untreated group during immune control and immune evasion. Since monocytes were almost absent in the DIVA[2]-treated group during immune control, the total number of CCL2-expressing cells was thus also lower. This indicates that CCR2^{+} cells are recruited to a lesser extent. However, we detected a strong increase in CCR2^{+} monocytes in the immune invasion phase, regardless of treatment, indicating that these monocytes could migrate into the TME via CCL2/CCR2 signaling. Notably, we observed strong Ly6C expression of these monocytes, allowing flow cytometry-based depletion analysis of those cells in a tumor experiment (Figure 4.14). Strikingly, only the macrophages in the DIVA[2]-treated group showed a strong expression of CD38 at the time of immune control compared to the other conditions. CD38 is a marker for pro-inflammatory macrophages of the M1 phenotype (Jablonski 2015) suggesting that the macrophages in the DIVA[2]-treated group had a pro-inflammatory phenotype at the time of immune control.
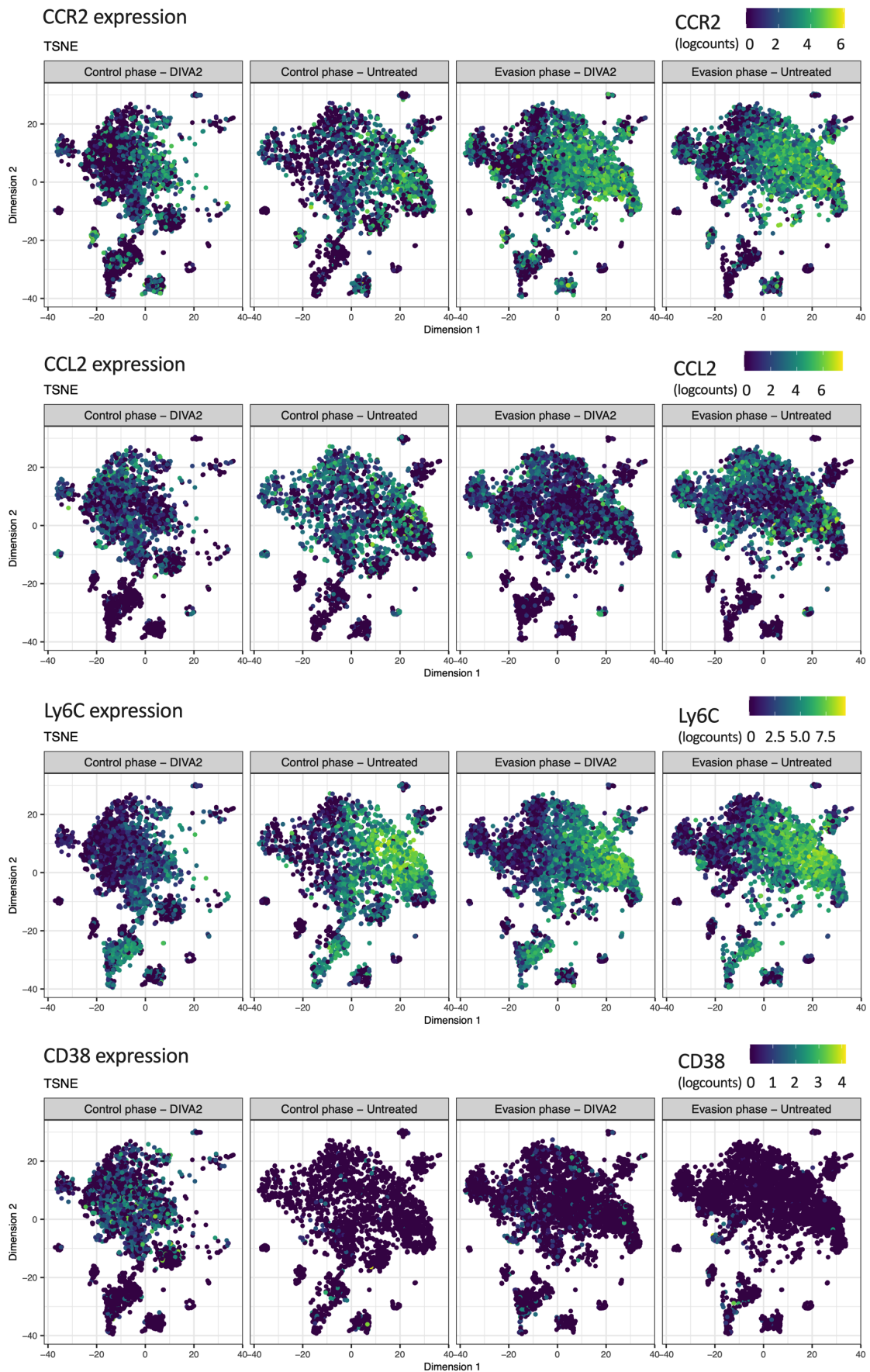
**Figure 4.14: Tumor-infiltrating monocytes express CCR2**

t-SNE plots visualizing the expression score of CCR2, CCL2, Ly6C and CD38, split by condition. Samples are merged per condition (n=2-3).

In summary, these results suggest that the DIVA[2]-induced cytotoxicity is mainly mediated by CD8^{+} T cells and ILCs but that CD8^{+} T cells also partly expressed exhaustion-related marker genes. Monocytes infiltrating the TME of DIVA[2]-treated mice until immune evasion exhibited an immunosuppressive phenotype indicated by the expression of a characteristic immunosuppressive gene signature. Furthermore, we detected a high expression of CCR2 by these monocytes, making them targetable with an anti-CCR2 antibody to prevent their migration to the peripheral tumor site. The increasing CCL2 expression in the DIVA[2]-treated group from immune control until immune evasion enhances the recruitment of CCR2^{+} monocytes, thereby favoring tumor growth. Only the macrophages of the DIVA[2]-treated group showed significantly increased expression of the pro-inflammatory M1 marker CD38 at the time of immune control. To verify the immunosuppressive effect of the CCR2^{+} monocytes, we targeted them in an *in vivo* tumor experiment with the anti-CCR2 antibody MC-21.

## 4.6 Depletion of immunosuppressive CCR2^{+} monocytes after therapeutic DIVA[2] demonstrates their tumor-promoting capacity

By analyzing the TILs by scRNA-seq, we further characterized the TME after DIVA[2] treatment by using an unbiased bioinformatic approach to precisely identify the immune cell types and describe their functional phenotype. Performing expression analysis of characteristic gene signatures allowed identifying the cytotoxic phenotype of CD8^{+} T cells and ILCs and the immunosuppressive phenotype of the CCR2^{+} monocytes, absent after DIVA[2] during immune control but present in the TME during immune evasion. In order to evaluate the immunosuppressive capacity of these monocytes and understand their influence on the tumor growth when they infiltrate the tumor, we decided to deplete the CCR2^{+} peripheral blood monocytes in a tumor experiment. The CCR2-CCL2 axis has been well described and represents a therapeutic target to prevent the infiltration of monocytic phagocytes into the TME (Kubli et al. 2021). To evaluate their tumor-promoting capacity we depleted them in a therapeutic tumor setting with the anti-CCR2 antibody MC-21 (Mack et al. 2001) (kindly provided by Prof. Dr. Matthias Mack, University Regensburg, Germany) and hypothesized a decrease of tumor growth after depletion (Figure 4.15a). In our previous work we showed that depletion of CCR2^{+} peripheral blood monocytes with MC-21 prior to DIVA abolished the immune response by preventing the dithranol-induced monocyte influx into the skin (Sohl et al. 2022). Therefore, we decided to start monocyte depletion only after the second immunization at day 15. Due to the formation of antibodies against the anti-CCR2 antibody MC-21, it can only be administered for 5 consecutive days (Mack et al. 2001). Administering 20 µg MC-21 antibody resulted at day 16 (24 h after the first injection) in a complete depletion of Ly6C^{high} CCR2^{+} peripheral blood monocytes. This depletion was accompanied by
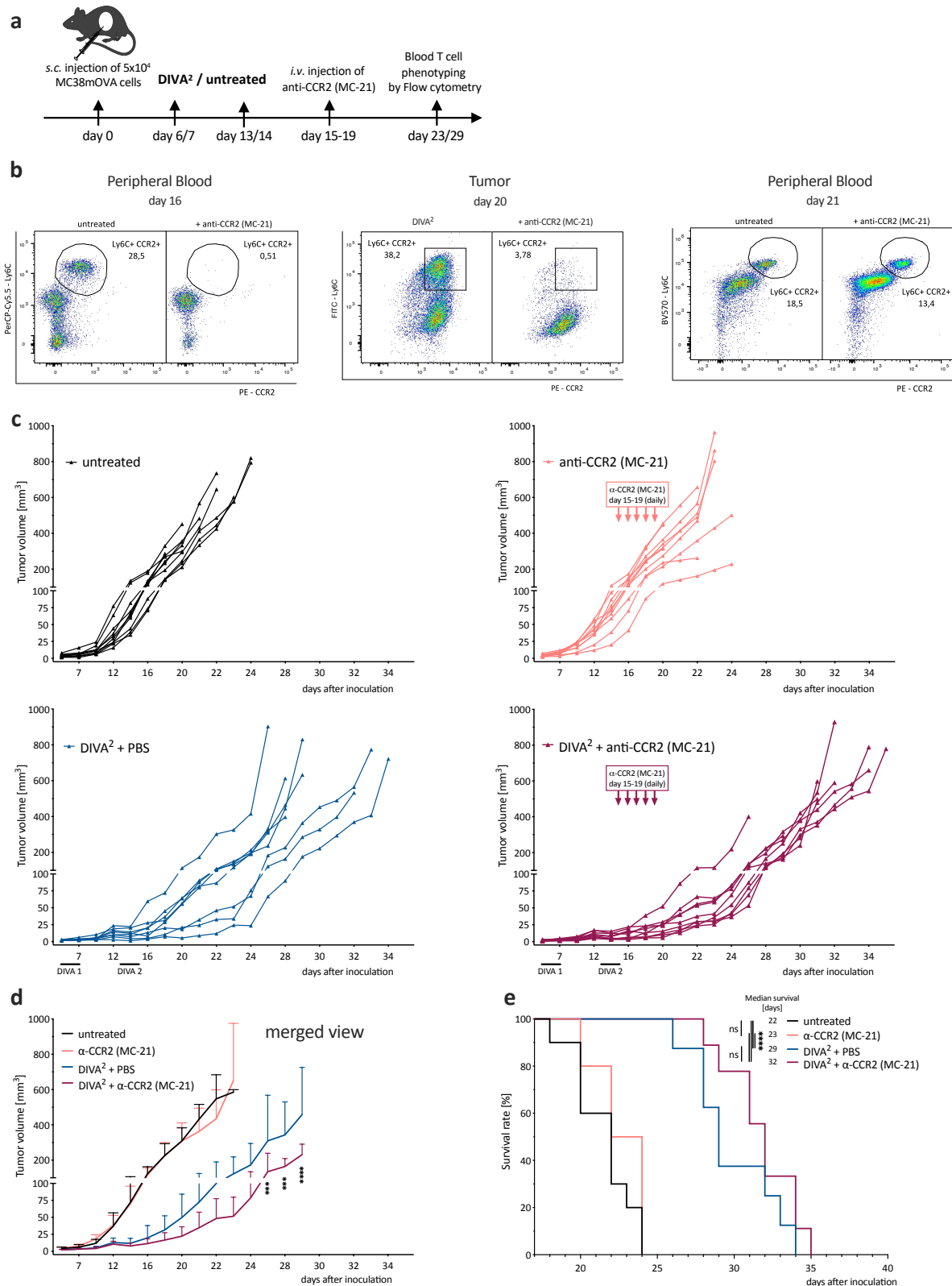
**Figure 4.15: Depletion of CCR2+ monocytes transiently decreases tumor growth demonstrating their immuno-suppressive capacity**

**a)** Schematic overview of the application pattern for DIVA[2] in a therapeutic tumor setting. DIVA[2]-treated or untreated mice were i.v. injected with anti-CCR2 antibody MC-21 from day 15-19 (20 µg daily) or left untreated. **b)** Representative flow cytometry dot plots of LY6C+ CCR2+ cells from peripheral blood or MC38mOVA tumor. Mice were treated either with MC-21 antibody, DIVA[2] or left untreated. **c)** Tumor volumes were assessed three times per week. Every curve represents the tumor volume of one individual mouse. **d)** Merged tumor volumes visualized as mean and SD per condition. **e)** Kaplan-Meier survival curve. p < 0.05 by two-way ANOVA with Sidaks multiple comparisons test and one-way ANOVA with Kruskal-Wallis test, when sample numbers were different. Comparisons of survival curves were performed by Log-rank (Mantel-Cox) test.

an almost complete depletion of these CCR2$^+$ monocytes in the tumors at day 20. These findings suggest that the CCR2$^+$ monocytes that we detected by scRNA-seq during immune evasion (day 20) infiltrate the TME from the peripheral blood, but that this infiltration can be prevented by the anti-CCR2 antibody MC-21. However, we detected CCR2$^+$ monocytes in the peripheral blood again 48 h after the last MC-21 injection at day 21, which is since the MC-21 antibody can only be administered for 5 consecutive days (Figure 4.15b). Combining DIVA$^2$ and MC-21 treatment in a therapeutic tumor setting reduced the tumor growth significantly, compared to DIVA$^2$ alone. However, this effect was limited and lasted only until about 5 days after the last MC-21 injection. Thereafter, we observed that the tumor volume increased more rapidly. Since the monocytes were detectable in the blood about 48 h after the last injection, these findings suggest that the CCR2$^+$ monocytes exhibit a tumor-promoting effect, which unfolds again when the depletion effect runs out. Notably, treatment with MC-21 alone did not induce a reduction in tumor growth, indicating that depletion of tumor-promoting monocytes no longer has an effect when started in the later immune evasion phase (Figure 4.15c, d). After treatment with MC-21 alone, we observed no prolongation of the median survival compared to the untreated group, which was 22 and 23 days, respectively. However, DIVA$^2$ significantly prolonged the median survival to 29 days and the combination of DIVA$^2$ and MC-21 to 32 days. The transiently stronger anti-tumoral character of the combination of DIVA$^2$ and MC-21 compared to DIVA$^2$ alone was mainly reflected in the survival curve in the period between day 27 and 32. This observation suggests that the effect of transient monocyte depletion in peripheral blood and in the tumor results in an equally transient prolonged survival after a time lag of about 10 to 12 days. The expiry of the depletion effect on day 21 was thus accompanied by the expiry of the discrepancy in prolonged survival, which can be seen at the end of the survival curves on day 34 and 35, respectively (Figure 4.15e).

We further checked if this anti-tumoral effect was due to depletion of tumor-promoting CCR2$^+$ monocytes or rather to an altered T cell immune response. For this purpose, we functionally characterized the circulating CD8$^+$ and CD4$^+$ T cells at different time points. Surprisingly, despite the lower tumor growth in the MC-21 treated animals, we found even fewer CD8$^+$ T cells and antigen-specific CD8$^+$ T cells. These cells produced similar amounts of IFN-$\gamma$, TNF-$\alpha$ and KLRG-1 upon stimulation with Ionomycin and phorbol-12-myristate-13-acetate (PMA), suggesting a functional, non-senescent phenotype. Even though CD8$^+$ T cells can express CCR2, depletion of CCR2$^+$ cells did not induce depletion of T cells, as we found no difference in CD8$^+$ T cell count after treatment with MC-21 alone compared to untreated mice (Figure 4.16a). In case of CD4$^+$ T cells, we also observed no differences between DIVA$^2$-treated and untreated mice (Figure 4.16b).
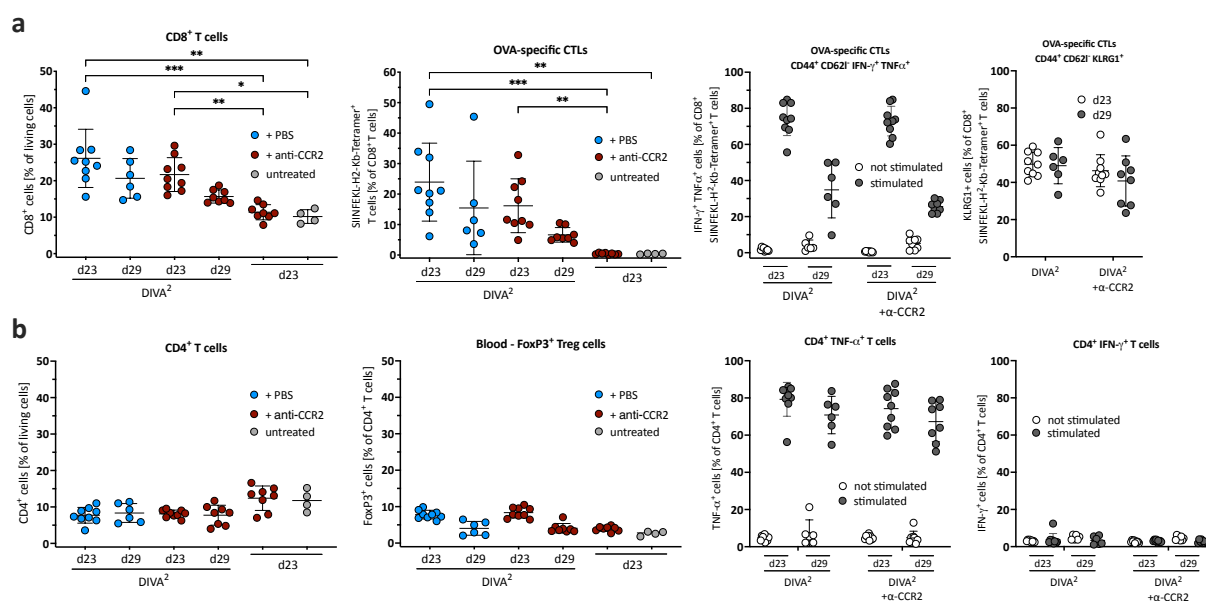
**Figure 4.16: Systemic depletion of CCR2⁺ cells does not lead to depletion of T cells**

T cell phenotyping of CD8⁺ T cells in **a)** and CD4⁺ T cells in **b)** was determined by flow cytometry at day 23 and 29. Stimulation of CD4⁺ and CD8⁺ T cells for assessing cytokine production by flow cytometry was performed for 4 h at 37 °C and stimulation with 0,5 µg/ml Ionomycin, 50 ng/ml PMA and 2 µM Monensin.

Taken together, these findings confirm the hypothesis that the Ly6C$^{high}$ CCR2⁺ tumor infiltrating monocytes contributed to the tumor-promoting microenvironment. The associated tumor growth could only be slowed down temporarily with the anti-CCR2 monocyte-depleting antibody MC-21. When the depletion effect was gone, the tumor growth did develop more rapidly indicating that alternative depleting or blocking substances are needed to permanently prevent the infiltration of tumor-promoting monocytes into the tumor.

## 4.7 Therapeutic DIVA² fails to increase anti-PD-1-mediated anti-tumor immunity to completely eliminate MC38mOVA tumors

To assess the biological capacity of DIVA² in relation to other immuno therapy approaches, we compared DIVA² with the immune checkpoint inhibitor (ICI) anti-PD-1. Ligation of PD-1 on the cell surface of T cells leads to downregulation of their immune response through tyrosine phosphatase activation and mediates immune tolerance in peripheral tissues and limits autoimmune responses (Chemnitz et al. 2004; Keir et al. 2008). Blocking PD-1 removes this immunological brake, allowing cytotoxic lymphocytes to continue their effector function against tumor cells. Therefore, we performed a therapeutic tumor experiment and treated mice with DIVA², anti-PD-1 or the combination of DIVA² and anti-PD-1 or left them untreated (Figure 4.17).
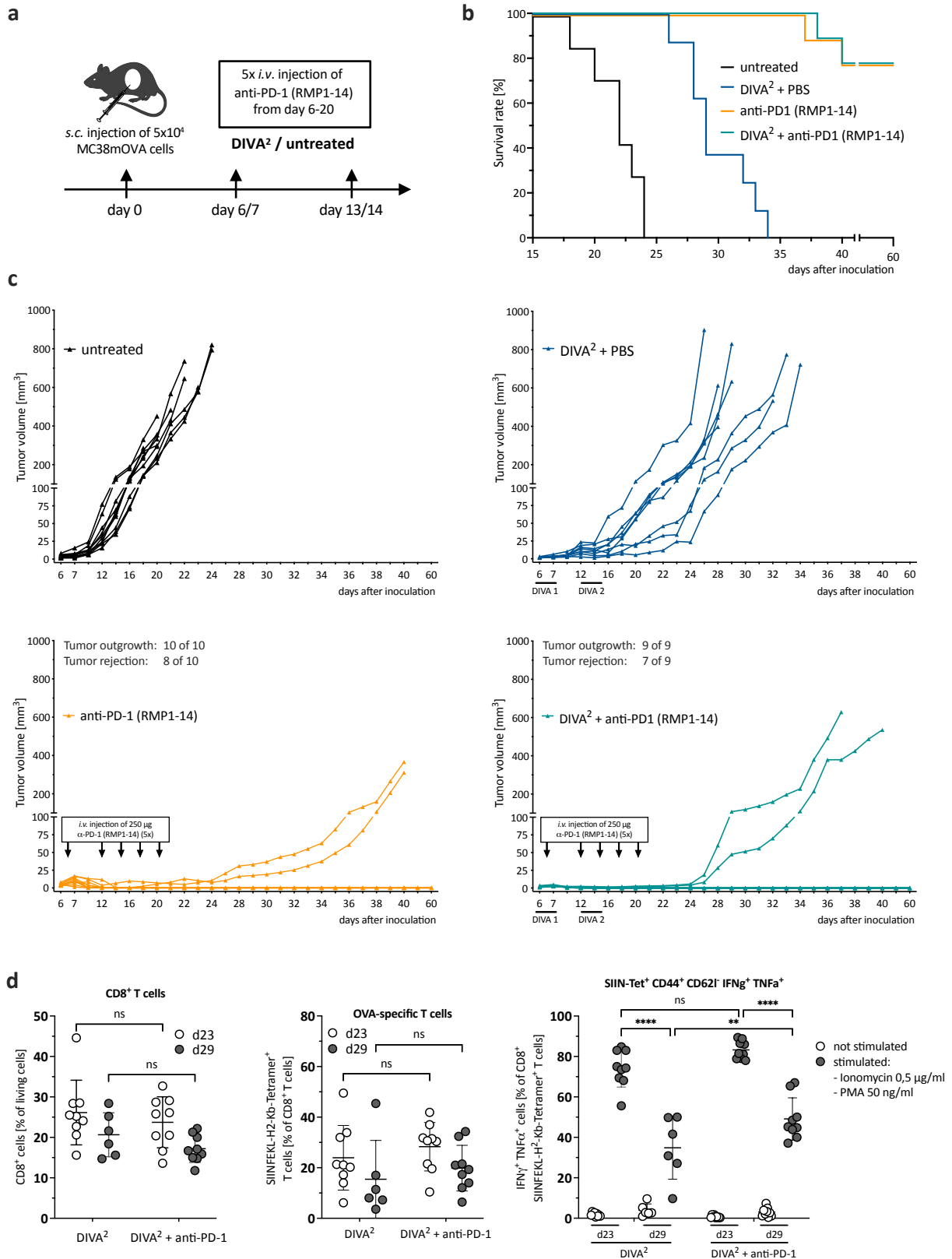
**Figure 4.17: Therapeutic DIVA² fails to increase anti-PD-1-induced anti-tumor immunity**

**a)** Schematic overview of the application pattern for combination of DIVA² and immune checkpoint blockade via anti-PD-1 in a therapeutic tumor setting. DIVA²-treated or untreated mice were i.v. injected 5x with anti-PD-1 antibody RMP1-14 between day 6 and 20 (250 µg each) or left untreated. **b)** Kaplan-Meier survival curve. Comparisons of survival curves were performed by Log-rank (Mantel-Cox) test. **c)** Tumor volumes were assessed three times per week. Every curve represents the tumor volume of one individual mouse. **d)** Frequency of CD8⁺ T cells and antigen-specific T cells and their expression of IFN-γ and TNF-α, assessed by flow cytometry after 4 h at 37 °C and stimulation with 0,5 µg/ml Ionomycin, 50 ng/ml PMA and 2 µM Monensin.

In contrast to the DIVA[2]-treated group, we observed that anti-PD-1 eliminated tumors in 8 of 10 mice. In the other two mice, immune evasion resulted in steadily progressive tumor growth. This indicates the strong anti-tumor capacity of anti-PD-1-mediated immune checkpoint blockade (ICB) in this MC38mOVA model. Since combining cancer vaccines with ICB is a common method to enhance induced anti-tumor immunity (J. Tang et al. 2018) we further tested whether DIVA[2] combined with anti-PD-1 acts synergistically enabling complete regression of tumors. However, this showed that 2 of the 9 outgrown tumors could not be rejected and the survival was not prolonged, indicating that DIVA[2] does not add anti-tumor capacity to anti-PD-1-based immunotherapy of MC38mOVA tumors (Figure 4.17). We quantified and characterized the effector function of the DIVA[2]-induced antigen-specific T cells by flow cytometry upon stimulation with ionomycin and PMA (Figure 4.17d). As expected, combining DIVA[2] and anti-PD-1 had no significant effect on the frequency of CD8^{+} T cells and antigen-specific T cells. On day 23, the effector function of antigen-specific T cells showed no significant difference between the two treatments. The frequency of IFN-$\gamma^+$ TNF-$\alpha^+$ antigen-specific CD8^{+} T cells was about 75 % and 80 %, respectively. However, until day 29, the frequencies differed significantly and dropped to about 35 % and 48 %, respectively. Taken together, these data indicate that combining DIVA[2] with anti-PD-1-mediated ICB only slightly increases the effector function of DIVA[2]-induced antigen-specific T cells but is not sufficient to synergistically enhance the anti-tumor capacity to enable complete regression of MC38mOVA tumors.

# 5    Discussion

The treatment of cancer is one of the greatest challenges for modern medicine. In addition to conventional cancer therapy approaches such as radiotherapy or chemotherapy, cancer immunotherapy has been gaining importance for more than two decades now. In this regard, the use of cancer vaccines that induce the generation of high-quality tumor-specific T cells is a promising tool that is now being researched intensively (J. Liu et al. 2022). Therapeutic approaches are needed that specifically sensitize the host immune system to the tumor, able to specifically address the targets in the complex immune-inhibitory network of the TME, a major obstacle that weakens the efficiency of immunotherapeutic approaches (T. Tang et al. 2021).

In this respect, the method of TCI is of increased interest. As TCI does not require injections, it allows for easy self-medication, which avoids needle-born accidents and thus drastically minimizes the risk of infection, which is a major concern of the WHO due to medical and socio-economic consequences (Hasak et al. 2018; Miller and Pisani 1999; World Health Organization 2015). However, the main focus of TCI is targeting of skin-resident professional APCs able to perform high quality T cell priming in dLNs. By targeting these skin-resident APCs, TCI enables superior immune responses compared to intra-muscular vaccine injection despite the use of lower vaccine doses (C.-M. Huang 2007). Thereby, tumor-reactive cytotoxic CD8$^+$ T cells can be generated, able to migrate to the tumor tissue to eliminate malignant cells. Since the development of TCI using cholera toxin by Glenn et al. 1998, various approaches have been developed to administer adjuvants and antigens, distinguishing between active and passive approaches (Engelke et al. 2015).

The TCI method developed in 2005 by Rechtsteiner and colleagues involved the passive delivery of antigenic peptides together with the TLR7-agonist imiquimod (Rechtsteiner et al. 2005). The combination of this TCI approach with immune checkpoint blockade by anti-CTLA-4 (Rausch et al. 2017) or Co-stimulation by CD40 ligation (Bialojan et al. 2019) enhanced the immune response and enabled prolonged protective immunity. However, the rejection of solid tumors could not be achieved by these methods. The TME, with its complex structure and multitude of immunosuppressive cells and soluble factors, is one of the main obstacles for cancer immunotherapy. Therefore, the central aim of this work was to characterize the TME upon TCI and to determine the extent to which immunosuppressive mechanisms within the TME inhibit the successful use of therapeutic TCI to control the growth of solid tumors. This should provide a more detailed understanding of how TCI must be adapted to circumvent these immunosuppressive mechanisms.

## 5.1   DIVA[2] enables protective tumor immune control

In a previous work, Sohl and colleagues developed a TCI method, called DIVA (Sohl et al. 2022). In this approach we used the adjuvants dithranol and imiquimod (IMQ) together with ovalbumin-derived peptides, to induce an antigen-specific cellular immune response. Compared to the previously developed IMQ-TCI, this enabled not only a stronger primary response but also, for the first time, the generation of a sustained memory T cell response. DIVA represents a general immunization platform that generates antigen-specific T cells making DIVA suitable for cancer immunotherapy.

### 5.1.1   Therapeutic DIVA has no impact on the growth of MC38mOVA tumors

We used the colorectal cancer model MC38 transfected with an eGFP-tagged membrane-bound version of the ovalbumin protein (MC38mOVA) (Stickdorn et al. 2022) to test DIVA in a tumor setting. MC38mOVA cells present ovalbumin-derived peptides through MHC class I molecules on their cell surface, reflecting a suitable antigen-specific target for DIVA-induced cytotoxic T cells. MC38mOVA tumor cells induced proliferation of OT-I T cells that express a transgenic T cell receptor specific for the $OVA_{257-264}$ peptide (Figure 4.1). Since we did not observe proliferation when OT-I splenocytes were co-cultured with MC38 control cells alone, this proves that antigen-specific activation of OT-I T cells by the $Ova_{257-264}$ peptide presented on MHC class I molecules on the surface of MC38mOVA tumor cells occurred.

We tested DIVA in a therapeutic tumor model. Therefore, we subcutaneously injected C57BL6/J mice with $5x10^4$ MC38mOVA tumor cells (Figure 4.2). However, we observed that DIVA had no effect on the growth of the MC38mOVA tumors. It is known from our previous work that DIVA produces frequencies of antigen-specific $CD8^+$ T cells of about 3 % after about one week and this rate increases up to 10 % by day 14 (Sohl et al. 2022). We performed DIVA in the tumor setting on day 5 and 6 after tumor cell inoculation. This means that 7 days later, when DIVA had induced about 3 % antigen-specific $CD8^+$ T cells, it was already day 12 or 13 after tumor cell inoculation and the averaged tumor volume was already about 80 mm³. In addition, we observed faster tumor growth from day 10 onwards, indicated by a steeper increase in the tumor growth curve between day 10 and day 13. However, the peak frequency of antigen-specific $CD8^+$ T cells is only reached on day 14 after immunization, or day 19 after tumor cell inoculation. Until then, we observed steady tumor growth, which exponentially increases from day 18 after inoculation onwards. This implies that the averaged tumor volume was already very advanced when the DIVA-induced immune response was fully developed. Therefore, the DIVA immunization protocol had to be adapted to induce a stronger antigen-specific T cell response that arises at an earlier stage to enable tumor control.

5.1.2　Multiple DIVA strongly increases T cell immune response protecting mice against MC38mOVA tumor cells

One possibility to induce stronger T cell immune responses is the multiple application of a vaccine. Boost immunizations build on the advantage of a natural immune response or basic immunization by eliciting stronger, prolonged or more specific immune responses (Schunk and Macallum 2005). However, since the application of dithranol to healthy human or murine skin leads to the formation of erythema and edema within 24 hours (Kemény et al. 1990), it is essential to reduce the dithranol concentration accordingly in the case of multiple applications in order to prevent excessive inflammation of the immunized skin tissue. It is known from previous work by Sohl and colleagues that multiple applications of DIVA led to a significantly increased T cell immune response (PhD thesis of Dr. Julian Sohl 2021). In this setting, DIVA was applied three times with a lower dithranol concentration of 75 ng/mg and 7 days between each immunization. This increased the frequency of antigen-specific CD8$^+$ T cells up to 35 % after 21 days. Based on these findings, we tested further application patterns (Figure 4.3). We performed double application of DIVA in a dithranol concentration of 300 ng/mg and triple immunization with 150 and 75 ng/mg, respectively. We observed that after using a dithranol concentration of 300 ng/mg, the antigen-specific CD8$^+$ T cell frequency was highest at about 60 %. Furthermore, the induced antigen-specific CD8$^+$ T cells showed the strongest functional phenotype, indicated by the most intense IFN-$\gamma$ production after restimulation in the ELISpot assay. As expected, we also observed due to multiple DIVA increased side effects in form of erythema and edema formation that were most intense after double application with 300 ng/mg. However, these recovered by the end of the experiment, as the ear thickness nearly returned to that of the other treated groups. In the further development of DIVA, it is conceivable that a lower concentration of dithranol in the boost immunization would still induce a sufficiently strong proinflammatory environment in the skin, but would reduce the side effects and prevent excessive skin irritation.

In our previous work, we showed that DIVA induces a massive recruitment of monocytes into the immunized skin tissue. Similarly, we observed the formation of hyperkeratosis in dithranol-treated skin tissue (Sohl et al. 2022). It is known from previous work that *in vitro* stimulation of keratinocytes with dithranol induces the secretion of pro-inflammatory cytokines (Lange et al. 1998). *In vitro* stimulation of keratinocytes did show that among their secreted pro-inflammatory cytokines are members of the IL-1 family IL-1a, IL-1b, IL-18, IL-33 and furthermore TNF-$\alpha$, IL-6, IL-8, IL-24, COX and ROS (Gröne 2002; Sun et al. 2017). This interaction is able to create an inflammatory milieu in the immunized skin tissue that supports the differentiation of moDCs. 24 hours after dithranol application, the application of IMQ leads to the activation of inflammatory DC populations in a TLR7-dependent manner (Stein et al. 2011). These take up the administered ovalbumin-derived peptides and migrate to the draining lymph nodes

where they induce strong T cell priming resulting in a strong antigen-specific T cell immune response (Sohl et al. 2022). For the process of multiple DIVA, it can be assumed that the first immunization induces the formation of the pro-inflammatory milieu, the recruitment of monocytes into the immunized skin tissue and a first wave of T cell priming in the draining lymph nodes. The second immunization with dithranol increasingly recruits monocytes and further strengthens the already prevailing pro-inflammatory milieu by reactivating keratinocytes, favoring pro-inflammatory cytokine production. In turn, leading to more differentiating moDCs, which potentiates the amount of inflammatory DCs that can be activated via TLR-7 by the second IMQ application. This results in a large increase of activated APCs able to take up the administered antigen and migrate to the draining lymph node. T cell priming is thus massively increased, which consequently induces an expansion of the antigen-specific T cell population. In this context, we observed a dose-dependent effect of dithranol in the generation of antigen-specific CD8$^+$ T cells. It can be assumed that the higher the dithranol concentration, the stronger the induced pro-inflammatory milieu in the immunized skin tissue and consequently the induced antigen-specific T cell immune response based on the pathway postulated above. The T cell immune response induced by DIVA$^2$ reached its maximum already on day 14, which made it the most promising application pattern of DIVA for a retest in a tumor setting.

We evaluated the anti-tumor capacity of DIVA$^2$ in a prophylactic tumor setting (Figure 4.4). We figured out that DIVA$^2$ induced full protection against MC38mOVA tumor cells injected subcutaneously into mice 7 days after the second immunization. In contrast, single application of DIVA did not provide full protection, as tumors grew in 2 of 12 mice. The fact that DIVA is not sufficient to establish full protection against MC38mOVA cells in a prophylactic tumor setting indicates that its induced immune response is consequently too weak to control an already established tumor in a therapeutic setting and that at least DIVA$^2$ should be applied to expect an anti-tumor effect in a therapeutic tumor setting.

In summary, we conclude that the **MC38mOVA tumor model is suitable as a target for DIVA-induced antigen-specific T cells**. DIVA had no effect on the growth of MC38mOVA tumors in a therapeutic setting. Therefore, we **adapted the DIVA protocol to a boost strategy, called DIVA$^2$**, resulting in massively increased CTL frequencies associated with a highly functional phenotype of T cells. This adaptation allowed **full protection in a prophylactic tumor setting**. Based on these observations, we decided to use DIVA$^2$ in a therapeutic tumor setting.

## 5.2 Therapeutic DIVA$^2$-induced tumor control turns into adaptive immune evasion

Within the last decade, therapeutic vaccination is one of the key developments in cancer immunotherapy. Therapeutic vaccines aim to induce tumor regression, establishing long-lasting antitumor memory immunity and preventing non-specific or adverse reactions (Saxena et al. 2021). Among approved immunotherapeutic agents, therapeutic cancer vaccines have the advantage of eliciting specific immune responses to tumor antigens (J. Wang, Mamuti, and Wang 2020). Therefore, the aim was to develop and characterize DIVA$^2$ in a therapeutic setting. The therapeutic use of DIVA$^2$ initially resulted in tumor growth control, which we observed from day 10 after inoculation. This initial tumor growth could be suppressed by DIVA$^2$ from day 13, leading to a reduction of tumor volumes (Figure 4.5). At this point, strong tumor growth had already taken place in the untreated mice. However, we did not observe a complete elimination of the tumors after DIVA$^2$, as their volumes increased again from day 18 and grew steadily. The underlying mechanisms are discussed in the following chapters.

### 5.2.1 DIVA$^2$ induces antigen-specific T cell infiltration of the Tumor microenvironment

Various cell types within the TME, including tumor cells, immune cells, endothelial cells and stroma cells can secrete chemokines that recruit different immune cell types to the peripheral tumor site. These secreted chemokines spread systemically throughout the blood vessels, creating a concentration gradient within the organism which immune cells migrate along to the peripheral tumor site and infiltrate the tumor. The main described interactions that significantly contribute to the recruitment of T cells to the tumor microenvironment include CXCR3 with its ligands CXCL9/CXCL10, CCR5 and its ligands CCL3/CCL4/ CCL5, and CCR2 and its ligand CCL2 (Fridman et al. 2012; Harlin et al. 2009). Furthermore, it is known from previous work that CXCL9 and CXCL10 are interferon-responsive genes that can be activated in DCs upon type I interferon activation, enhancing the T cell recruitment into the TME (Woo et al. 2014). Similarly, professional APCs such as DCs capture and cross-present antigens released by tumor cells, thereby activating naïve T cells (Balan, Radford, and Bhardwaj 2020; Mollica Poeta et al. 2019) that can contribute to already DIVA$^2$-induced T cells that migrate to the tumor in an activated state. These mechanisms could explain how the DIVA$^2$-induced Tumor-reactive T cells are recruited to the TME establishing initial tumor control by day 13, which in the context of cancer immunoediting is called immune control phase or elimination phase (Schreiber, Old, and Smyth 2011). Boost immunization on day 13 and 14 significantly enhances the already induced immune response through the processes discussed in chapter 5.1.2 and leads to a massive T cell expansion. This results in the regression of the tumors, indicated by decreasing tumor volumes in the immune control phase until day 16. This anti-tumor effect induced by DIVA$^2$ is illustrated by the significantly different tumor volumes on day 16 (Figure 4.5c).

### 5.2.2 DIVA[2]-induced T cell immune response enables transient tumor immune control

To better understand how this initial DIVA[2]-induced immune control occurs we further analyzed the CD8^{+} T cells regarding their antigen-specificity and characterized their functional phenotype by IFN-γ ELISpot assay (Figure 4.6). DIVA[2] led to a significantly increased number of CD8^{+} T cells and especially to a high number of antigen-specific CD8^{+} T cells in the TME during immune control. These antigen-specific CD8^{+} T cells exhibited a high PD-1 expression along with a very low expression of CTLA-4 and Lag3 and a strong IFN-γ production after $Ova_{257-264}$ restimulation in the IFN-γ ELISpot assay indicating a strongly activated phenotype (Gros et al. 2014; Inozume et al. 2010; Pauken and Wherry 2015). CD8^{+} cytotoxic T cells take a lead role in the elimination of tumor cells. If an activated antigen-specific CD8^{+} T cell, in this case induced by DIVA[2], encounters a tumor cell in the TME that presents antigen on its cell surface via MHC class I molecules, this tumor cell gets eliminated by the T cell. The effector molecule IFN-γ, which the DIVA[2] induced antigen-specific CD8^{+} T cells produced in large quantities, plays a key role in the antitumor effect of cytotoxic lymphocytes (Shen et al. 2018). IFN-γ inhibits the proliferation of tumor cells by enhancing their expression of the cell cycle inhibitors p27Kip, p16 or p21 which has been described for breast cancer (Kochupurakkal et al. 2015), colorectal cancer (L. Wang et al. 2015) and hepatocellular cancer (W. Li et al. 2012). IFN-γ thus reduces tumor cell growth by inducing cell cycle arrest, apoptosis and necroptosis (Ni and Lu 2018). Inhibition of tumor angiogenesis is another function of IFN-γ that inhibits tumor progression by reducing the nutrient supply of tumor cells (Coughlin et al. 1998; Qin et al. 2003; Rüegg et al. 1998). Furthermore, in a murine neuroblastoma model, IFN-γ has been described to indirectly support tumor regression by inducing the polarization of macrophages into inflammatory M1 macrophages (Relation et al. 2018). Other effector molecules secreted by cytotoxic T cells as well as NK cells are perforins and granzymes. In the course of granule exocytosis-mediated cell death, granzyme and perforin-containing granules fuse with the cell membrane of the T cell or NK cell, thereby releasing granzyme and perforins into the synaptic cleft. Perforin forms large in the membrane of the tumor cell, enabling the diffusion of granzymes into the cytosol of the tumor cell. This leads to caspase-dependent and -independent cell death of the tumor cells (Chowdhury and Lieberman 2008; Voskoboinik et al 2015). These are possible immunological mechanisms for the initial DIVA[2]-induced tumor immune control that led to the reduction in tumor volume.

### 5.2.3 Initial DIVA[2]-induced tumor immune control is limited and turns into immune evasion

During the therapeutic tumor experiment, we observed that complete elimination of the tumors did not occur. Between day 16 and 18 after inoculation, the average tumor volume of the DIVA[2]-treated mice stagnated, which is referred to as **immune equilibrium** and then started to increase (Figure 4.5d) which is referred to as **immune evasion** or immune escape (Schreiber, Old, and Smyth 2011). In this

respect, a distinction is made between innate immune evasion, in which the recruitment of T cells into the TME is prevented, and adaptive immune evasion, in which T cell recruitment into the TME takes place but further immunosuppressive mechanisms induce immune evasion (Spranger and Gajewski 2018). Since we detected CD8^{+} T cells in both untreated mice and DIVA[2] treated mice, the immune evasion in the TME of MC38mOVA tumors from both untreated and DIVA[2] treated mice can be classified as adaptive immune evasion (Figure 4.6). Numerous mechanisms have been described that promote the transition of the immune control via the state of immune equilibrium to immune evasion. Tumors that exhibit a rich immune cell infiltrate are described as immunologically 'hot' or inflamed tumors and are associated with a better prognosis and response to anticancer immunotherapy. In contrast, non-inflamed tumors are also described as 'cold' tumors (O'Donnell, Teng, and Smyth 2019). The MC38mOVA tumors can be classified as hot or inflamed tumors both in the untreated group and after DIVA[2] treatment, as they have a rich immune cell infiltrate, including CD8^{+} T cells. For this type of inflammation signature, it is known from previous work that the immune response is ongoing but can often be functionally suppressed favoring immune evasion (Y.-P. Chen et al. 2017). This condition is further described as adaptive immune resistance and can be associated with the presence of immunosuppressive molecules in the TME, such as PD-L1 (Teng et al. 2015).

Based on the activated and functional phenotype of DIVA[2]-induced CD8^{+} T cells, we first postulated that the T cell immune response is sufficiently strong, but that immunosuppression of these cells occurs, preventing ongoing elimination of tumor cells thereby promoting immune evasion. We first considered myeloid cells within the TME as a possible cause and therefore analyzed them by high-dimensional flow cytometry (Figure 4.7). The FlowSOM map showed that the myeloid compartment of the TME mainly consists of monocyte and macrophage populations. More detailed clustering analysis in tSNE plots split by condition revealed that the myeloid compartment of the TME after DIVA[2] during immune control differed greatly from that of the untreated mice. The differences in clustering were mainly related to differentially clustered monocyte and macrophage populations after DIVA[2] treatment. However, this discrepancy between the conditions was gone in immune evasion, suggesting that the phenotypic development of myeloid cells after DIVA[2] treatment from immune control until immune evasion may be a factor that initiates the immune evasion. Analysis of characteristic surface markers by flow cytometry allows the assignment of monocytes and macrophages to a pro- or anti-inflammatory phenotype, supporting or inhibiting tumor progression. A more detailed flow cytometry-based functional analysis of these monocyte and macrophage populations with the pro-inflammatory marker TNF-$\alpha$ and inducible nitric oxide synthase (iNOS) (Hibbs et al. 1988; Hibbs et al. 1987) and with the anti-inflammatory marker arginase-1 (Arg1) (Pesce et al. 2009) could not provide further insights into the phenotype (data not shown). Therefore, based on the high-dimensional flow cytometry TME

analysis, no conclusion can be drawn about the functional phenotype of the monocyte and macrophage populations and the question if these cells could be initiators for immune evasion. These data suggest that after DIVA[2], the myeloid compartment in the TME differs greatly across conditions during immune control but this must be analyzed with an alternative method for more detailed characteristics due to limitation of flow cytometry. Single-cell RNA-sequencing (scRNA-seq) would be best suited for such a characterization.

The strongly activated phenotype of antigen-specific CD8^{+} T cells was also characterized by a strong IFN-$\gamma$ production after restimulation with Ova$_{257-264}$ in the ELISpot assay. Up to immune evasion, we observed that this phenotype even increased (Figure 4.6b). In addition to the central anti-tumor role of IFN-$\gamma$, it has been described several times that IFN-$\gamma$ can also act as a pro-tumor cytokine (Aqbi et al. 2018; Castro et al. 2018; Kursunel and Esendagli 2016; C.-F. Lin et al. 2017; Mojic, Takeda, and Hayakawa 2017; Zaidi 2019; Zaidi and Merlino 2011). IFN-$\gamma$ signaling pathways have been shown to regulate immune evasion by activating immune checkpoint genes. One of the most important IFN-$\gamma$-regulated immune checkpoint mechanisms is the expression of PD-L1 and PD-L2 on the cell surface of tumor cells and tumor infiltrating stromal cells (Zaidi 2019). IFN-$\gamma$-induced PD-L1 and PD-L2 bind to PD-1 on the cell surface of T cells or NK cells, leading to their immunosuppression (Abiko et al. 2015; Bellucci et al. 2015; Garcia-Diaz et al. 2017; Jiang et al. 2019). This could indicate that the large amount of IFN-$\gamma$ produced by the DIVA[2]-induced antigen-specific CD8^{+} T cells upon contact with their antigen can lead to PD-L1/PD-L2 expression of the tumor cells in the TME. Since we observed a strong PD-1 expression of the DIVA[2]-induced antigen-specific CD8^{+} T cells, this could represent a target for IFN-$\gamma$ induced PD-L1/PD-L2, indirectly causing immunosuppression of the DIVA[2]-induced T cells. However, what must be critically questioned with regard to the IFN-$\gamma$ production of the T cells is the fact that IFN-$\gamma$ production was measured in an artificial *ex vivo* assay after 20 h restimulation with the peptide Ova$_{257-264}$. In this regard, it is conceivable that the T cells within the TME are suppressed and may be less lytic than their *ex vivo* analyzed phenotype would suggest. It is possible that this suppression is reversible and enables strong antigen-specific IFN-$\gamma$ production in an *ex vivo* ELISpot assay, falsely suggesting a strong functional phenotype. To consider this differentially, the phenotype of DIVA[2]-induced T cells would need to be analyzed without *ex vivo* stimulation. Again, scRNA-seq would be ideally suited for such a characterization.

A tumor cell intrinsic molecular aberration that can lead to poor T cell-mediated tumor control is due to loss of sensitivity of the tumor cells towards IFN-$\gamma$ or TNF-$\alpha$. Thereby, T cells are functional and secrete the effector molecules IFN-$\gamma$ or TNF-$\alpha$, however, these cannot induce apoptosis in the tumor cells due to prohibited signaling inside the tumor cell (Benci et al. 2016; Zaretsky et al. 2016). However,

tumor cells also contribute to the alteration of the TME through the production of other immune modulatory molecules. For example, they reduce the pH and glucose concentration in the TME and produce large amounts of pro-angiogenic VEGFA, death ligands such as FasL and TRAIL, anti-inflammatory cytokines or tumor cell metabolites such as Indoleamine 2,3-dioxygenase (IDO), reactive oxygen species (ROS) and reactive nitrogen species (RNS) (Labani-Motlagh et al. 2020). These molecules form an immunosuppressive environment, which can have considerable effects on the differentiation of tumor-infiltrating immune cells thereby favoring tumor progression. However, these possible causes for the initiation of immune evasion could not be clarified in the present study.

### 5.2.4 Tumor immune evasion is not caused by antigen loss of MC38mOVA tumor cells

Another possible reason for the initiation of immune evasion is the development of tumor cell intrinsic immune evasion mechanisms. Pre-clinical models have shown that strong immune selective pressure can lead to an outgrowth of antigen-loss variants of tumor cells (DuPage et al. 2012; Matsushita et al. 2012). This can be due to the loss or mutation of $\beta$2-microglobulin that drastically reduces the MHC class I molecule expression of tumor cells (Roh et al. 2017; Zaretsky et al. 2016). Reeves and James describe that this process can also be driven by the downregulation of other proteins involved in antigen processing, such as Transporter associated with antigen processing (TAP) and Endoplasmic reticulum aminopeptidase (ERAP) (Reeves and James 2017). These mechanisms avoid recognition of tumor cells by antigen-specific CD8^{+} T cells due to lack of presented antigen leading to tumor progression and consequently to immune evasion. We verified whether the MC38mOVA tumor cells show a reduction or loss of antigen presentation after initial DIVA[2]-induced tumor immune control that could cause immune evasion. Therefore, we performed an *in vitro* proliferation assay of *ex vivo* MC38mOVA tumor cells together with OT-I splenocytes (Figure 4.8). The T cells from OT-I mice exhibit a transgenic T cell receptor that is able to specifically bind $Ova_{257-264}$ peptides presented on MHC class I molecules (Clarke et al. 2000; Hogquist et al. 1994). This binding induces proliferation of the OT-I T cells, which can be measured by flow cytometry and proves the existence of the antigen on the surface of the APC, in this case the tumor cell. In the *in vitro* proliferation assay, we observed that the *ex vivo* MC38mOVA tumor cells contributed to the proliferation of OT-I T cells. This was independent of the treatment of the mice and whether the tumor cells were isolated during immune control or immune evasion. Thus, we were able to exclude the reduction or loss of antigen presentation of tumor cells as a possible cause for initiating immune evasion.

In conclusion, we found that **DIVA[2] enables initial tumor immune control** in a therapeutic setting. This was maintained for over two weeks, most likely due to the DIVA[2]-induced adaptive immune response. However, this phase then progressed through a brief immune equilibrium to the state of **adaptive**

**immune evasion**. This could be due, among other things, to **immunosuppressive myeloid** cells or IFN-γ-induced PD-L1/PD-L2 expression by tumor cells, which in turn leads to suppression of DIVA[2]-induced T cells. An *in vitro* proliferation assay with *ex vivo* MC38mOVA tumor cells did show that DIVA[2] did not induce antigen loss on the surface of MC38mOVA tumor cells, indicating that **we can exclude antigen loss as initiator for immune evasion**. Due to limitations of flow cytometry-based TME analysis, we decided to analyze the tumor-infiltrating leukocytes by scRNA-seq. This method offers the possibility to characterize the immune status of individual cells in the TME much more precisely.

## 5.3 Single-cell RNA-sequencing reveals tumor-infiltrating monocytes to be immunosuppressive

When we used DIVA[2] in a therapeutic tumor experiment, we figured out that after DIVA[2]-induced tumor immune control, there was a switch to immune evasion. Due to the limitations of flow cytometry-based analysis of the TILs in the TME, we were unable to identify any specific causes for the initiation of immune evasion. Therefore, we decided to investigate the TILs by scRNA-seq. This method offers the possibility to sequence, bioinformatically process and analyze the transcriptome at single cell level and thus obtain information about the immune status of each individual cell of the processed single cell suspension. We used this to investigate the immunological phenotype of the TILs in more detail in order to find causes for immune evasion after initial DIVA[2]-induced immune control. We put the main focus on the cytotoxic lymphocytes and the monocytes that scRNA-seq revealed to be absent during DIVA[2]-induced immune control.

### 5.3.1 DIVA[2]-induced immune control is associated with an altered TME composition

To analyze the TILs of MC38mOVA tumors by scRNA-seq, we performed DIVA[2] in a therapeutic tumor setting (Figure 4.9) which showed the characteristic tumor growth curve firstly shown in the flow cytometry-based TME analysis (Figure 4.5). We selected the time point for scRNA-seq analysis for immune control samples based on the fact that a DIVA[2]-induced decrease in tumor volume had occurred (day 16). We chose the time point for the analysis of the immune evasion samples as late as possible in the course of the tumor experiment (day 20). Although the average tumor volumes of the two groups were different at this time due to DIVA[2], this was based on the fact that a renewed increase in tumor volumes had taken place after initial DIVA[2]-induced immune control.

ScRNA-seq is a powerful tool for dissecting the very heterogeneous TME at the cellular and molecular level (Lei et al. 2021). After bioinformatic processing of the scRNA-seq data, we assigned the single cells to immune cell types based on the database *immunological Genome Project* (ImmGen, annotation *immgen main*) (Aguilar et al. 2020). In this regard, dimensionality reduction is an important step in the

visualization of scRNA-seq data, which are highly dimensional due to the high number of analyzed genes. The visualization of these data by t-SNE plots offers a very well-suited possibility to represent the heterogeneity of the data in a two-dimensional compact way (Linderman et al. 2019). Therefore, we visualized the transcriptome data of the TILs from MC38mOVA tumors in t-SNE plots (Figure 4.9) and plotted the quantitative differences between the cell types for better comparability (Figure 4.10). The t-SNE plots (Figure 4.9) showed a discrepancy between the clustering of the DIVA[2]-treated and untreated group at the time of immune control. However, at the time of immune evasion, the populations clustered very similarly. Thus, we conclude that scRNA-seq generally confirmed the results of the flow cytometry-based TME analysis, supporting the robustness of the results. This was evident in the scRNA-seq data at the time of immune control by an altered myeloid compartment and by a DIVA[2]-induced increase in cytotoxic lymphocytes (including T cells NKT cells, NK cells and ILCs). However, a closer look at the myeloid cells revealed a difference from flow cytometry-based analysis. Surprisingly, in the scRNA-seq analysis, we detected hardly any monocytes in the DIVA[2]-treated group, with macrophages being more represented. In contrast, in the flow cytometry-based analysis, monocytes clustered in four different populations. The scRNA-seq analysis is based on a much higher number of markers when compared to flow cytometry and is performed in an automated approach. Thus, a much larger number of marker genes is used for cell type annotation. Therefore, it can be expected to lead to a more accurate and un-biased result than the flow cytometry-based analysis, in which we probably partially detected macrophages as monocytes due to an insufficient number of molecular markers. Another reason for this difficult cell type classification of myeloid cells by flow cytometry may be the large number of differentiation stages in myelopoiesis, especially within the TME (Ugel et al. 2021). This is better explained by a higher number of molecular markers, as scRNA-seq analysis uses. In this respect, flow cytometry reaches its limits when the complete myeloid diversity has to be covered in one panel. For these reasons, the result of the scRNA-seq analysis can be preferred to the flow cytometry-based analysis.

The recruitment of peripheral blood monocytes to the peripheral tumor site occurs through the migration of monocytes along chemokine gradients. Chemokines produced by tumor cells in the TME include chemokine (C-C motif 2) ligand 2 (CCL2), also known as monocyte chemoattractant protein-1 (MCP-1) (Kubli et al. 2021). The secretion of CCL2 and CCL5 creates concentration gradients within the organism. Monocytes expressing the CCL2/CCL5 receptor CC chemokine receptor 2 (CCR2) are recruited along these gradients to the peripheral tumor site (Hao et al. 2020; Hardy et al. 2004). In the TME of the untreated mice, uncontrolled growth of the tumor cells occurred from the beginning (Figure 4.9). It can be assumed that the tumor cells produce a large number of chemokines that recruit peripheral blood monocytes, for example through the CCL2/CCL5-CCR2 axis. After DIVA[2], we detected

the monocytes only in immune evasion when tumor growth was already advanced. During DIVA[2]-induced immune control, tumor cells are eliminated by the processes discussed in the previous chapters, controlling and reducing the tumor growth. It is conceivable that, in contrast to the untreated group, this leads to a lower number of secreted chemokines, whereby in this phase no or much fewer monocytes are recruited to the peripheral tumor site. This would represent a possible mechanism for the earlier monocyte migration into the TME in the untreated group compared to the DIVA[2]-treated group. However, it remains unclear at this time whether infiltration of these monocytes into the TME is a possible cause for initiating immune evasion after initial DIVA[2]-induced immune control. When CCR2^{+} monocytes infiltrate the TME, for example through CCL2/CCL5-mediated migration, they mature and can develop pro-tumor functions (Franklin et al. 2014; Y. Liu and Cao 2015). In this process, they can mature into tumor-associated macrophages (TAM), which can decisively support tumor growth (Noy and Pollard 2014). This is supported by previous work in pre-clinical models showing that inhibiting monocyte attraction by targeting the CCR2-CCL2 axis through genetic or therapeutic blockade reduces tumor growth (Mantovani et al. 2017). Therefore, monocytes infiltrating the TME may be a key contributor to tumor progression. To clarify whether the monocytes we detected in the TME of DIVA[2]-treated mice at the time of immune evasion exhibit such a tumor-promoting phenotype, an expression analysis of monocytes with an anti-inflammatory gene signature had to be performed.

Quantitative analysis of cell types, in addition to the t-SNE plots, showed that the main differences we detected during DIVA[2]-induced immune control were related to cytotoxic lymphocytes in addition to monocytes (Figure 4.10a). We split these cytotoxic lymphocytes into subtypes (Figure 4.10b). This showed that the CD8^{+} T cells were duplicated by DIVA[2] and, surprisingly, this was also observed in the ILCs, which extended the findings of the flow cytometry-based TME analysis. In addition to the possible mechanisms for T cell recruitment discussed in 5.2.1, the DIVA[2]-induced milieu also appears to recruit ILCs into the TME during immune control. ILCs can be divided into three subsets, including NK/ILC1s, ILC2s and ILC3/LTi (lymphoid tissue inducer) (Artis and Spits 2015). Since the ILCs clustered very closely together with the NK cells in the t-SNE plot, it can be assumed that their transcriptional pattern is indicative of the ILC1 phenotype. ILC1s are activated by several cytokines, including tumor cell-derived IL-15 or immune cell-derived IL-12 and IL-18, and subsequently produce IFN-$\gamma$ to contribute to early anti-tumor immunity (A. Fuchs et al. 2013). In colorectal cancer, CD86 stimulation on DCs and T cells by ILC1s has been described to further enhance tumor-specific immunity (Dadi et al. 2016). In contrast to CD8^{+} T cells and ILCs, the CD4^{+} T cells, NK cells and NKT cells were less conspicuous as they did not show large quantitative differences in immune control phase across conditions. These data suggest that **DIVA[2]-induced antitumor immunity is realized by ILCs in addition to CD8^{+} T cells**. However, in order to further characterize the functional phenotype of the CD8^{+} T cells and ILCs and thus making a

precise statement on the extent to which the two cell types contribute to cytotoxicity in the TME, a more detailed expression analysis of a cytotoxic gene signature is required. However, at the time of immune evasion, the number of ILCs in the DIVA$^2$-treated group decreased by half. The reduction in these potentially cytotoxic cells would represent a decrease in overall anti-tumor immunity and therefore represents a factor favoring tumor growth after initial immune control. The cause for this decrease cannot be assessed based on the data available. However, it is conceivable that an altered cytokine and chemokine milieu in the TME from the onset of immune evasion is associated with the decrease in ILCs.

Treg cells have the task of regulating the function of effector immune cells to prevent an exuberant immune response that could lead to host tissue damage. Treg cells have been described to suppress anti-tumor immune responses and thereby contribute to the development of an immunosuppressive TME that supports immune evasion and cancer progression (Elkord et al. 2010; Nishikawa and Sakaguchi 2014). However, it is unlikely that the immunosuppressive effect of Treg cells is an initiator of immune evasion after initial DIVA$^2$-induced immune control. This is because the Treg cell frequency in the DIVA$^2$-treated group did not increase from immune control to immune evasion and the Treg cells were present in a very low cell count in the TME of the DIVA$^2$-treated group (Figure 4.10b).

In summary, we conclude that the composition of the TME after DIVA$^2$ treatment was confirmed by scRNA-seq analysis and furthermore characterized in more detail. It was confirmed that the CD8$^+$ T cells were significantly increased due to DIVA$^2$, but this was also the case for the ILCs, which are probably ILC1s, as they clustered very close to the NK cells. It was shown that the monocytes were nearly absent in the TME during DIVA$^2$-induced immune control, but these appeared until immune evasion. It remains to be assessed to what extent the CD8$^+$ T cells and the ILCs enable initial tumor control and whether the monocytes detected in the TME during immune evasion are possible initiators for immune evasion. To address this question in more detail, we performed expression analyses with marker gene signatures of the potentially cytotoxic cells and the monocytes.

### 5.3.2 scRNA-seq reveals DIVA$^2$-induced immune control to be mainly mediated by cytotoxic CD8$^+$ T cells and ILC1s

To accurately characterize the phenotype of the potentially cytotoxic cells, we performed an expression analysis of a cytotoxic gene signature (Figure 4.11a). The analysis of a cell population with a gene signature offers the advantage that a whole repertoire of characteristic genes is analyzed and thus a more comprehensive picture of the population with regard to a certain function is obtained. In the cytotoxic gene signature, we included Granzyme A (Gzma) (Z. Zhou et al. 2020), Granzyme B (Gzmb)

(J. A. Lopez et al. 2013), PD-1 (Pdcd1) (Gros et al. 2014; Inozume et al. 2010), Perforin-1 (Prf1) (Voskoboinik, Whisstock, and Trapani 2015), IFN-$\gamma$ (Ifng) (Shen et al. 2018) and Natural Killer cell protein 7 (NKG7) (X.-Y. Li et al. 2022; Malarkannan 2020). The t-SNE plots showed that the cytotoxic signature was mainly expressed by the T cells, NKT cells, NK cells and ILCs, regardless of the condition. A more detailed impression of the cell types from which the cytotoxicity originated was provided by splitting the cytotoxic subtypes (Figure 4.11b).

With regard to CD8^{+} T cells, scRNA-seq confirmed the results of the flow cytometry-based analysis. The averaged signature score increased after DIVA[2] until immune evasion, which is probably due to the delayed effect of boost immunization from day 13/14 and the associated activation and expansion of T cells. Since CD8^{+} T cells also made up the most frequent subtype of cytotoxic lymphocytes in the DIVA[2]-treated tumors, it is very likely that the DIVA[2]-induced CD8^{+} T cells expressing cytotoxic marker genes contribute decisively to immune control. However, T cells expressing cytotoxic marker genes may still be in a state of T cell exhaustion. Initiators of T cell exhaustion can be suppression by other immune cells and tumor cells or continuous exposure to their antigen (Wherry and Kurachi 2015). We therefore checked in a gene expression analysis with T cell exhaustion marker genes whether the DIVA[2]-induced CD8^{+} T cells are exhausted. This showed that PD-1 expression increased after DIVA[2] from immune control to immune evasion. This in itself is a sign of antigen contact and T cell activation. However, this was accompanied by the expression of CTLA-4, Lag3, Tim-3 and Tigit in about half of the CD8^{+} T cells. The T cell exhaustion markers indicate that these CD8^{+} T cells are inhibited in their effector function and therefore cannot contribute to anti-tumor immunity, which promotes tumor growth. This means that the CD8^{+} T cells can contribute decisively to immune control based on the expression of cytotoxic marker genes through tumor cell elimination, but this only applies to a part of the CD8^{+} T cells, since a part of them also expressed T cell exhaustion marker genes.

The ILCs were conspicuous in the quantitative analysis and also showed a cytotoxic phenotype for the most part, regardless of condition. The clustering of ILCs in the tSNE plots which was close to the NK cells already suggested an ILC1 phenotype (Figure 4.9). This is confirmed by the analysis of the cytotoxic gene signature (Figure 4.11b) (Jacquelot et al. 2022). Since they were most abundant after DIVA[2] at the time of immune control, this means that as part of the innate immune defense they made a decisive contribution to the initial tumor immune control in addition to the CD8^{+} T cells. However, based on the data, it is not possible to say why the number of ILCs had halved from immune control to immune evasion. As a result, significantly fewer ILCs were able to contribute to the continued elimination of tumor cells, which favors tumor growth and thus the switch to immune evasion.

In the case of NKT cells, we detected no significant differences across treatment during immune control. However, the rate of NKT cells halved regardless of treatment until immune evasion. Although the NKT cells did not show particularly high expression of the cytotoxic gene signature, they were able to contribute to immune control at baseline. The expression of the cytotoxic marker genes suggests an NKT type I phenotype (Bae et al. 2019), which are able to produce the cytokines IFN-$\gamma$, IL-2, -4, -6, -17, -22, TNF-$\alpha$, TGF-$\beta$ and GM-CSF, among others, which can activate a broad spectrum of immune cells and thus contribute directly and indirectly to immune control (Coquet et al. 2007, 2008). However, due to the decrease over time until immune evasion, they were less able to contribute to ongoing immune control because of the lower cell number, which favors tumor growth.

The CD4^{+} T cells showed the lowest average signature score of all cytotoxic lymphocyte subsets, which is why we assume that they contributed the least to cytotoxicity within the TME. It is known from previous work that the DIVA-mediated CD8^{+} T cell immune response is weakened when CD4^{+} T cells are systemically depleted during immunization, indicating that CD4^{+} T cell help is important for potent CD8^{+} T cell immunity (Sohl et al. 2022). Such an interplay of CD4^{+} T cells and CD8^{+} T cells is also likely in DIVA[2]-mediated T cell immunity in the TME of MC38mOVA tumors, whereby CD4^{+} T cells contribute directly to optimal CD8^{+} T cell immunity and thus indirectly to initial tumor control. The phenotype of the CD4^{+} T cells of the DIVA[2]-treated group showed no significant changes quantitatively and qualitatively between immune control and immune evasion. Therefore, it can be assumed that the CD4^{+} T cells do not represent an initiator for immune evasion after initial DIVA[2]-induced immune control.

NK cells were slightly increased during DIVA[2]-induced immune control, but accounted for only a small proportion of cytotoxic lymphocytes. However, since they had the highest average signature score of the cytotoxic gene signature, it is conceivable that they contributed to immune control. With regard to NK cell-mediated cell death, the rapid release of lytic granules is studied best. These contain granzymes and perforins and induce apoptosis in the tumor cell (Ewen et al. 2012). In addition, NK cells also eliminate tumor cells by engaging death receptors. CD95L on the NK cell can bind to CD95 on the tumor cell surface inducing apoptosis of the tumor cell (Prager et al. 2019). Since we did not observe any quantitative or qualitative decrease of NK cells from immune control to immune evasion, we conclude that they do not represent an initiator for immune evasion.

In conclusion, the cytotoxicity in the TME of MC38mOVA tumors induced by DIVA[2] mainly originates from CD8^{+} T cells and ILCs. These were most abundant in the DIVA[2]-treated group during immune control. However, we observed that the CD8^{+} T cells partly expressed T cell exhaustion marker genes,

lowering the number of cytotoxic cells that enable tumor immune control. The other cytotoxic lymphocyte subtypes most likely exert less cytotoxicity due to their lower cell numbers, excepting the NK cells. This is due to their strong expression of cytotoxic marker genes despite a low cell number, wherefore they still likely contribute to cytotoxicity. In the DIVA$^2$-treated group, we detected a quantitative decrease in cytotoxic subtypes from immune control to immune evasion. This was most evident in the ILCs and also slightly in the NKT cells. Overall, these changes represent a decrease in total cytotoxicity in the TME when comparing immune control to immune evasion, favoring the initiation of evasion. To find more precise causes for these effects, we also performed an expression analysis of monocytes, as their absence at the time of immune control and appearance at the time of immune evasion is a major clue for the initiation of immune evasion.

### 5.3.3 scRNA-seq reveals Monocytes appearing after DIVA$^2$-induced immune control to be immunosuppressive

A key finding of the scRNA-seq analysis was that monocytes were absent in DIVA$^2$-induced immune control, but detected in immune evasion. We performed expression analysis with a gene signature containing genes related to pro-tumorigenic functions to further describe the phenotype of these monocytes and thus find out to what extent they act tumor-promoting in the TME (Figure 4.13a). The merged t-SNE plot and the signature score plot showed that the expression of the immunosuppressive marker genes was mainly related to the myeloid cells, but among them the monocytes showed the strongest expression (Figure 4.13b). Since the absence of monocytes in the DIVA$^2$-treated group during immune control, the total number of cells expressing those immunosuppressive marker genes was therefore comparatively low, favoring the cytotoxic activity of DIVA$^2$-induced cytotoxic lymphocytes to contribute to immune control. Thus, at this stage, it can be assumed that immunosuppression in the TME was at a low level, which allowed elimination of tumor cells. At the time of immune evasion, immunosuppressive monocytes were much more prevalent in the DIVA$^2$-treated group. This means that immune evasion must be largely driven by these cells, contributing significantly to tumor growth. This characteristic represents the main difference in the composition of the TME of the DIVA$^2$-treated group comparing immune control and immune evasion.

The VEGFA expression of monocytes in the DIVA$^2$-treated group at the time of immune evasion suggests that it supports tumor angiogenesis. This increases the nutrient transport, thereby promoting tumor growth (Hanahan and Coussens 2012). In addition, monocytes also expressed PD-L1, which binds to PD-1 on the cell surface of T cells and suppresses their effector function (D. H. Kim et al. 2019; Yu et al. 2020). Since we detected by flow cytometry and scRNA-seq that DIVA$^2$-induced T cells expressed PD-1 to a high extent (Figure 4.6 and Figure 4.11) PD-L1-expressing monocytes, and to some

extent PD-L1-expressing macrophages, might suppress the T cell immune response via PD-L1/PD-1 signaling, causing T cell exhaustion which is promoting tumor growth. The genes Ifitm6, Chil3, Lyz2, Cybb, CD177, Aldh2, Arhgdib, Btg1, CCL9, Thbs1, Srgn, CD14 included in the immunosuppressive gene signature represent marker genes for myeloid derived suppressor cells (MDSC) (Veglia et al. 2021). The monocytes, that infiltrated the TME of the DIVA[2]-treated group, expressed these markers indicating a MDSC-like phenotype of the monocytes which contributes to tumor progression (Figure 4.13). Their strong Ly6C and CCR2 expression further suggests a monocyte derived-MDSC (M-MDSC) phenotype (Figure 4.14) (Veglia, Perego, and Gabrilovich 2018). We further observed that these monocytes and to some extent the macrophages expressed CCL2 (Figure 4.14). Since the infiltration of classical monocytes from the peripheral blood into the TME occurs predominantly via the CCL2-CCR2 axis (Qian et al. 2011) this means that CCL2 expressed by monocytes and macrophages further increased the recruitment of CCR2^{+} monocytes. CCR2^{+} monocytes are actually pro-inflammatory cells that are recruited to the site of inflammation via the CCR2-CCL2 axis. However, the infiltration or presence of such CCR2^{+} monocytes in the TME is often associated with pro-tumoral effects. This means that the actual pro-inflammatory cells can become immunosuppressive cells when they enter the TME. In this regard, it has been described that the infiltration of those monocytes is associated with the suppression of T cell function in various cancer models (Lesokhin et al. 2012; X. Li et al. 2017; Movahedi et al. 2010; Sanford et al. 2013). The major suppressive function of these CCR2^{+} monocytes is reported to be due to the production of the suppressive factors arginase-1 (Arg1) and inducible nitric oxide synthase (iNOS), as well as increased production of nitric oxides (NO) and reactive oxygen species (ROS) (D. I. Gabrilovich and Nagaraj 2009). This suppresses the function of cytotoxic CD8^{+} T cells, which in turn promotes tumor growth (Lesokhin et al. 2012). In line with this, the CCR2^{+} monocytes expressed Irf8 (Figure 4.13) which is described for monocyte-derived cells to be associated with the induction of T cell exhaustion, further promoting tumor growth (Nixon et al. 2022). Another main aspect is that tumor-infiltrating monocytes differentiate into tumor-associated macrophages (TAM) shortly after entering the TME, able to contribute essentially to tumor progression (Franklin et al. 2014; Qian et al. 2011). Furthermore, tumor-infiltrating monocytes induce the recruitment of tumor-promoting Treg cells, which also drive the suppression of pro-inflammatory mechanisms (Sanford et al. 2013; Schlecker et al. 2012). However, since we found that the frequency of Treg cells in the DIVA[2]-treated group was the same during immune control and immune evasion (Figure 4.10), the Treg cell-recruiting effect of monocytes cannot be classified as an initiator of immune evasion. The suppressive effect of CCR2^{+} monocytes is supported by the fact that inhibition of CCR2 prevented monocyte-derived cell accumulation in murine pancreatic, liver and melanoma tumors, which was associated with increased infiltration of CD8^{+} T cells and reduced tumor growth (X. Li et al. 2017; Mitchem et al. 2013). All these properties of monocytes infiltrating the TME of DIVA[2]-treated mice suggest an immunosuppressive

phenotype that crucially promotes tumor growth. Accordingly, we conclude that monocytes contributed substantially to immune evasion. This explains how tumor growth is significantly promoted, resulting in exponential growth, but does not explain why the tumor cells were not completely eliminated in the immune control phase, resulting in the switch to immune evasion.

A possible clue to explain this switch is linked to the expression of CD38 by macrophages (Figure 4.14). During immune control, almost exclusively macrophages in the DIVA[2]-treated group showed marked CD38 expression. This CD38 expression decreased significantly until immune evasion. In the untreated group, we detected almost no CD38 expressing cells, regardless of the timepoint. CD38 is an ectoenzyme and surface receptor that catalyzes nicotinamide adenine dinucleotide (NAD^{+}) to adenosine diphosphate ribose (ADPR) or cyclic ADPR (cADPR) and is expressed by several immune cell types, including macrophages, T cells, NK cells or DCs (Malavasi et al. 2008). Besides reducing NAD+, CD38 influences calcium signaling cascades and contributes to the production of the immunosuppressive adenosine (Konen, Fradette, and Gibbons 2019). In this respect, CD38 is considered to play an immunosuppressive role in the context of TME of solid tumors (L. Chen et al. 2018; Karakasheva et al. 2015; Levy et al. 2012). However, this does not mean for the macrophages in the DIVA[2]-treated group at the time of immune control that their pronounced CD38 expression implies an anti-inflammatory phenotype per se. Rather, Jablonski et al. showed that CD38 is an exclusive marker for macrophages of the pro-inflammatory M1 phenotype that can be induced by IFN-γ (Jablonski et al. 2015). It is conceivable that the strong DIVA[2]-induced IFN-γ immune response in the TME triggers this pro-inflammatory phenotype of macrophages, indicated by a marked CD38 expression. However, only the continued expression of CD38 leads to a marked decrease of NAD+ via adenosine pathway, which brings the immunosuppressive properties in form of adenosine production to front (Konen, Fradette, and Gibbons 2019). The immunosuppressive effect of adenosine is driven by adenosine-receptor A2AR/A2BR-mediated inhibition of T cell activation, accompanied by the recruitment of tumor-promoting cells such as MDSCs or TAMs (Cekic et al. 2014; Vijayan et al. 2017). Thus, IFN-γ-associated CD38 expression of macrophages during immune control represents a potential bridge from DIVA[2]-induced immune control to immune evasion. To prevent the production of adenosine, which is promoted by CD38-expressing macrophages, neutralizing antibodies can be used. In this context, the anti-CD38 antibody daratumumab has been widely described. Daratumumab is a human anti-CD38 IgG1 antibody approved for the treatment of recurrent/refractory multiple myeloma. CD38-expressing myeloma cells are eliminated by daratumumab via antibody-dependent cellular cytotoxicity (ADCC) or complement-dependent cytotoxicity (CDC). It also inhibits the production of the immunosuppressive adenosine by CD38^{+} macrophages or MDSCs, thereby enhancing anti-tumor immunity (Dwivedi et al. 2021). Daratumumab thus enabled an increase in cytotoxic T cells in patients who showed a partial to

good response to daratumumab, thereby enhancing anti-tumor immunity (Krejcik et al. 2016). Adenosine-dependent inhibition of T cells also plays a role in melanoma. In this context, the use of CD38 inhibitors showed a reverting effect that restored T cell proliferation (Ben Baruch et al. 2018; Morandi et al. 2015). Due to the CD38-expressing macrophages in the DIVA$^2$-induced immune control, the use of a CD38 inhibitor to suppress adenosine production and the thus suppressed immunosuppressive effect is a conceivable target to prevent immune evasion.

In summary, we conclude that the **DIVA$^2$-induced cytotoxicity is mainly mediated by CD8$^+$ T cells and ILCs**, however the CD8$^+$ T Cell-mediated cytotoxicity is decreased since a **portion of CD8$^+$ T cells expressed T cell exhaustion marker genes**. The TME of the DIVA$^2$-treated group was devoid of monocytes at the time of immune control, but we detected them at the time of immune evasion. These monocytes expressed pro-tumorigenic marker genes indicative of a **suppressive MDSC-like phenotype**. An explanation for this switch from immune control to immune evasion is offered by the IFN-$\gamma$-associated **CD38 expression of macrophages** in the DIVA$^2$-treated group at the time of immune control, which primarily suggests a pro-inflammatory M1 phenotype, but when expressed continuously **implies the formation of the immunosuppressive adenosine**, additionally associated with the recruitment of myeloid immunosuppressive cells into the TME. In order to verify the immunosuppressive effect of those monocytes *in vivo*, the use of blocking agents that prevent the recruitment of monocytes into the tumor is suggested. For this purpose, we tested the use of the anti-CCR2 antibody MC-21 in a therapeutic tumor experiment.

## 5.4 Depleting CCR2$^+$ monocytes after DIVA$^2$ transiently diminishes tumor growth showing their tumor-promoting capacity

The monocytes that we detected in the DIVA$^2$-treated group in immune evasion by scRNA-seq strongly expressed CCR2 in addition to the immunosuppressive marker genes. CCR2 represents a promising target to prevent the migration of these cells to the tumor with an anti-CCR2 antibody and to further evaluate their immunosuppressive potential (Fei et al. 2021). However, in our previous work, we found that CCR2$^+$ peripheral blood monocytes are crucial for a successful immunization by DIVA. They are recruited into the treated skin tissue by the adjuvant effect of Dithranol and generate an inflammatory milieu essential for T cell priming by local DC populations (Sohl et al. 2022). Depletion of these monocytes with the anti-CCR2 antibody MC-21 (Mack et al. 2001) resulted in a significantly reduced T cell immune response (Sohl et al. 2022). Therefore, in the therapeutic tumor experiment it was important to start the depletion of the CCR2$^+$ monocytes only when the second immunization had already been performed, but the monocytes had not yet infiltrated the TME of the MC38mOVA tumors. This time window was given from day 15 (Figure 4.15a). MC-21 almost completely depleted

the CCR2^{+} Ly6C^{+} monocytes in the blood preventing their migration to the tumor (Figure 4.15b). Combination of DIVA[2] and MC-21 transiently reduced tumor growth compared to DIVA[2] alone and slightly increased the overall survival (Figure 4.15c-e). These observations support the findings from the scRNA-seq analysis that the CCR2^{+} monocytes are immunosuppressive cells that enhance immune evasion and promote tumor growth when entering the TME. However, the combination of DIVA[2] and MC-21 failed to completely eliminate the tumor cells and the tumors showed accelerated growth from about day 23.

Besides monocytes and monocyte-derived macrophages, T cells can also express CCR2. To prove that MC-21 exclusively depletes monocytes and not T cells, which could explain the accelerated growth from day 23, we analyzed the T cells during the depletion experiment (Figure 4.16). This showed that the MC-21 treated group had similar frequencies to the untreated group in both CD4^{+} and CD8^{+} T cells, proving that MC-21 did not lead to depletion of T cells. Only the CD8^{+} T cells of the group treated with DIVA[2] and MC-21 showed a slightly lower frequency of CD8^{+} T cells. This is probably due to the fact that, despite the start time of depletion two days after boost immunization, the MC-21-induced depletion of monocytes weakened the immunization performance to a slight extent, caused by a weaker inflammatory milieu in the treated skin tissue. However, it is very unlikely that the DIVA[2]-induced T cell immune response became too weak to be able to eliminate tumor cells in the TME.

A disadvantage of the performed depletion experiment is due to the fact that the chosen antibody MC-21 can only be administered once per day for 5 consecutive days, otherwise the immune system will produce antibodies against MC-21. Hence, CCR2^{+} monocytes were detectable in the blood again on day 21, allowing their migration to the tumor (Figure 4.15b). Therefore, it is more likely that the monocytes infiltrating the TME released their immunosuppressive potential and suppressed the cytotoxic lymphocytes when the depletion effect was gone. This explains the greater increase in tumor growth from around day 23 in the group receiving the combination of DIVA[2] and MC-21 (Figure 4.15c). Since the **time window in which infiltration of the TME by immunosuppressive monocytes could be prevented was not sufficient** for the DIVA[2]-induced cytotoxic lymphocytes to eliminate the tumor cells, monocytes entered the TME, able to suppress cytotoxic lymphocyte activity, favoring accelerated tumor growth.

In addition to the mechanisms discussed in 5.3.3, an indirect immunosuppressive effect of monocytes also emanates from TAMs they can differentiate to in the TME. TAMs mediate immunosuppression, among other things, via secretion of the cytokines IL-6, IL-8 and IL-10 (Sanmamed et al. 2017; J. Zhou et al. 2020), which promotes tumor growth. Furthermore, it has been described that monocyte-derived

TAMs maturing in the TME are capable of self-renewal and proliferation (Franklin et al. 2014), which in turn increases the number of these cells in the TME. In addition, TAMs can also produce CCL2, which again increases the recruitment of CCR2^{+} monocytes (Dongbo Li et al. 2020). However, if the recruitment of monocytes is prevented, continued proliferation of TAMs is significantly reduced, thereby reducing tumor growth. MC-21 could not persistently prevent the recruitment of CCR2^{+} monocytes to the tumor. Therefore, further work is needed to find an alternative therapeutic approach that persistently mediates this recruitment.

One alternative to MC-21 is selective CCR2 antagonist RS504393. It also inhibits infiltration of the TME by immunosuppressive cells such as MDSCs, which improved the survival in pre-clinical bladder cancer mouse models (Mu et al. 2019) and was associated with reduced numbers of TAMs and significantly reduced tumor volume (Z. Yang et al. 2019). The CCR2 antagonist CAS445479-97-0 reversed the induction of A549 cell proliferation by CCL2 and decreased their CCL2-mediated capacity to migrate (An et al. 2017). BMS CCR2 22 is a CCR2 antagonist that also reduced infiltration of TAMs in the MC38 colorectal cancer model and equally enhanced the efficiency of the chemotherapeutic agent FOLFOX, leading to improved survival of the mice (Grossman et al. 2018). In addition, some inhibitors or antibodies targeting CCL2 have also been described, which minimizes the recruitment of CCR2^{+} cells. C1142 can specifically neutralize CCL2 and significantly reduced the recruitment of TAMs and MDSCs in a glioma model, which inhibited tumor proliferation and enabled prolonged survival of glioma-bearing mice (X. Zhu et al. 2011). Bindarit inhibits the synthesis of CCL2 and was also able to prevent infiltration of the TME by TAMs and MDSCs in pre-clinical models, inducing tumor regression (Zollo et al. 2012). In addition to CCL2, CSF1 as a chemoattractant also leads to monocyte recruitment to the TME (Laoui et al. 2014) inducing tumor progression in pre-clinical models (Y. Zhu et al. 2014). Blocking the CSF1 receptor (CSF1R) prevented monocyte recruitment in pre-clinical models, promoting antitumour immunity and enhancing the efficacy of checkpoint inhibitors (Ngambenjawong, Gustafson, and Pun 2017). The cytotoxicity of myeloid cells is regulated by inhibitory and activating receptors. The immunoglobulin CD47 is secreted by tumor cells and represents a "do not eat me" signal upon binding to signal-regulatory protein alpha (Sirp$\alpha$) receptor on the cell surface of myeloid cells (Logtenberg 2020). Blocking the CD47-Sirp1$\alpha$ axis therefore offers a possible target to enhance the cytotoxicity of myeloid cells after DIVA[2] treatment, as the myeloid cells also expressed Sirp1$\alpha$ (data not shown). These formulations offer alternatives to the anti-CCR2 antibody MC-21 to persistently inhibit the recruitment of CCR2^{+} monocytes to the TME.

## 5.5 DIVA[2] failed to increase the anti-tumor immunity against MC38mOVA tumors mediated by anti-PD-1 immune checkpoint blockade

To assess the biological capacity of DIVA[2] in relation to other immunotherapeutic approaches, we compared DIVA[2]-induced anti-tumor immunity with that mediated by immune checkpoint blockade (ICB). For the MC38 tumor model, it has been described that ICB targeting the PD-1/PD-L1 axis achieves very successful therapeutic effects and can lead to complete regression, making anti-PD-1-mediated immunotherapy a gold standard in the MC38 tumor model (Juneja et al. 2017; Kleinovink et al. 2017). Therefore, we treated mice in a therapeutic tumor setting with DIVA[2] or anti-PD-1 (Figure 4.17). In contrast to DIVA[2], anti-PD-1 could prohibit immune evasion in 8 of 10 tumors, allowing their regression. In the other two mice, immune evasion resulted in steadily progressive tumor growth. These findings imply that the ligation of PD-1 on the surface of cytotoxic T cells after DIVA[2] treatment by PD-L1, plays a significant role in the induction of immunosuppression in the TME in addition to the influx of immunosuppressive monocytes and thus contributes decisively to immune evasion. PD-L1 is produced not only by immunosuppressive cells in the TME but also by tumor cells (Wu et al. 2021). The binding of PD-L1 to PD-1 on the surface of T cells leads to phosphorylation of ITIMs and ITSMs at the intracellular domain of PD-1, which recruits the tyrosine phosphatases SHP-1 and SHP-2 (Lázár-Molnár et al. 2008; D. Y. Lin et al. 2008). These phosphatases dephosphorylate several key proteins downstream of the TCR, suppressing signaling pathways such as PI3K/AKT, Ras, MAPK, ERK and ultimately inhibiting the T cell cycle, cytokine production and therefore T cell proliferation and differentiation. Consequently, this leads to loss of immune function (Hui et al. 2017; Patsoukis et al. 2012; Sharpe and Pauken 2018).

To test whether combining DIVA[2] with anti-PD-1 acts synergistically to enable complete regression of tumors, we further treated mice with the combination of DIVA[2] and anti-PD-1 (Figure 4.17). Although combining DIVA[2] with anti-PD-1-mediated ICB slightly increased the effector function of the DIVA[2]-induced antigen-specific CD8^{+} T cells compared to DIVA[2] alone, this did not increase the induced anti-tumour capacity (Figure 4.17). For this reason, we observed that 2 of the 9 outgrown tumors could not be rejected. A significant problem in the use of immune checkpoint inhibitors (ICI) is posed by tumor types that exhibit no response or lower response rates to ICB (Jenkins et al. 2018). Response rates vary greatly depending on the tumor type. They range for anti-PD-1 from almost non-existent in pancreatic cancer to 10-30 % in most other tumor types and reach 40-60 % in melanoma, Hodgkin lymphoma, squamous-cell carcinoma of the skin or Merkel cell carcinoma (S. Chen et al. 2021; Esfahani et al. 2020). Such resistance may be due to inadequate generation of T cells, impaired T cell effector function or impaired formation of T cell memory (O'Donnell et al. 2017). In this work, it was clearly shown that DIVA[2] leads to a strong cellular immune response in the form of functional antigen-specific tumor-

reactive T cells that are still detectable in the memory phase. The use of the vaccination platform DIVA$^2$ is therefore conceivable for the treatment of tumor types that show no response or a lower response rate to ICIs. Even if the combination of DIVA$^2$ and anti-PD-1 did not offer any added value compared to anti-PD-1, testing of DIVA$^2$ combined with anti-PD-1 or combined with other ICIs is promising for tumor types that show lower response rates. This provides an opportunity for further pre-clinical development of DIVA$^2$ as a therapeutic immunotherapy approach.

## 5.6   Limitations of DIVA$^2$ for treating solid tumors and possibilities for further development

The dithranol-imiquimod-based TCI method DIVA developed in the group of Prof. Dr. Markus Radsak should be optimized with regard the generation of a stronger primary and memory T cell response to characterize its effects on the TME of solid tumors in a therapeutic tumor model. This should provide insights how DIVA can be adapted to achieve a successful therapeutic treatment. Figure 5.1 graphically summarizes the immunological mechanisms in the TME after DIVA$^2$ treatment.
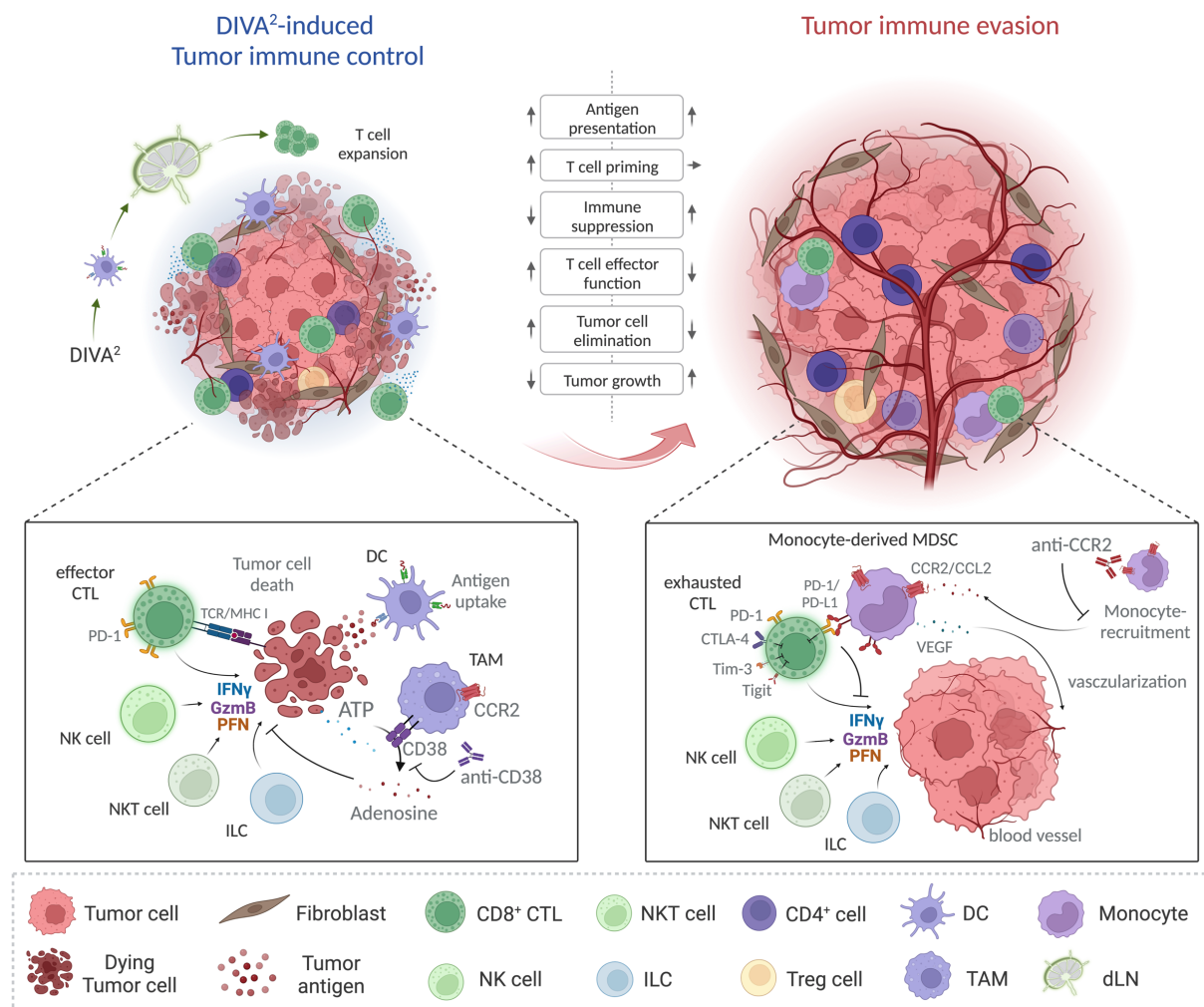


**Figure 5.1: Immunological mechanisms in the TME after DIVA$^2$ treatment**

DIVA$^2$ induces antigen-specific CD8$^+$ T cells that migrate from the dLN to the tumor to eliminate tumor cells. This immunization enables transient tumor immune control that is maintained for over two weeks. The TME of DIVA$^2$-treated mice showed marked CD38 expression by macrophages. The adenosine produced by CD38 is a possible initiator of immunosuppression in the TME, as it inhibits T cell effector function and results in the inability to completely eliminate tumor cells. This leads to the development of an immune equilibrium which turns into immune evasion through further immunosuppressive mechanisms. CCL2 produced by macrophages and tumor cells in the TME recruits inflammatory CCR2$^+$ monocytes, which differentiate into an MDSC phenotype in the TME producing immunosuppressive factors such as PD-L1 and VEGF. These inhibit T cell effector function and promote vascularization, inhibiting tumor cell elimination and significantly promoting tumor progression. Possible targets to counteract these mechanisms are CD38 and CCR2 to prevent the production of adenosine and the infiltration of immunosuppressive monocytes. Created with BioRender.com.

DIVA$^2$ induces generation of antigen-specific CD8$^+$ T cells that migrate from the draining lymph node to the TME to eliminate tumor cells. This enables transient tumor immune control which is maintained for over two weeks. The TME of DIVA$^2$-treated mice showed marked CD38 expression by macrophages during immune control. The adenosine produced by CD38 is a possible initiator of immunosuppression in the TME, as it inhibits T cell effector function and results in the inability to completely eliminate tumor cells. Furthermore, we observed the expression of T cell exhaustion marker genes by around half of the CD8$^+$ T cells, indicating that their cytotoxic capacity is hindered. This leads to the development of an immune equilibrium which, through further immunosuppressive mechanisms, transitions to the state of immune evasion. CCL2 produced by macrophages and tumor cells in the TME recruits inflammatory CCR2$^+$ monocytes, which differentiate into an MDSC phenotype in the TME producing immunosuppressive factors such as PD-L1 and VEGF. These inhibit the effector function of PD-1 expressing T cells and promote vascularization, thereby inhibiting tumor cell elimination and significantly promoting tumor progression. Possible targets to counteract these mechanisms are CD38 and CCR2.

The further development of DIVA$^2$ in the present work produced a significant optimization of the primary and memory t cell immune response. This enabled complete protection in the prophylactic tumor model as well as transient immune control in the therapeutic tumor setting. However, it must be mentioned that the model antigens Ova$_{257-264/323-337}$ represent immunogenic peptides and cannot congruently represent the immunogenicity of tumor-associated antigens. Furthermore, the MC38mOVA tumor model represents an artificial system whose TME character may differ from that of spontaneously occurring tumors. Therefore, further development of DIVA$^2$ in other spontaneous or inducible tumor models is necessary.

To prevent the infiltration of immunosuppressive monocytes into the TME, alternative CCR2- or CCL2-blocking antibodies can be used, which, in contrast to MC-21, can be applied for longer and thus continuously prevent infiltration. In chapter 5.4, alternatives were presented that can be tested in tumor experiments. Furthermore, the CD38 expression of the macrophages at the time of immune control offers a target to prevent the production of the immunosuppressive adenosine. For this purpose, the use of an anti-CD38 antibody, such as daratumumab, would be appropriate. In order to understand the immunosuppressive processes that originate from monocytic cells in the TME even more precisely, it would be useful to investigate the phenotype of the tumor-infiltrating monocytes more detailed using bioinformatics automated pathway analyses. This could provide crucial insights into how T cell suppression occurs after initial DIVA$^2$-induced immune control and offer possible

alternative targets to prevent this. The use of the B16OVA tumor model could also provide insights into the extent to which the metabolic character of the TME influences the cytotoxic capacity of DIVA[2]. One of the main obstacles for translation into the human system reflects the different nature of human skin tissue and the associated altered permeability which is crucial for diffusion of adjuvants and peptides. To begin translation into the human system, the development of microneedle-based TCI with dithranol and imiquimod offers a promising basis. In this context, a microneedle-based system allows to bypass the stratum corneum and the upper epidermal skin layers to deliver the adjuvants and peptides into the epidermal and dermal skin layers where APCs are localized to enable potent TCI-mediated immunity.

# 6    Abstract

The treatment of cancer diseases is one of the greatest challenges for modern medicine. In addition to conventional cancer therapy approaches, cancer immunotherapy has been gaining importance for more than two decades. In this context, the use of cancer vaccines that induce the formation of high-quality tumor-specific T cells is a promising tool that is now being intensively researched. Therapeutic approaches are needed that specifically sensitize the host immune system to the tumor and are able to specifically address targets in the complex immune-inhibitory network of the tumor microenvironment, a major obstacle affecting the efficiency of immunotherapeutic approaches.

The transcutaneous immunization method developed in the research group of Prof. Dr. Markus Radsak enables the generation of antigen-specific CD8$^+$ and CD4$^+$ T cells by activating skin tissue-resident antigen-presenting cells. With the aim of first optimizing the memory T cell response, the frequency of antigen-specific activated T cells was massively increased in the present work by multiple TCI. The optimized Dithranol-Imiquimod-based transcutaneous immunization (DIVA$^2$) enabled protection against MC38mOVA tumor cells in a prophylactic tumor setting. Applied in a therapeutic Tumor setting, DIVA$^2$ resulted in transient tumor immune control. High-dimensional flow cytometry analysis and single-cell mRNA-sequencing of tumor-infiltrating leukocytes showed that DIVA$^2$-induced cytotoxic CD8$^+$ T cells facilitate initial tumor immune control, but are inhibited by immunosuppressive CCR2$^+$ PD-L1$^+$ monocyte-derived myeloid-derived suppressor cells (M-MDSC), resulting in partial T-cell exhaustion. Furthermore, CD38 expression by macrophages during immune control implicated production of the immunosuppressive adenosine. Anti-CCR2 antibody-based depletion of CCR2$^+$ monocytes in the tumor experiment highlighted their immunosuppressive nature, but could not persistently limit tumor growth as depletion could not be continuously ensured. The use of the immune checkpoint inhibitor anti-PD-1 enabled a strong regression of the tumors in a therapeutic tumor setting, which illustrates the immunosuppressive role of the PD-1/PD-L1 axis in the tumor microenvironment of MC38mOVA tumors after initial DIVA$^2$-induced immune control.

In summary, the present work provides a platform for generating a strong antigen-specific primary and memory T cell immune response using the optimized transcutaneous immunization method DIVA$^2$. This enables protection against tumor cells and transient therapeutic immune control of solid tumors. For a successful therapeutic elimination of tumors, the identification of specific immune targets is necessary.

# 6 Zusammenfassung

Die Behandlung von Krebs-Erkrankungen ist eine der größten Hürden für die moderne Medizin. Neben den konventionellen Krebstherapieansätzen gewinnt die Krebsimmuntherapie seit mehr als zwei Jahrzehnten an Bedeutung. In diesem Zusammenhang ist der Einsatz von Krebsimpfstoffen, die die Bildung hochwertiger Tumor-spezifischer T-Zellen induzieren, ein vielversprechendes Instrument, das inzwischen intensiv erforscht wird. Es werden therapeutische Ansätze benötigt, die das Wirtsimmunsystem spezifisch für den Tumor sensibilisieren und in der Lage sind, gezielt Strukturen im komplexen immunsupprimierenden Netzwerk des Tumor Mikromilieus anzusprechen, ein Haupthindernis für effiziente Immuntherapie.

Die in der Forschungsgruppe von Prof. Dr. Markus Radsak entwickelte transkutane Immunisierungsmethode ermöglicht durch die Aktivierung Hautgewebs-residenter Antigen-präsentierender Zellen die Entstehung antigenspezifischer $CD8^+$ und $CD4^+$ T Zellen. Mit dem Ziel die T-Gedächtniszell-Antwort zunächst zu optimieren, wurde in der vorliegenden Arbeit durch mehrfache TCI die Frequenz Antigen-spezifischer aktivierter T-Zellen massiv gesteigert. Die optimierte Dithranol-Imiquimod-basierte transkutane Immunisierung ($DIVA^2$) ermöglichte eine Protektion gegen MC38mOVA Tumorzellen in einem prophylaktischen Tumorversuch. Bei therapeutischer Anwendung ermöglichte $DIVA^2$ eine transiente Tumorimmunkontrolle. Hochdimensionale Durchflusszytometrie-Analysen und Einzel-Zell-mRNA-Sequenzierung Tumor-infiltrierender Leukozyten zeigten, dass $DIVA^2$-induzierte cytotoxische $CD8^+$ T-Zellen die initiale Tumorimmunkontrolle ermöglichen, jedoch durch immunsuppressive $CCR2^+$ $PD-L1^+$ Monozyten-abstammende myeloide Suppressorzellen (M-MDSC) inhibiert werden, was in Teilen zu T-Zell Exhaustion führte. Ferner implizierte die CD38-Expression von Makrophagen während der Immunkontrolle die Produktion des immunsuppressiven Adenosins. Die anti-CCR2 Antikörper-basierte Depletion $CCR2^+$ Monozyten im Tumorexperiment verdeutlichte deren immunsuppressiven Charakter, konnte das Tumorwachstum jedoch nicht anhalten einschränken, da die Depletion nicht fortwährend sichergestellt werden konnte. Der therapeutische Einsatz des Immun-checkpoint Inhibitors anti-PD-1 ermöglichte eine starke Regression der Tumore, was die suppressive Rolle der PD-1/PD-L1 Achse im Tumor Mikromilieu nach initialer $DIVA^2$-induzierter Immunkontrolle verdeutlicht.

Zusammenfassend liefert die vorliegende Arbeit mit der optimierten transkutanen Immunisierungsmethode $DIVA^2$ eine Plattform zur Generierung einer starken antigen-spezifischen Primär- und T-Gedächtniszell Immunantwort. Diese ermöglicht Protektion gegen Tumorzellen und eine transiente therapeutische Immunkontrolle solider Tumoren. Für eine erfolgreiche therapeutische Eliminierung der Tumoren ist die Identifizierung spezifischer Immun-Targets notwendig.

# 7 Appendix

## 7.1 Literature directory

Abiko, K et al. 2015. 'IFN-γ from Lymphocytes Induces PD-L1 Expression and Promotes Progression of Ovarian Cancer'. *British Journal of Cancer* 112(9): 1501–9.

Agata, Yasutoshi et al. 1996. 'Expression of the PD-1 Antigen on the Surface of Stimulated Mouse T and B Lymphocytes'. *International Immunology* 8(5): 765–72.

Aguilar, Stephanie Vargas et al. 2020. 'ImmGen at 15'. *Nature Immunology* 21(7): 700–703.

Alimardani, Vahid, Samira Sadat Abolmaali, Ali Mohammad Tamaddon, and Mohammad Ashfaq. 2021. 'Recent Advances on Microneedle Arrays-Mediated Technology in Cancer Diagnosis and Therapy'. *Drug Delivery and Translational Research* 11(3): 788–816.

Allard, Bertrand, Maria Serena Longhi, Simon C. Robson, and John Stagg. 2017. 'The Ectonucleotidases CD39 and CD73: Novel Checkpoint Inhibitor Targets'. *Immunological Reviews* 276(1): 121–44.

Alshamsan, Aws. 2012. 'Induction of Tolerogenic Dendritic Cells by IL-6-Secreting CT26 Colon Carcinoma'. *Immunopharmacology and Immunotoxicology* 34(3): 465–69.

An, Jun et al. 2017. 'Targeting CCR2 with Its Antagonist Suppresses Viability, Motility and Invasion by Downregulating MMP-9 Expression in Non-Small Cell Lung Cancer Cells'. *Oncotarget* 8(24): 39230–40.

Ansell, Stephen M. et al. 2015. 'PD-1 Blockade with Nivolumab in Relapsed or Refractory Hodgkin's Lymphoma'. *New England Journal of Medicine* 372(4): 311–19.

Aqbi, Hussein F et al. 2018. 'IFN-γ Orchestrates Tumor Elimination, Tumor Dormancy, Tumor Escape, and Progression'. *Journal of Leukocyte Biology* 103(6): 1219–23.

Artis, David, and Hergen Spits. 2015. 'The Biology of Innate Lymphoid Cells'. *Nature* 517(7534): 293–301.

Austin, James W. et al. 2014. 'STAT3, STAT4, NFATc1, and CTCF Regulate PD-1 through Multiple Novel Regulatory Regions in Murine T Cells'. *The Journal of Immunology* 192(10): 4876–86.

Bae, Eun-Ah et al. 2019. 'Roles of NKT Cells in Cancer Immunotherapy'. *Archives of Pharmacal Research* 42(7): 543–48.

Bai, Haiqing, Gillian M. Schiralli Lester, Laura C. Petishnok, and David A. Dean. 2017. 'Cytoplasmic Transport and Nuclear Import of Plasmid DNA'. *Bioscience Reports* 37(6).

Balan, Sreekumar, Kristen J Radford, and Nina Bhardwaj. 2020. 'Unexplored Horizons of CDC1 in Immunity and Tolerance.' *Advances in immunology* 148: 49–91.

Ben Baruch, Bar et al. 2018. 'Stromal CD38 Regulates Outgrowth of Primary Melanoma and Generation of Spontaneous Metastasis'. *Oncotarget* 9(61): 31797–811.

Baumgaertner, P. et al. 2016. 'Vaccination of Stage III/IV Melanoma Patients with Long NY-ESO-1 Peptide and CpG-B Elicits Robust CD8 [+] and CD4 [+] T-Cell Responses with Multiple Specificities Including a Novel DR7-Restricted Epitope'. *OncoImmunology* 5(10): e1216290.

Beatty, Gregory L., and Yvonne Paterson. 2001. 'IFN-γ-Dependent Inhibition of Tumor Angiogenesis by Tumor-Infiltrating CD4+ T Cells Requires Tumor Responsiveness to IFN-γ'. *The Journal of Immunology* 166(4): 2276–82.

Belai, E. B. et al. 2014. 'PD-1 Blockage Delays Murine Squamous Cell Carcinoma Development'. *Carcinogenesis* 35(2): 424–31.

Bellmunt, Joaquim et al. 2017. 'Pembrolizumab as Second-Line Therapy for Advanced Urothelial Carcinoma'. *New England Journal of Medicine* 376(11): 1015–26.

Bellucci, Roberto et al. 2015. 'Interferon-γ-Induced Activation of JAK1 and JAK2 Suppresses Tumor Cell Susceptibility to NK Cells through Upregulation of PD-L1 Expression'. *OncoImmunology* 4(6): e1008824.

Belnap, LeGrand P., Patrick H. Cleveland, M. E.M. Colmerauer, and Robert M. Barone. 1979. 'Immunogenicity of Chemically Induced Murine Colon Cancers'. *Cancer Research* 39(4): 1174–79.

Benci, Joseph L. et al. 2016. 'Tumor Interferon Signaling Regulates a Multigenic Resistance Program to Immune Checkpoint Blockade'. *Cell* 167(6): 1540-1554.e12.

Bernink, Jochem H et al. 2013. 'Human Type 1 Innate Lymphoid Cells Accumulate in Inflamed Mucosal Tissues'. *Nature Immunology* 14(3): 221–29.

Bertrand, Anne et al. 2015. 'Immune Related Adverse Events Associated with Anti-CTLA-4 Antibodies: Systematic Review and Meta-Analysis'. *BMC Medicine* 13(1): 211.

Bialojan, Ariane et al. 2019. 'Transcutaneous Immunization with CD40 Ligation Boosts Cytotoxic T Lymphocyte Mediated Antitumor Immunity Independent of CD4 Helper Cells in Mice'. *European Journal of Immunology* 49(11): 2083–94.

Böttcher, Jan P., and Caetano Reis e Sousa. 2018. 'The Role of Type 1 Conventional Dendritic Cells in Cancer Immunity'. *Trends in Cancer* 4(11): 784–92.

Brayer, Jason et al. 2015. 'WT1 Vaccination in AML and MDS: A Pilot Trial with Synthetic Analog Peptides'. *American Journal of Hematology* 90(7): 602–7.

Brentjens, Renier J. et al. 2013. 'CD19-Targeted T Cells Rapidly Induce Molecular Remissions in Adults with Chemotherapy-Refractory Acute Lymphoblastic Leukemia'. *Science Translational Medicine* 5(177).

Brown, Ross D. et al. 2001. 'Dendritic Cells from Patients with Myeloma Are Numerically Normal but Functionally Defective as They Fail to Up-Regulate CD80 (B7-1) Expression after HuCD40LT Stimulation Because of Inhibition by Transforming Growth Factor-B1 and Interleukin-10'. *Blood* 98(10): 2992–98.

Broz, Miranda L. et al. 2014. 'Dissecting the Tumor Myeloid Compartment Reveals Rare Activating Antigen-Presenting Cells Critical for T Cell Immunity'. *Cancer Cell* 26(5): 638–52.

Brunet, Jean-François et al. 1987. 'A New Member of the Immunoglobulin Superfamily—CTLA-4'. *Nature* 328(6127): 267–70.

Cafri, Gal et al. 2020. 'MRNA Vaccine–Induced Neoantigen-Specific T Cell Immunity in Patients with Gastrointestinal Cancer'. *Journal of Clinical Investigation* 130(11): 5976–88.

del Campo, Ana B. et al. 2014. 'Immune Escape of Cancer Cells with Beta2-Microglobulin Loss over the Course of Metastatic Melanoma'. *International Journal of Cancer* 134(1): 102–13.

Castro, Flávia et al. 2018. 'Interferon-Gamma at the Crossroads of Tumor Immune Surveillance or Evasion'. *Frontiers in Immunology* 9.

Cekic, Caglar, Yuan-Ji Day, Duygu Sag, and Joel Linden. 2014. 'Myeloid Expression of Adenosine A2A Receptor Suppresses T and NK Cell Responses in the Solid Tumor Microenvironment'. *Cancer Research* 74(24): 7250–59.

Chappell, John C., David M. Wiley, and Victoria L. Bautch. 2011. 'Regulation of Blood Vessel Sprouting'. *Seminars in Cell & Developmental Biology* 22(9): 1005–11.

Chemnitz, Jens M. et al. 2004. 'SHP-1 and SHP-2 Associate with Immunoreceptor Tyrosine-Based Switch Motif of Programmed Death 1 upon Primary Human T Cell Stimulation, but Only Receptor Ligation Prevents T Cell Activation'. *The Journal of Immunology* 173(2): 945–54.

Chen, Limo et al. 2018. 'CD38-Mediated Immunosuppression as a Mechanism of Tumor Cell Escape from PD-1/PD-L1 Blockade'. *Cancer Discovery* 8(9): 1156–75.

Chen, Shixue et al. 2021. 'Response Efficacy of PD-1 and PD-L1 Inhibitors in Clinical Trials: A Systematic Review and Meta-Analysis'. *Frontiers in Oncology* 11.

Chen, Yu-Pei et al. 2017. 'Genomic Analysis of Tumor Microenvironment Immune Types across 14 Solid Cancer Types: Immunotherapeutic Implications.' *Theranostics* 7(14): 3585–94.

Cheng, Min et al. 2013. 'NK Cell-Based Immunotherapy for Malignant Diseases'. *Cellular & Molecular Immunology* 10(3): 230–52.

Chiossone, Laura, Pierre-Yves Dumas, Margaux Vienne, and Eric Vivier. 2018. 'Natural Killer Cells and Other Innate Lymphoid Cells in Cancer'. *Nature Reviews Immunology* 18(11): 671–88.

Chomarat, Pascale, Jacques Banchereau, Jean Davoust, and A. Karolina Palucka. 2000. 'IL-6 Switches the Differentiation of Monocytes from Dendritic Cells to Macrophages'. *Nature Immunology* 1(6): 510–14.

Chowdhury, Dipanjan, and Judy Lieberman. 2008. 'Death by a Thousand Cuts: Granzyme Pathways of Programmed Cell Death'. *Annual Review of Immunology* 26(1): 389–420.

Chun, Eunyoung et al. 2015. 'CCL2 Promotes Colorectal Carcinogenesis by Enhancing Polymorphonuclear Myeloid-Derived Suppressor Cell Population and Function'. *Cell Reports* 12(2): 244–57.

Clarke, Sally RMcK et al. 2000. 'Characterization of the Ovalbumin-Specific TCR Transgenic Line OT-I: MHC Elements for Positive and Negative Selection'. *Immunology and Cell Biology* 78(2): 110–17.

Cohen, Ezra E W et al. 2019. 'Pembrolizumab versus Methotrexate, Docetaxel, or Cetuximab for Recurrent or Metastatic Head-and-Neck Squamous Cell Carcinoma (KEYNOTE-040): A Randomised, Open-Label, Phase 3 Study'. *The Lancet* 393(10167): 156–67.

Condamine, Thomas, and Dmitry I. Gabrilovich. 2011. 'Molecular Mechanisms Regulating Myeloid-Derived Suppressor Cell Differentiation and Function'. *Trends in Immunology* 32(1): 19–25.

Coquet, Jonathan M. et al. 2007. 'IL-21 Is Produced by NKT Cells and Modulates NKT Cell Activation and Cytokine Production'. *The Journal of Immunology* 178(5): 2827–34.

Coquet, Jonathan M et al. 2008. 'Diverse Cytokine Production by NKT Cell Subsets and Identification of an IL-17-Producing CD4-NK1.1- NKT Cell Population.' *Proceedings of the National Academy of Sciences of the United States of America* 105(32): 11287–92.

Coughlin, Christina M. et al. 1998. 'Tumor Cell Responses to IFNγ Affect Tumorigenicity and Response to IL-12 Therapy and Antiangiogenesis'. *Immunity* 9(1): 25–34.

Crews, Davis W., Jenna A. Dombroski, and Michael R. King. 2021. 'Prophylactic Cancer Vaccines Engineered to Elicit Specific Adaptive Immune Response'. *Frontiers in Oncology* 11.

Curiel, Tyler J et al. 2004. 'Specific Recruitment of Regulatory T Cells in Ovarian Carcinoma Fosters Immune Privilege and Predicts Reduced Survival'. *Nature Medicine* 10(9): 942–49.

Dadi, Saïda et al. 2016. 'Cancer Immunosurveillance by Tissue-Resident Innate Lymphoid Cells and Innate-like T Cells'. *Cell* 164(3): 365–77.

Damo, Martina, and Nikhil S. Joshi. 2019. 'Treg Cell IL-10 and IL-35 Exhaust CD8+ T Cells in Tumors'. *Nature Immunology* 20(6): 674–75.

Damuzzo, Vera et al. 2015. 'Complexity and Challenges in Defining Myeloid-Derived Suppressor Cells'. *Cytometry Part B: Clinical Cytometry* 88(2): 77–91.

Dannull, Jens et al. 2005. 'Enhancing the Immunostimulatory Function of Dendritic Cells by Transfection with MRNA Encoding OX40 Ligand'. *Blood* 105(8): 3206–13.

Deaglio, Silvia et al. 2007. 'Adenosine Generation Catalyzed by CD39 and CD73 Expressed on Regulatory T Cells Mediates Immune Suppression'. *Journal of Experimental Medicine* 204(6): 1257–65.

DeGregori, James. 2011. 'Evolved Tumor Suppression: Why Are We So Good at Not Getting Cancer?' *Cancer Research* 71(11): 3739–44.

Diao, Jun et al. 2018. 'Tumor Dendritic Cells (DCs) Derived from Precursors of Conventional DCs Are Dispensable for Intratumor CTL Responses'. *The Journal of Immunology* 201(4): 1306–14.

Díaz-Basabe, Angélica, Francesco Strati, and Federica Facciotti. 2020. 'License to Kill: When INKT Cells Are Granted the Use of Lethal Cytotoxicity'. *International Journal of Molecular Sciences* 21(11): 3909.

Dieu-Nosjean, Marie-Caroline et al. 2008. 'Long-Term Survival for Patients With Non–Small-Cell Lung Cancer With Intratumoral Lymphoid Structures'. *Journal of Clinical Oncology* 26(27): 4410–17.

Doering, Travis A. et al. 2012. 'Network Analysis Reveals Centrally Connected Genes and Pathways Involved in CD8+ T Cell Exhaustion versus Memory'. *Immunity* 37(6): 1130–44.

Dolcetti, Luigi et al. 2009. 'Hierarchy of Immunosuppressive Strength among Myeloid-Derived Suppressor Cell Subsets Is Determined by GM-CSF'. *European Journal of Immunology* 40(1): 22–35.

Donninger, Howard, Chi Li, John W. Eaton, and Kavitha Yaddanapudi. 2021. 'Cancer Vaccines: Promising Therapeutics or an Unattainable Dream'. *Vaccines* 9(6): 668.

DuPage, Michel et al. 2012. 'Expression of Tumour-Specific Antigens Underlies Cancer Immunoediting'. *Nature* 482(7385): 405–9.

Duperret, Elizabeth K. et al. 2019. 'A Synthetic DNA, Multi-Neoantigen Vaccine Drives Predominately MHC Class I CD8+ T-Cell Responses, Impacting Tumor Challenge'. *Cancer Immunology Research* 7(2): 174–82.

Dwivedi, Sanyog, Erika P. Rendón-Huerta, Vianney Ortiz-Navarrete, and Luis F. Montaño. 2021. 'CD38 and Regulation of the Immune Response Cells in Cancer'. *Journal of Oncology* 2021: 1–11.

El-Khoueiry, Anthony B et al. 2017. 'Nivolumab in Patients with Advanced Hepatocellular Carcinoma (CheckMate 040): An Open-Label, Non-Comparative, Phase 1/2 Dose Escalation and Expansion Trial'. *The Lancet* 389(10088): 2492–2502.

Elkord, Eyad et al. 2010. 'T Regulatory Cells in Cancer: Recent Advances and Therapeutic Potential'. *Expert Opinion on Biological Therapy* 10(11): 1573–86.

Engelke, Laura, Gerhard Winter, Sarah Hook, and Julia Engert. 2015. 'Recent Insights into Cutaneous Immunization: How to Vaccinate via the Skin'. *Vaccine* 33(37): 4663–74.

Esfahani, K. et al. 2020. 'A Review of Cancer Immunotherapy: From the Past, to the Present, to the Future'. *Current Oncology* 27(12): 87–97.

Ewen, C L, K P Kane, and R C Bleackley. 2012. 'A Quarter Century of Granzymes'. *Cell Death & Differentiation* 19(1): 28–35.

Fei, Liyang, Xiaochen Ren, Haijia Yu, and Yifan Zhan. 2021. 'Targeting the CCL2/CCR2 Axis in Cancer Immunotherapy: One Stone, Three Birds?' *Frontiers in Immunology* 12.

Ferris, Robert L. et al. 2016. 'Nivolumab for Recurrent Squamous-Cell Carcinoma of the Head and Neck'. *New England Journal of Medicine* 375(19): 1856–67.

Fife, Brian T., and Jeffrey A. Bluestone. 2008. 'Control of Peripheral T-Cell Tolerance and Autoimmunity via the CTLA-4 and PD-1 Pathways'. *Immunological Reviews* 224(1): 166–82.

Franklin, Ruth A. et al. 2014. 'The Cellular and Molecular Origin of Tumor-Associated Macrophages'. *Science* 344(6186): 921–25.

Fridman, Wolf Herman, Franck Pagès, Catherine Sautès-Fridman, and Jérôme Galon. 2012. 'The Immune Contexture in Human Tumours: Impact on Clinical Outcome'. *Nature Reviews Cancer* 12(4): 298–306.

Fuchs, Anja et al. 2013. 'Intraepithelial Type 1 Innate Lymphoid Cells Are a Unique Subset of IL-12- and IL-15-Responsive IFN-γ-Producing Cells'. *Immunity* 38(4): 769–81.

Fuchs, Charles S. et al. 2018. 'Safety and Efficacy of Pembrolizumab Monotherapy in Patients With Previously Treated Advanced Gastric and Gastroesophageal Junction Cancer'. *JAMA Oncology* 4(5): e180013.

Gabrilovich, D et al. 1998. 'Vascular Endothelial Growth Factor Inhibits the Development of Dendritic Cells and Dramatically Affects the Differentiation of Multiple Hematopoietic Lineages in Vivo.' *Blood* 92(11): 4150–66.

Gabrilovich, Dmitry I., and Srinivas Nagaraj. 2009. 'Myeloid-Derived Suppressor Cells as Regulators of the Immune System'. *Nature Reviews Immunology* 9(3): 162–74.

Gabrilovich, Dmitry I., Suzanne Ostrand-Rosenberg, and Vincenzo Bronte. 2012. 'Coordinated Regulation of Myeloid Cells by Tumours'. *Nature Reviews Immunology* 12(4): 253–68.

Garcia-Diaz, Angel et al. 2017. 'Interferon Receptor Signaling Pathways Regulating PD-L1 and PD-L2 Expression'. *Cell Reports* 19(6): 1189–1201.

Gardner, Alycia, Álvaro de Mingo Pulido, and Brian Ruffell. 2020. 'Dendritic Cells and Their Role in Immunotherapy'. *Frontiers in Immunology* 11.

Gardner, Thomas, Bennett Elzey, and Noah M. Hahn. 2012. 'Sipuleucel-T (Provenge) Autologous Vaccine Approved for Treatment of Men with Asymptomatic or Minimally Symptomatic Castrate-Resistant Metastatic Prostate Cancer'. *Human Vaccines & Immunotherapeutics* 8(4): 534–39.

Ginhoux, Florent et al. 2016. 'New Insights into the Multidimensional Concept of Macrophage Ontogeny, Activation and Function'. *Nature Immunology* 17(1): 34–40.

Glenn, G M et al. 1998. 'Transcutaneous Immunization with Cholera Toxin Protects Mice against Lethal Mucosal Toxin Challenge.' *Journal of immunology (Baltimore, Md. : 1950)* 161(7): 3211–14.

Godfrey, Dale I. et al. 2004. 'NKT Cells: What's in a Name?' *Nature Reviews Immunology* 4(3): 231–37.

Godfrey, Dale I., and Stuart P. Berzins. 2007. 'Control Points in NKT-Cell Development'. *Nature Reviews Immunology* 7(7): 505–18.

Gogoll, Karsten et al. 2016. 'Solid Nanoemulsion as Antigen and Immunopotentiator Carrier for Transcutaneous Immunization'. *Cellular Immunology* 308: 35–43.

Gonda, Kenji et al. 2017. 'Myeloid-Derived Suppressor Cells Are Increased and Correlated with Type 2 Immune Responses, Malnutrition, Inflammation, and Poor Prognosis in Patients with Breast Cancer'. *Oncology Letters* 14(2): 1766–74.

Gong, Jun, Alexander Chehrazi-Raffle, Srikanth Reddi, and Ravi Salgia. 2018. 'Development of PD-1 and PD-L1 Inhibitors as a Form of Cancer Immunotherapy: A Comprehensive Review of Registration Trials and Future Considerations'. *Journal for ImmunoTherapy of Cancer* 6(1): 8.

Gröne, A. 2002. 'Keratinocytes and Cytokines'. *Veterinary Immunology and Immunopathology* 88(1–2): 1–12.

Gros, Alena et al. 2014. 'PD-1 Identifies the Patient-Specific CD8+ Tumor-Reactive Repertoire Infiltrating Human Tumors'. *Journal of Clinical Investigation* 124(5): 2246–59.

Grossman, Julie G et al. 2018. 'Recruitment of CCR2+ Tumor Associated Macrophage to Sites of Liver Metastasis Confers a Poor Prognosis in Human Colorectal Cancer'. *OncoImmunology* 7(9): e1470729.

Guerra, Nadia et al. 2008. 'NKG2D-Deficient Mice Are Defective in Tumor Surveillance in Models of Spontaneous Malignancy'. *Immunity* 28(4): 571–80.

Guilliams, Martin et al. 2016. 'Unsupervised High-Dimensional Analysis Aligns Dendritic Cells across Tissues and Species'. *Immunity* 45(3): 669–84.

den Haan, Joke M.M., Sophie M. Lehar, and Michael J. Bevan. 2000. 'Cd8+ but Not Cd8– Dendritic Cells Cross-Prime Cytotoxic T Cells in Vivo'. *Journal of Experimental Medicine* 192(12): 1685–96.

Hanahan, Douglas, and Lisa M. Coussens. 2012. 'Accessories to the Crime: Functions of Cells Recruited to the Tumor Microenvironment'. *Cancer Cell* 21(3): 309–22.

Hanahan, Douglas, and Robert A. Weinberg. 2011. 'Hallmarks of Cancer: The Next Generation'. *Cell* 144(5): 646–74.

Hao, Qiongyu, Jaydutt v. Vadgama, and Piwen Wang. 2020. 'CCL2/CCR2 Signaling in Cancer Pathogenesis'. *Cell Communication and Signaling* 18(1): 82.

Hardy, Lynne A et al. 2004. 'Examination of MCP-1 (CCL2) Partitioning and Presentation during Transendothelial Leukocyte Migration'. *Laboratory Investigation* 84(1): 81–90.

Harlin, Helena et al. 2009. 'Chemokine Expression in Melanoma Metastases Associated with CD8+ T-Cell Recruitment'. *Cancer Research* 69(7): 3077–85.

Harper, K et al. 1991. 'CTLA-4 and CD28 Activated Lymphocyte Molecules Are Closely Related in Both Mouse and Human as to Sequence, Message Expression, Gene Structure, and Chromosomal Location.' *Journal of Immunology* 147(3): 1037–44.

Hasak, Jessica M., Christine B. Novak, Jennifer Megan M. Patterson, and Susan E. Mackinnon. 2018. 'Prevalence of Needlestick Injuries, Attitude Changes, and Prevention Practices Over 12 Years in an Urban Academic Hospital Surgery Department'. *Annals of Surgery* 267(2): 291–96.

Vander Heiden, Matthew G, Lewis C Cantley, and Craig B Thompson. 2009. 'Understanding the Warburg Effect: The Metabolic Requirements of Cell Proliferation.' *Science (New York, N.Y.)* 324(5930): 1029–33.

Hibbs, J B, Z Vavrin, and R R Taintor. 1987. 'L-Arginine Is Required for Expression of the Activated Macrophage Effector Mechanism Causing Selective Metabolic Inhibition in Target Cells.' *Journal of Immunology* 138(2): 550–65.

Hibbs, John B., Read R. Taintor, Zdenek Vavrin, and Elliot M. Rachlin. 1988. 'Nitric Oxide: A Cytotoxic Activated Macrophage Effector Molecule'. *Biochemical and Biophysical Research Communications* 157(1): 87–94.

Hirano, Fumiya et al. 2005. 'Blockade of B7-H1 and PD-1 by Monoclonal Antibodies Potentiates Cancer Therapeutic Immunity.' *Cancer research* 65(3): 1089–96.

Hodi, F. Stephen et al. 2010. 'Improved Survival with Ipilimumab in Patients with Metastatic Melanoma'. *New England Journal of Medicine* 363(8): 711–23.

Hogquist, Kristin A. et al. 1994. 'T Cell Receptor Antagonist Peptides Induce Positive Selection'. *Cell* 76(1): 17–27.

Hori, Shohei, Takashi Nomura, and Shimon Sakaguchi. 2003. 'Control of Regulatory T Cell Development by the Transcription Factor *Foxp3*'. *Science* 299(5609): 1057–61.

Hos, Brett J. et al. 2020. 'Identification of a Neo-Epitope Dominating Endogenous CD8 T Cell Responses to MC-38 Colorectal Cancer'. *OncoImmunology* 9(1).

Huang, Chun-Ming. 2007. 'Topical Vaccination: The Skin as a Unique Portal to Adaptive Immune Responses'. *Seminars in Immunopathology* 29(1): 71–80.

Huang, Li-Yun et al. 2001. 'IL-12 Induction by a Th1-Inducing Adjuvant In Vivo: Dendritic Cell Subsets and Regulation by IL-10'. *The Journal of Immunology* 167(3): 1423–30.

Hui, Enfu et al. 2017. 'T Cell Costimulatory Receptor CD28 Is a Primary Target for PD-1–Mediated Inhibition'. *Science* 355(6332): 1428–33.

Inozume, Takashi et al. 2010. 'Selection of CD8+PD-1+ Lymphocytes in Fresh Human Melanomas Enriches for Tumor-Reactive T Cells'. *Journal of Immunotherapy* 33(9): 956–64.

Itahashi, Kota, Takuma Irie, and Hiroyoshi Nishikawa. 2022. 'Regulatory T-cell Development in the Tumor Microenvironment'. *European Journal of Immunology* 52(8): 1216–27.

Iwai, Yoshiko et al. 2002. 'Involvement of PD-L1 on Tumor Cells in the Escape from Host Immune System and Tumor Immunotherapy by PD-L1 Blockade'. *Proceedings of the National Academy of Sciences* 99(19): 12293–97.

Iwai, Yoshiko, Seigo Terawaki, and Tasuku Honjo. 2005. 'PD-1 Blockade Inhibits Hematogenous Spread of Poorly Immunogenic Tumor Cells by Enhanced Recruitment of Effector T Cells.' *International immunology* 17(2): 133–44.

Jablonski, Kyle A. et al. 2015. 'Novel Markers to Delineate Murine M1 and M2 Macrophages'. *PLOS ONE* 10(12): e0145342.

Jacquelot, Nicolas, Cyril Seillet, Eric Vivier, and Gabrielle T. Belz. 2022. 'Innate Lymphoid Cells and Cancer'. *Nature Immunology* 23(3): 371–79.

Jain, Nitya, Hai Nguyen, Cynthia Chambers, and Joonsoo Kang. 2010. 'Dual Function of CTLA-4 in Regulatory T Cells and Conventional T Cells to Prevent Multiorgan Autoimmunity'. *Proceedings of the National Academy of Sciences* 107(4): 1524–28.

Jakubzick, Claudia et al. 2013. 'Minimal Differentiation of Classical Monocytes as They Survey Steady-State Tissues and Transport Antigen to Lymph Nodes'. *Immunity* 39(3): 599–610.

Jarnicki, Andrew G., Joanne Lysaght, Stephen Todryk, and Kingston H. G. Mills. 2006. 'Suppression of Antitumor Immunity by IL-10 and TGF-β-Producing T Cells Infiltrating the Growing Tumor: Influence of Tumor Environment on the Induction of CD4+ and CD8+ Regulatory T Cells'. *The Journal of Immunology* 177(2): 896–904.

Jenkins, Russell W, David A Barbie, and Keith T Flaherty. 2018. 'Mechanisms of Resistance to Immune Checkpoint Inhibitors'. *British Journal of Cancer* 118(1): 9–16.

Jiang, Xianjie et al. 2019. 'Role of the Tumor Microenvironment in PD-L1/PD-1-Mediated Tumor Immune Escape'. *Molecular Cancer* 18(1): 10.

Juneja, Vikram R. et al. 2017. 'PD-L1 on Tumor Cells Is Sufficient for Immune Evasion in Immunogenic Tumors and Inhibits CD8 T Cell Cytotoxicity'. *Journal of Experimental Medicine* 214(4): 895–904.

Van Kaer, L. 2007. 'NKT Cells: T Lymphocytes with Innate Effector Functions'. *Current Opinion in Immunology* 19(3): 354–64.

Kantoff, Philip W. et al. 2010. 'Sipuleucel-T Immunotherapy for Castration-Resistant Prostate Cancer'. *New England Journal of Medicine* 363(5): 411–22.

Karakasheva, Tatiana A. et al. 2015. 'CD38-Expressing Myeloid-Derived Suppressor Cells Promote Tumor Growth in a Murine Model of Esophageal Cancer'. *Cancer Research* 75(19): 4074–85.

De Keersmaecker, Brenda et al. 2020. 'TriMix and Tumor Antigen MRNA Electroporated Dendritic Cell Vaccination plus Ipilimumab: Link between T-Cell Activation and Clinical Responses in Advanced Melanoma'. *Journal for ImmunoTherapy of Cancer* 8(1): e000329.

Keir, Mary E., Manish J. Butte, Gordon J. Freeman, and Arlene H. Sharpe. 2008. 'PD-1 and Its Ligands in Tolerance and Immunity'. *Annual Review of Immunology* 26(1): 677–704.

Kemény, Lajos, Thomas Ruzicka, and Otto Braun-Falco. 1990. 'Dithranol: A Review of the Mechanism of Action in the Treatment of Psoriasis Vulgaris'. *Skin Pharmacol* 3: 1–20.

Kim, Chae Won, Kyun-Do Kim, and Heung Kyu Lee. 2021. 'The Role of Dendritic Cells in Tumor Microenvironments and Their Uses as Therapeutic Targets'. *BMB Reports* 54(1): 31–43.

Kim, Dong Ha et al. 2019. 'Exosomal PD-L1 Promotes Tumor Growth through Immune Escape in Non-Small Cell Lung Cancer'. *Experimental & Molecular Medicine* 51(8): 1–13.

Kitamura, Hidemitsu et al. 1999. 'The Natural Killer T (NKT) Cell Ligand α-Galactosylceramide Demonstrates Its Immunopotentiating Effect by Inducing Interleukin (IL)-12 Production by Dendritic Cells and IL-12 Receptor Expression on NKT Cells'. *Journal of Experimental Medicine* 189(7): 1121–28.

Kleinovink, Jan Willem et al. 2017. 'PD-L1 Expression on Malignant Cells Is No Prerequisite for Checkpoint Therapy'. *OncoImmunology* 6(4): e1294299.

Klose, Christoph S.N. et al. 2014. 'Differentiation of Type 1 ILCs from a Common Progenitor to All Helper-like Innate Lymphoid Cell Lineages'. *Cell* 157(2): 340–56.

Kochupurakkal, Bose S. et al. 2015. 'RelA-Induced Interferon Response Negatively Regulates Proliferation'. *PLOS ONE* 10(10): e0140243.

Konen, Jessica M., Jared J. Fradette, and Don L. Gibbons. 2019. 'The Good, the Bad and the Unknown of CD38 in the Metabolic Microenvironment and Immune Cell Functionality of Solid Tumors'. *Cells* 9(1): 52.

Krejcik, Jakub et al. 2016. 'Daratumumab Depletes CD38+ Immune Regulatory Cells, Promotes T-Cell Expansion, and Skews T-Cell Repertoire in Multiple Myeloma'. *Blood* 128(3): 384–94.

Krummel, M F, and J P Allison. 1995. 'CD28 and CTLA-4 Have Opposing Effects on the Response of T Cells to Stimulation.' *Journal of Experimental Medicine* 182(2): 459–65.

Kubli, Shawn P. et al. 2021. 'Beyond Immune Checkpoint Blockade: Emerging Immunological Strategies'. *Nature Reviews Drug Discovery* 20(12): 899–919.

Kuhn, Nicholas F. et al. 2019. 'CD40 Ligand-Modified Chimeric Antigen Receptor T Cells Enhance Antitumor Function by Eliciting an Endogenous Antitumor Response'. *Cancer Cell* 35(3): 473-488.e6.

Kumar, Vivek et al. 2017. 'Current Diagnosis and Management of Immune Related Adverse Events (IrAEs) Induced by Immune Checkpoint Inhibitor Therapy'. *Frontiers in Pharmacology* 8.

Kursunel, M. Alper, and Gunes Esendagli. 2016. 'The Untold Story of IFN-γ in Cancer Biology'. *Cytokine & Growth Factor Reviews* 31: 73–81.

Kwon, Eugene D et al. 2014. 'Ipilimumab versus Placebo after Radiotherapy in Patients with Metastatic Castration-Resistant Prostate Cancer That Had Progressed after Docetaxel Chemotherapy (CA184-043): A Multicentre, Randomised, Double-Blind, Phase 3 Trial'. *The Lancet Oncology* 15(7): 700–712.

Labani-Motlagh, Alireza, Mehrnoush Ashja-Mahdavi, and Angelica Loskog. 2020. 'The Tumor Microenvironment: A Milieu Hindering and Obstructing Antitumor Immune Responses'. *Frontiers in Immunology* 11.

Lange, R. W., P. J. Hayden, C. F. Chignell, and M. I. Luster. 1998. 'Anthralin Stimulates Keratinocyte-Derived Proinflammatory Cytokines via Generation of Reactive Oxygen Species'. *Inflammation Research* 47(4): 174–81.

Laoui, Damya et al. 2014. 'Functional Relationship between Tumor-Associated Macrophages and Macrophage Colony-Stimulating Factor as Contributors to Cancer Progression'. *Frontiers in Immunology* 5.

Lavin, Yonit et al. 2017. 'Innate Immune Landscape in Early Lung Adenocarcinoma by Paired Single-Cell Analyses'. *Cell* 169(4): 750-765.e17.

Lázár-Molnár, Eszter et al. 2008. 'Crystal Structure of the Complex between Programmed Death-1 (PD-1) and Its Ligand PD-L2'. *Proceedings of the National Academy of Sciences* 105(30): 10483–88.

Leach, Dana R., Matthew F. Krummel, and James P. Allison. 1996. 'Enhancement of Antitumor Immunity by CTLA-4 Blockade'. *Science* 271(5256): 1734–36.

Lebegge, Els et al. 2020. 'Innate Immune Defense Mechanisms by Myeloid Cells That Hamper Cancer Immunotherapy'. *Frontiers in Immunology* 11.

Lei, Yalan et al. 2021. 'Applications of Single-Cell Sequencing in Cancer Research: Progress and Perspectives'. *Journal of Hematology & Oncology* 14(1): 91.

Lesokhin, Alexander M. et al. 2012. 'Monocytic CCR2+ Myeloid-Derived Suppressor Cells Promote Immune Escape by Limiting Activated CD8 T-Cell Infiltration into the Tumor Microenvironment'. *Cancer Research* 72(4): 876–86.

Levy, Ayelet et al. 2012. 'CD38 Deficiency in the Tumor Microenvironment Attenuates Glioma Progression and Modulates Features of Tumor-Associated Microglia/Macrophages'. *Neuro-Oncology* 14(8): 1037–49.

Li, Dongbo et al. 2020. 'Tumor-associated Macrophages Secrete CC-chemokine Ligand 2 and Induce Tamoxifen Resistance by Activating PI3K/Akt/MTOR in Breast Cancer'. *Cancer Science* 111(1): 47–58.

Li, Dongdong et al. 2021. 'Progress and Perspective of Microneedle System for Anti-Cancer Drug Delivery'. *Biomaterials* 264: 120410.

Li, Lei, and Nikolai Petrovsky. 2016. 'Molecular Mechanisms for Enhanced DNA Vaccine Immunogenicity'. *Expert Review of Vaccines* 15(3): 313–29.

Li, Lihong et al. 2020. 'Effects of Immune Cells and Cytokines on Inflammation and Immunosuppression in the Tumor Microenvironment'. *International Immunopharmacology* 88: 106939.

Li, Wei et al. 2012. 'Comparison of the Regulation of β-Catenin Signaling by Type I, Type II and Type III Interferons in Hepatocellular Carcinoma Cells'. *PLoS ONE* 7(10): e47040.

Li, Xian-Yang et al. 2022. 'NKG7 Is Required for Optimal Antitumor T-Cell Immunity'. *Cancer Immunology Research* 10(2): 154–61.

Li, Xiaoguang et al. 2017. 'Targeting of Tumour-Infiltrating Macrophages via CCL2/CCR2 Signalling as a Therapeutic Strategy against Hepatocellular Carcinoma'. *Gut* 66(1): 157–67.

Lin, Chiou-Feng et al. 2017. 'Escape from IFN-γ-Dependent Immunosurveillance in Tumorigenesis'. *Journal of Biomedical Science* 24(1): 10.

Lin, David Yin-wei et al. 2008. 'The PD-1/PD-L1 Complex Resembles the Antigen-Binding Fv Domains of Antibodies and T Cell Receptors'. *Proceedings of the National Academy of Sciences* 105(8): 3011–16.

Lin, Matthew J. et al. 2022. 'Cancer Vaccines: The next Immunotherapy Frontier'. *Nature Cancer* 3(8): 911–26.

Linderman, George C. et al. 2019. 'Fast Interpolation-Based t-SNE for Improved Visualization of Single-Cell RNA-Seq Data'. *Nature Methods* 16(3): 243–45.

Linsley, Peter S. et al. 1994. 'Human B7-1 (CD80) and B7-2 (CD86) Bind with Similar Avidities but Distinct Kinetics to CD28 and CTLA-4 Receptors'. *Immunity* 1(9): 793–801.

Liu, Jian et al. 2022. 'Cancer Vaccines as Promising Immuno-Therapeutics: Platforms and Current Progress'. *Journal of Hematology & Oncology* 15(1): 28.

Liu, Yang, and Xuetao Cao. 2015. 'The Origin and Function of Tumor-Associated Macrophages'. *Cellular & Molecular Immunology* 12(1): 1–4.

Lopes, Alessandra, Gaëlle Vandermeulen, and Véronique Préat. 2019. 'Cancer DNA Vaccines: Current Preclinical and Clinical Developments and Future Perspectives'. *Journal of Experimental & Clinical Cancer Research* 38(1): 146.

Lopez, Jamie A. et al. 2013. 'Perforin Forms Transient Pores on the Target Cell Plasma Membrane to Facilitate Rapid Access of Granzymes during Killer Cell Attack'. *Blood* 121(14): 2659–68.

Lopez, Pamela Aranda et al. 2017. 'Transcutaneous Immunization with a Novel Imiquimod Nanoemulsion Induces Superior T Cell Responses and Virus Protection'. *Journal of Dermatological Science* 87(3): 252–59.

Lynch, Thomas J. et al. 2012. 'Ipilimumab in Combination With Paclitaxel and Carboplatin As First-Line Treatment in Stage IIIB/IV Non–Small-Cell Lung Cancer: Results From a Randomized, Double-Blind, Multicenter Phase II Study'. *Journal of Clinical Oncology* 30(17): 2046–54.

Ma, Daphne Y., and Edward A. Clark. 2009. 'The Role of CD40 and CD154/CD40L in Dendritic Cells'. *Seminars in Immunology* 21(5): 265–72.

Mack, Matthias et al. 2001. 'Expression and Characterization of the Chemokine Receptors CCR2 and CCR5 in Mice'. *The Journal of Immunology* 166(7): 4697–4704.

Maher, John et al. 2002. 'Human T-Lymphocyte Cytotoxicity and Proliferation Directed by a Single Chimeric TCRζ /CD28 Receptor'. *Nature Biotechnology* 20(1): 70–75.

Malarkannan, Subramaniam. 2020. 'NKG7 Makes a Better Killer'. *Nature Immunology* 21(10): 1139–40.

Malavasi, Fabio et al. 2008. 'Evolution and Function of the ADP Ribosyl Cyclase/CD38 Gene Family in Physiology and Pathology'. *Physiological Reviews* 88(3): 841–86.

Mantovani, Alberto et al. 2017. 'Tumour-Associated Macrophages as Treatment Targets in Oncology'. *Nature Reviews Clinical Oncology* 14(7): 399–416.

Martini, Matteo et al. 2010. 'IFN-γ-Mediated Upmodulation of MHC Class I Expression Activates Tumor-Specific Immune Response in a Mouse Model of Prostate Cancer'. *Vaccine* 28(20): 3548–57.

Mass, Elvira et al. 2016. 'Specification of Tissue-Resident Macrophages during Organogenesis'. *Science* 353(6304).

Matsushita, Hirokazu et al. 2012. 'Cancer Exome Analysis Reveals a T-Cell-Dependent Mechanism of Cancer Immunoediting'. *Nature* 482(7385): 400–404.

McCarthy, Edward F. 2006. 'The Toxins of William B. Coley and the Treatment of Bone and Soft-Tissue Sarcomas.' *The Iowa orthopaedic journal* 26: 154–58.

Le Mercier, Isabelle, J. Louise Lines, and Randolph J. Noelle. 2015. 'Beyond CTLA-4 and PD-1, the Generation Z of Negative Checkpoint Regulators'. *Frontiers in Immunology* 6.

Miller, M A, and E Pisani. 1999. 'The Cost of Unsafe Injections.' *Bulletin of the World Health Organization* 77(10): 808–11.

Mishra, Rabinarayan, Alex T. Chen, Raymond M. Welsh, and Eva Szomolanyi-Tsuda. 2010. 'NK Cells and Γδ T Cells Mediate Resistance to Polyomavirus–Induced Tumors'. *PLoS Pathogens* 6(5): e1000924.

Mitchem, Jonathan B. et al. 2013. 'Targeting Tumor-Infiltrating Macrophages Decreases Tumor-Initiating Cells, Relieves Immunosuppression, and Improves Chemotherapeutic Responses'. *Cancer Research* 73(3): 1128–41.

Mojic, Marija, Kazuyoshi Takeda, and Yoshihiro Hayakawa. 2017. 'The Dark Side of IFN-γ: Its Role in Promoting Cancer Immunoevasion'. *International Journal of Molecular Sciences* 19(1): 89.

Mollica Poeta, Valeria, Matteo Massara, Arianna Capucetti, and Raffaella Bonecchi. 2019. 'Chemokines and Chemokine Receptors: New Targets for Cancer Immunotherapy'. *Frontiers in Immunology* 10.

Morandi, Fabio et al. 2015. 'A Non-Canonical Adenosinergic Pathway Led by CD38 in Human Melanoma Cells Induces Suppression of T Cell Proliferation'. *Oncotarget* 6(28): 25602–18.

Moskowitz, Craig H. et al. 2016. 'Pembrolizumab in Relapsed/Refractory Classical Hodgkin Lymphoma: Primary End Point Analysis of the Phase 2 Keynote-087 Study'. *Blood* 128(22): 1107–1107.

Motz, Gregory T et al. 2014. 'Tumor Endothelium FasL Establishes a Selective Immune Barrier Promoting Tolerance in Tumors'. *Nature Medicine* 20(6): 607–15.

Motzer, Robert J. et al. 2015. 'Nivolumab versus Everolimus in Advanced Renal-Cell Carcinoma'. *New England Journal of Medicine* 373(19): 1803–13.

Movahedi, Kiavash et al. 2010. 'Different Tumor Microenvironments Contain Functionally Distinct Subsets of Macrophages Derived from Ly6C(High) Monocytes'. *Cancer Research* 70(14): 5728–39.

Mu, Xing-Yu et al. 2019. 'RS 504393 Inhibits M-MDSCs Recruiting in Immune Microenvironment of Bladder Cancer after Gemcitabine Treatment'. *Molecular Immunology* 109: 140–48.

Neelapu, Sattva S. et al. 2018. 'Chimeric Antigen Receptor T-Cell Therapy — Assessment and Management of Toxicities'. *Nature Reviews Clinical Oncology* 15(1): 47–62.

Ngambenjawong, Chayanon, Heather H. Gustafson, and Suzie H. Pun. 2017. 'Progress in Tumor-Associated Macrophage (TAM)-Targeted Therapeutics'. *Advanced Drug Delivery Reviews* 114: 206–21.

Ni, Ling, and Jian Lu. 2018. 'Interferon Gamma in Cancer Immunotherapy'. *Cancer Medicine* 7(9): 4509–16.

Nishikawa, Hiroyoshi, and Shimon Sakaguchi. 2014. 'Regulatory T Cells in Cancer Immunotherapy'. *Current Opinion in Immunology* 27: 1–7.

Nixon, Briana G. et al. 2022. 'Tumor-Associated Macrophages Expressing the Transcription Factor IRF8 Promote T Cell Exhaustion in Cancer'. *Immunity* 55(11): 2044-2058.e5.

Noy, Roy, and Jeffrey W. Pollard. 2014. 'Tumor-Associated Macrophages: From Mechanisms to Therapy'. *Immunity* 41(1): 49–61.

O'Donnell, Jake S. et al. 2017. 'Resistance to PD1/PDL1 Checkpoint Inhibition'. *Cancer Treatment Reviews* 52: 71–81.

O'Donnell, Jake S., Michele W. L. Teng, and Mark J. Smyth. 2019. 'Cancer Immunoediting and Resistance to T Cell-Based Immunotherapy'. *Nature Reviews Clinical Oncology* 16(3): 151–67.

Ogonek, Justyna et al. 2016. 'Immune Reconstitution after Allogeneic Hematopoietic Stem Cell Transplantation'. *Frontiers in Immunology* 7.

Ohta, Akio et al. 2012. 'The Development and Immunosuppressive Functions of CD4+ CD25+ FoxP3+ Regulatory T Cells Are under Influence of the Adenosine-A2A Adenosine Receptor Pathway'. *Frontiers in Immunology* 3.

Orozco, Susana L, Susan P Canny, and Jessica A Hamerman. 2021. 'Signals Governing Monocyte Differentiation during Inflammation'. *Current Opinion in Immunology* 73: 16–24.

O'Shea, Jesse, Mark R. Prausnitz, and Nadine Rouphael. 2021. 'Dissolvable Microneedle Patches to Enable Increased Access to Vaccines against SARS-CoV-2 and Future Pandemic Outbreaks'. *Vaccines* 9(4): 320.

Oyewole-Said, Damilola et al. 2020. 'Beyond T-Cells: Functional Characterization of CTLA-4 Expression in Immune and Non-Immune Cell Types'. *Frontiers in Immunology* 11.

Pahne-Zeppenfeld, Jennifer et al. 2014. 'Cervical Cancer Cell-Derived Interleukin-6 Impairs CCR7-Dependent Migration of MMP-9-Expressing Dendritic Cells'. *International Journal of Cancer* 134(9): 2061–73.

van Panhuis, Willem G. et al. 2013. 'Contagious Diseases in the United States from 1888 to the Present'. *New England Journal of Medicine* 369(22): 2152–58.

Pardi, Norbert, Michael J. Hogan, Frederick W. Porter, and Drew Weissman. 2018. 'MRNA Vaccines — a New Era in Vaccinology'. *Nature Reviews Drug Discovery* 17(4): 261–79.

Pasparakis, Manolis, Ingo Haase, and Frank O. Nestle. 2014. 'Mechanisms Regulating Skin Immunity and Inflammation'. *Nature Reviews Immunology* 14(5): 289–301.

Patsoukis, Nikolaos et al. 2012. 'Selective Effects of PD-1 on Akt and Ras Pathways Regulate Molecular Components of the Cell Cycle and Inhibit T Cell Proliferation'. *Science Signaling* 5(230).

Pauken, Kristen E., and E. John Wherry. 2015. 'SnapShot: T Cell Exhaustion'. *Cell* 163(4): 1038-1038.e1.

Peng, Weiyi et al. 2016. 'Loss of PTEN Promotes Resistance to T Cell–Mediated Immunotherapy'. *Cancer Discovery* 6(2): 202–16.

Pépin, Jacques et al. 2014. 'Evolution of the Global Burden of Viral Infections from Unsafe Medical Injections, 2000–2010'. *PLoS ONE* 9(6): e99677.

Pesce, John T. et al. 2009. 'Arginase-1–Expressing Macrophages Suppress Th2 Cytokine–Driven Inflammation and Fibrosis'. *PLoS Pathogens* 5(4): e1000371.

Porter, David L. et al. 2011. 'Chimeric Antigen Receptor–Modified T Cells in Chronic Lymphoid Leukemia'. *New England Journal of Medicine* 365(8): 725–33.

Prager, Isabel et al. 2019. 'NK Cells Switch from Granzyme B to Death Receptor–Mediated Cytotoxicity during Serial Killing'. *Journal of Experimental Medicine* 216(9): 2113–27.

Qian, Bin-Zhi et al. 2011. 'CCL2 Recruits Inflammatory Monocytes to Facilitate Breast-Tumour Metastasis'. *Nature* 475(7355): 222–25.

Qin, Zhihai et al. 2003. 'A Critical Requirement of Interferon Gamma-Mediated Angiostasis for Tumor Rejection by CD8+ T Cells.' *Cancer research* 63(14): 4095–4100.

Quail, Daniela F, and Johanna A Joyce. 2013. 'Microenvironmental Regulation of Tumor Progression and Metastasis'. *Nature Medicine* 19(11): 1423–37.

Rausch, Johanna et al. 2017. 'Combined Immunotherapy: CTLA-4 Blockade Potentiates Anti-Tumor Response Induced by Transcutaneous Immunization'. *Journal of Dermatological Science* 87(3): 300–306. http://dx.doi.org/10.1016/j.jdermsci.2017.06.013.

Rechtsteiner, Gerd et al. 2005. 'Cutting Edge: Priming of CTL by Transcutaneous Peptide Immunization with Imiquimod'. *The Journal of Immunology* 174(5): 2476–80.

Reck, M. et al. 2013. 'Ipilimumab in Combination with Paclitaxel and Carboplatin as First-Line Therapy in Extensive-Disease-Small-Cell Lung Cancer: Results from a Randomized, Double-Blind, Multicenter Phase 2 Trial'. *Annals of Oncology* 24(1): 75–83.

Reeves, Emma, and Edward James. 2017. 'Antigen Processing and Immune Regulation in the Response to Tumours'. *Immunology* 150(1): 16–24.

Relation, Theresa et al. 2018. 'Intratumoral Delivery of Interferony-Secreting Mesenchymal Stromal Cells Repolarizes Tumor-Associated Macrophages and Suppresses Neuroblastoma Proliferation In Vivo'. *Stem Cells* 36(6): 915–24.

Riabov, Vladimir et al. 2014. 'Role of Tumor Associated Macrophages in Tumor Angiogenesis and Lymphangiogenesis'. *Frontiers in Physiology* 5.

Ribas, Antoni. 2012. 'Tumor Immunotherapy Directed at PD-1'. *New England Journal of Medicine* 366(26): 2517–19.

Robert, Caroline et al. 2015. 'Pembrolizumab versus Ipilimumab in Advanced Melanoma'. *New England Journal of Medicine* 372(26): 2521–32.

Roh, Whijae et al. 2017. 'Integrated Molecular Analysis of Tumor Biopsies on Sequential CTLA-4 and PD-1 Blockade Reveals Markers of Response and Resistance'. *Science Translational Medicine* 9(379).

Rosenberg, S. A. et al. 1994. 'Treatment of Patients With Metastatic Melanoma With Autologous Tumor-Infiltrating Lymphocytes and Interleukin 2'. *JNCI Journal of the National Cancer Institute* 86(15): 1159–66.

Rosenberg, Steven A. et al. 1988. 'Use of Tumor-Infiltrating Lymphocytes and Interleukin-2 in the Immunotherapy of Patients with Metastatic Melanoma'. *New England Journal of Medicine* 319(25): 1676–80.

Rosenberg, Steven A et al. 2011. 'Durable Complete Responses in Heavily Pretreated Patients with Metastatic Melanoma Using T-Cell Transfer Immunotherapy.' *Clinical cancer research* 17(13): 4550–57.

Rossin, Aurélie, Giorgia Miloro, and Anne-Odile Hueber. 2019. 'TRAIL and FasL Functions in Cancer and Autoimmune Diseases: Towards an Increasing Complexity'. *Cancers* 11(5): 639.

Rue-Albrecht, Kevin, Federico Marini, Charlotte Soneson, and Aaron T L Lun. 2018. 'ISEE: Interactive SummarizedExperiment Explorer'. *F1000Research* 7: 741.

Rüegg, Curzio et al. 1998. 'Evidence for the Involvement of Endotheliai Cell Integrin AVβ3 in the Disruption of the Tumor Vascuiature Induced by TNF and IFN-γ'. *Nature Medicine* 4(4): 408–14.

Sadelain, Michel, Renier Brentjens, and Isabelle Rivière. 2013. 'The Basic Principles of Chimeric Antigen Receptor Design'. *Cancer Discovery* 3(4): 388–98.

Sahin, Ugur et al. 2017. 'Personalized RNA Mutanome Vaccines Mobilize Poly-Specific Therapeutic Immunity against Cancer'. *Nature* 547(7662): 222–26.

Sahin, Ugur et al. 2020. 'An RNA Vaccine Drives Immunity in Checkpoint-Inhibitor-Treated Melanoma.' *Nature* 585(7823): 107–12.

Saito, Yasuyuki et al. 2022. 'The Role of Type-2 Conventional Dendritic Cells in the Regulation of Tumor Immunity'. *Cancers* 14(8): 1976.

Sakaguchi, S et al. 1995. 'Immunologic Self-Tolerance Maintained by Activated T Cells Expressing IL-2 Receptor Alpha-Chains (CD25). Breakdown of a Single Mechanism of Self-Tolerance Causes Various Autoimmune Diseases.' *Journal of immunology* 155(3): 1151–64.

Saman, Harman, Syed Shadab Raza, Shahab Uddin, and Kakil Rasul. 2020. 'Inducing Angiogenesis, a Key Step in Cancer Vascularization, and Treatment Approaches'. *Cancers* 12(5): 1172.

Sanford, Dominic E. et al. 2013. 'Inflammatory Monocyte Mobilization Decreases Patient Survival in Pancreatic Cancer: A Role for Targeting the CCL2/CCR2 Axis'. *Clinical Cancer Research* 19(13): 3404–15.

Sanmamed, M.F. et al. 2017. 'Changes in Serum Interleukin-8 (IL-8) Levels Reflect and Predict Response to Anti-PD-1 Treatment in Melanoma and Non-Small-Cell Lung Cancer Patients'. *Annals of Oncology* 28(8): 1988–95.

Saxena, Mansi, Sjoerd H. van der Burg, Cornelis J. M. Melief, and Nina Bhardwaj. 2021. 'Therapeutic Cancer Vaccines'. *Nature Reviews Cancer* 21(6): 360–78.

Schadendorf, Dirk et al. 2015. 'Pooled Analysis of Long-Term Survival Data From Phase II and Phase III Trials of Ipilimumab in Unresectable or Metastatic Melanoma'. *Journal of Clinical Oncology* 33(17): 1889–94.

Schlecker, Eva et al. 2012. 'Tumor-Infiltrating Monocytic Myeloid-Derived Suppressor Cells Mediate CCR5-Dependent Recruitment of Regulatory T Cells Favoring Tumor Growth'. *The Journal of Immunology* 189(12): 5602–11.

Schreiber, Robert D., Lloyd J. Old, and Mark J. Smyth. 2011. 'Cancer Immunoediting: Integrating Immunity's Roles in Cancer Suppression and Promotion'. *Science* 331(6024): 1565–70.

Schunk, M. K., and G. E. Macallum. 2005. 'Applications and Optimization of Immunization Procedures'. *ILAR Journal* 46(3): 241–57.

Serbina, Natalya V, and Eric G Pamer. 2006. 'Monocyte Emigration from Bone Marrow during Bacterial Infection Requires Signals Mediated by Chemokine Receptor CCR2'. *Nature Immunology* 7(3): 311–17.

Sharma, Padmanee et al. 2017. 'Nivolumab in Metastatic Urothelial Carcinoma after Platinum Therapy (CheckMate 275): A Multicentre, Single-Arm, Phase 2 Trial'. *The Lancet Oncology* 18(3): 312–22.

Sharpe, Arlene H., and Kristen E. Pauken. 2018. 'The Diverse Functions of the PD1 Inhibitory Pathway'. *Nature Reviews Immunology* 18(3): 153–67.

Shen, Jing et al. 2018. 'Anti-Cancer Therapy with TNFα and IFNγ: A Comprehensive Review'. *Cell Proliferation* 51(4): e12441.

Smyth, Mark J. et al. 2005. 'NKG2D Function Protects the Host from Tumor Initiation'. *Journal of Experimental Medicine* 202(5): 583–88.

Sohl, Julian. 2021. *Anthralin Als Neues Adjuvans in Der Transkutanen Immunisierung*. 3. Medizinische Klinik der Universitätsmedizin, Johannes Gutenberg-Universität Mainz, Germany.

Sohl, Julian et al. 2022. 'Dithranol as Novel Co-Adjuvant for Non-Invasive Dermal Vaccination'. *npj Vaccines* 7(1).

Soria, Gali, and Adit Ben-Baruch. 2008. 'The Inflammatory Chemokines CCL2 and CCL5 in Breast Cancer'. *Cancer Letters* 267(2): 271–85.

Sorrentino, Claudia et al. 2015. 'Myeloid-Derived Suppressor Cells Contribute to A2B Adenosine Receptor-Induced VEGF Production and Angiogenesis in a Mouse Melanoma Model'. *Oncotarget* 6(29): 27478–89.

Spolski, Rosanne, Peng Li, and Warren J. Leonard. 2018. 'Biology and Regulation of IL-2: From Molecular Mechanisms to Human Therapy'. *Nature Reviews Immunology* 18(10): 648–59.

Spranger, Stefani, Riyue Bao, and Thomas F. Gajewski. 2015. 'Melanoma-Intrinsic β-Catenin Signalling Prevents Anti-Tumour Immunity'. *Nature* 523(7559): 231–35.

Spranger, Stefani, and Thomas F. Gajewski. 2018a. 'Mechanisms of Tumor Cell–Intrinsic Immune Evasion'. *Annual Review of Cancer Biology* 2(1): 213–28.

Spranger, Stefani, and Thomas F Gajewski. 2018b. 'Mechanisms of Tumor Cell-Intrinsic Immune Evasion'. *Annu. Rev. Cancer Biol* 2: 213–28. https://doi.org/10.1146/annurev-cancerbio-.

Stagg, John et al. 2011. 'CD73-Deficient Mice Have Increased Antitumor Immunity and Are Resistant to Experimental Metastasis'. *Cancer Research* 71(8): 2892–2900.

Stein, Pamela et al. 2011. 'UV Exposure Boosts Transcutaneous Immunization and Improves Tumor Immunity: Cytotoxic T-Cell Priming through the Skin'. *Journal of Investigative Dermatology* 131(1): 211–19.

Stickdorn, Judith et al. 2022. 'Systemically Administered TLR7/8 Agonist and Antigen-Conjugated Nanogels Govern Immune Responses against Tumors'. *ACS Nano* 16(3): 4426–43.

Stoitzner, Patrizia et al. 2006. 'Langerhans Cells Cross-Present Antigen Derived from Skin'. *Proceedings of the National Academy of Sciences* 103(20): 7783–88.

Sun, Yue et al. 2017. 'CCN1 Promotes IL-1β Production in Keratinocytes by Activating P38 MAPK Signaling in Psoriasis'. *Scientific Reports* 7(1): 43310.

Sunderkötter, Cord et al. 2004. 'Subpopulations of Mouse Blood Monocytes Differ in Maturation Stage and Inflammatory Response'. *The Journal of Immunology* 172(7): 4410–17.

Suschak, John J., James A. Williams, and Connie S. Schmaljohn. 2017. 'Advancements in DNA Vaccine Vectors, Non-Mechanical Delivery Methods, and Molecular Adjuvants to Increase Immunogenicity'. *Human Vaccines & Immunotherapeutics* 13(12): 2837–48.

Tan, M H, E D Holyoke, and M H Goldrosen. 1976. 'Brief Communication: Murine Colon Adenocarcinomas: Methods for Selective Culture In Vitrol,2'. *Journal of the national Cancer Institute* 56(4).

Tang, Jun, Laura Pearce, Jill O'Donnell-Tormey, and Vanessa M. Hubbard-Lucey. 2018. 'Trends in the Global Immuno-Oncology Landscape'. *Nature Reviews Drug Discovery* 17(11): 783–84.

Tang, Tianyu et al. 2021. 'Advantages of Targeting the Tumor Immune Microenvironment over Blocking Immune Checkpoint in Cancer Immunotherapy'. *Signal Transduction and Targeted Therapy* 6(1): 72.

Taraban, Vadim Y. et al. 2008. 'Invariant NKT Cells Promote CD8+ Cytotoxic T Cell Responses by Inducing CD70 Expression on Dendritic Cells'. *The Journal of Immunology* 180(7): 4615–20.

Teng, Michele W.L., Shin Foong Ngiow, Antoni Ribas, and Mark J. Smyth. 2015. 'Classifying Cancers Based on T-Cell Infiltration and PD-L1'. *Cancer Research* 75(11): 2139–45.

Thijssen, Victor LJL et al. 2018. 'Targeting PDGF-Mediated Recruitment of Pericytes Blocks Vascular Mimicry and Tumor Growth'. *The Journal of Pathology* 246(4): 447–58.

Tomić, Sergej et al. 2019. 'Prostaglanin-E2 Potentiates the Suppressive Functions of Human Mononuclear Myeloid-Derived Suppressor Cells and Increases Their Capacity to Expand IL-10-Producing Regulatory T Cell Subsets'. *Frontiers in Immunology* 10.

Turnis, Meghan E. et al. 2016. 'Interleukin-35 Limits Anti-Tumor Immunity'. *Immunity* 44(2): 316–29.

Tuthill, Mark, and Hatzimichael. 2010. 'Hematopoietic Stem Cell Transplantation'. *Stem Cells and Cloning: Advances and Applications*: 105.

Ugel, Stefano, Stefania Canè, Francesco De Sanctis, and Vincenzo Bronte. 2021. 'Monocytes in the Tumor Microenvironment'. *Annual Review of Pathology: Mechanisms of Disease* 16(1): 93–122.

Umansky, Viktor, and Alexandra Sevko. 2013. 'Tumor Microenvironment and Myeloid-Derived Suppressor Cells'. *Cancer Microenvironment* 6(2): 169–77.

Vansteenkiste, Johan F et al. 2016. 'Efficacy of the MAGE-A3 Cancer Immunotherapeutic as Adjuvant Therapy in Patients with Resected MAGE-A3-Positive Non-Small-Cell Lung Cancer (MAGRIT): A

Randomised, Double-Blind, Placebo-Controlled, Phase 3 Trial'. *The Lancet Oncology* 17(6): 822–35.

Veglia, Filippo et al. 2021. 'Analysis of Classical Neutrophils and Polymorphonuclear Myeloid-Derived Suppressor Cells in Cancer Patients and Tumor-Bearing Mice'. *Journal of Experimental Medicine* 218(4).

Veglia, Filippo, Michela Perego, and Dmitry Gabrilovich. 2018. 'Myeloid-Derived Suppressor Cells Coming of Age'. *Nature Immunology* 19(2): 108–19.

Vijayan, Dipti, Arabella Young, Michele W.L. Teng, and Mark J. Smyth. 2017. 'Targeting Immunosuppressive Adenosine in Cancer'. *Nature Reviews Cancer* 17(12): 709–24.

Voskoboinik, Ilia, James C. Whisstock, and Joseph A. Trapani. 2015. 'Perforin and Granzymes: Function, Dysfunction and Human Pathology'. *Nature Reviews Immunology* 15(6): 388–400.

Waldhauer, I, and A Steinle. 2008. 'NK Cells and Cancer Immunosurveillance'. *Oncogene* 27(45): 5932–43.

Wang, Jie, Muhetaerjiang Mamuti, and Hao Wang. 2020. 'Therapeutic Vaccines for Cancer Immunotherapy'. *ACS Biomaterials Science & Engineering* 6(11): 6036–52.

Wang, Lu et al. 2015. 'Deficiency of Interferon-Gamma or Its Receptor Promotes Colorectal Cancer Development'. *Journal of Interferon & Cytokine Research* 35(4): 273–80.

Wang, Peng-Fei et al. 2017. 'Immune-Related Adverse Events Associated with Anti-PD-1/PD-L1 Treatment for Malignancies: A Meta-Analysis'. *Frontiers in Pharmacology* 8.

Warger, Tobias et al. 2007. 'Transcutaneous Immunization with Imiquimod Is Amplified by CD40 Ligation and Results in Sustained Cytotoxic T-Lymphocyte Activation and Tumor Protection'. *Clinical Reviews in Allergy and Immunology* 32(1): 57–65.

Wherry, E John. 2011. 'T Cell Exhaustion'. *Nature Immunology* 12(6): 492–99.

Wherry, E. John, and Makoto Kurachi. 2015. 'Molecular and Cellular Insights into T Cell Exhaustion'. *Nature Reviews Immunology* 15(8): 486–99.

Whiteside, T L. 2008. 'The Tumor Microenvironment and Its Role in Promoting Tumor Growth'. *Oncogene* 27(45): 5904–12.

Woo, Seng-Ryong et al. 2014. 'STING-Dependent Cytosolic DNA Sensing Mediates Innate Immune Recognition of Immunogenic Tumors'. *Immunity* 41(5): 830–42.

World Health Organization. 2015. *WHO Guideline on the Use of Safety-Engineered Syringes for Intramuscular, Intradermal and Subcutaneous Injections in Health Care Settings.*

Wu, Qian et al. 2021. 'Small Molecule Inhibitors Targeting the PD-1/PD-L1 Signaling Pathway'. *Acta Pharmacologica Sinica* 42(1): 1–9.

Xu, Maosen et al. 2021. 'Role of the CCL2-CCR2 Signalling Axis in Cancer: Mechanisms and Therapeutic Targeting'. *Cell Proliferation* 54(10).

Yang, Arvin S, and Edmund C Lattime. 2003. 'Tumor-Induced Interleukin 10 Suppresses the Ability of Splenic Dendritic Cells to Stimulate CD4 and CD8 T-Cell Responses.' *Cancer research* 63(9): 2150–57.

Yang, Hui et al. 2020. 'CCL2-CCR2 Axis Recruits Tumor Associated Macrophages to Induce Immune Evasion through PD-1 Signaling in Esophageal Carcinogenesis'. *Molecular Cancer* 19(1): 41.

Yang, James C. et al. 2007. 'Ipilimumab (Anti-CTLA4 Antibody) Causes Regression of Metastatic Renal Cell Cancer Associated With Enteritis and Hypophysitis'. *Journal of Immunotherapy* 30(8): 825–30.

Yang, Yi-Fu et al. 2000. 'Requirement for IFN-γ in IL-12 Production Induced by Collaboration between Vα14+ NKT Cells and Antigen-Presenting Cells'. *International Immunology* 12(12): 1669–75.

Yang, Zihui et al. 2019. 'CCL2/CCR2 Axis Promotes the Progression of Salivary Adenoid Cystic Carcinoma via Recruiting and Reprogramming the Tumor-Associated Macrophages'. *Frontiers in Oncology* 9.

Yona, Simon et al. 2013. 'Fate Mapping Reveals Origins and Dynamics of Monocytes and Tissue Macrophages under Homeostasis'. *Immunity* 38(1): 79–91.

Yu, Wendan et al. 2020. 'PD-L1 Promotes Tumor Growth and Progression by Activating WIP and β-Catenin Signaling Pathways and Predicts Poor Prognosis in Lung Cancer'. *Cell Death & Disease* 11(7): 506.

Zaidi, M. Raza. 2019. 'The Interferon-Gamma Paradox in Cancer'. *Journal of Interferon & Cytokine Research* 39(1): 30–38.

Zaidi, M. Raza, and Glenn Merlino. 2011. 'The Two Faces of Interferon-γ in Cancer'. *Clinical Cancer Research* 17(19): 6118–24.

Zaretsky, Jesse M. et al. 2016. 'Mutations Associated with Acquired Resistance to PD-1 Blockade in Melanoma'. *New England Journal of Medicine* 375(9): 819–29.

Zhan, Xianbao et al. 2020. 'Phase I Trial of Personalized MRNA Vaccine Encoding Neoantigen in Patients with Advanced Digestive System Neoplasms.' *Journal of Clinical Oncology* 38(15_suppl): e15269–e15269.

Zhong, Zhenyu, Elsa Sanchez-Lopez, and Michael Karin. 2016. 'Autophagy, Inflammation, and Immunity: A Troika Governing Cancer and Its Treatment'. *Cell* 166(2): 288–98.

Zhou, Jiawei et al. 2020. 'Tumor-Associated Macrophages: Recent Insights and Therapies'. *Frontiers in Oncology* 10.

Zhou, Zhiwei et al. 2020. 'Granzyme A from Cytotoxic Lymphocytes Cleaves GSDMB to Trigger Pyroptosis in Target Cells'. *Science* 368(6494).

Zhu, Xinmei, Mitsugu Fujita, Linda A. Snyder, and Hideho Okada. 2011. 'Systemic Delivery of Neutralizing Antibody Targeting CCL2 for Glioma Therapy'. *Journal of Neuro-Oncology* 104(1): 83–92.

Zhu, Yu et al. 2014. 'CSF1/CSF1R Blockade Reprograms Tumor-Infiltrating Macrophages and Improves Response to T-Cell Checkpoint Immunotherapy in Pancreatic Cancer Models'. *Cancer Research* 74(18): 5057–69.

Zhu, Yu et al. 2017. 'Tissue-Resident Macrophages in Pancreatic Ductal Adenocarcinoma Originate from Embryonic Hematopoiesis and Promote Tumor Progression'. *Immunity* 47(2): 323-338.e6.

Ziegler-Heitbrock, Loems et al. 2010. 'Nomenclature of Monocytes and Dendritic Cells in Blood'. *Blood* 116(16): e74–80.

Zilionis, Rapolas et al. 2019. 'Single-Cell Transcriptomics of Human and Mouse Lung Cancers Reveals Conserved Myeloid Populations across Individuals and Species'. *Immunity* 50(5): 1317-1334.e10.

Zollo, Massimo et al. 2012. 'Targeting Monocyte Chemotactic Protein-1 Synthesis with Bindarit Induces Tumor Regression in Prostate and Breast Cancer Animal Models'. *Clinical & Experimental Metastasis* 29(6): 585–601.

Zong, Jinbao, Anton A. Keskinov, Galina V. Shurin, and Michael R. Shurin. 2016. 'Tumor-Derived Factors Modulating Dendritic Cell Function'. *Cancer Immunology, Immunotherapy* 65(7): 821–33.

## 7.2 Figure directory

## 7.3  Table directory

## 7.4   scRNA-seq Workflow

The data of the mRNA isolation process for scRNA-seq analysis are shown in Table 7.1 and Table 7.2.

**Table 7.1: Quality control steps during mRNA isolation process for scRNA-seq analysis**

| Isolation step | Immune control experiment | | Immune evasion experiment | |
|---|---|---|---|---|
| | DIVA$^2$ | untreated | DIVA$^2$ | untreated |
| Viability of isolated TILs | 91,3 % | 89,9 % | 93,7 % | 93,6 % |
| Cell load on cartridge | 18091 | | 17353 | |
| Cells with one bead in a well | 13490 | | 13512 | |
| Final Cell multiplet rate | 12,7 % | | 4,9 % | |

**Table 7.2: Metrics summary of the scRNA-seq analysis**

| Category | Immune control experiment | Immune evasion experiment |
|---|---|---|
| Total Reads in FASTQ | 1474959367 | 1907358571 |
| Total Filtered Reads | 1364949296 | 1774267864 |
| Aligned Reads by Type | 776311637 | 1170073411 |
| Putative Cell Count | 9799 | 10742 |
| Sample Tag Filtered Reads | 36197188 | 61266418 |

# 8 Curriculum vitae

## 9 Danksagung

An dieser Stelle möchte ich mich bei den vielen Personen ganz herzlich bedanken, die mich während meiner Promotionszeit begleitet und unterstützt haben.

Besonders möchte ich mich bei meinem Betreuer Prof. Dr. Markus Radsak bedanken. Bereits in der Projekt- und Masterarbeit erhielt ich von Dir die Möglichkeit, an dem sehr interessanten Projekt der Transkutanen Immunisierung zu arbeiten und dies mit der anschließenden Promotion deutlich zu vertiefen. Ich danke Dir sehr für die vielen intensiven wissenschaftlichen Gespräche und die Ratschläge, die ich in meiner Promotionszeit von Dir erhielt. Ich habe in dieser Zeit sehr viel gelernt.

Prof. Dr. Eckhard Thines danke ich für die freundliche Übernahme des Zweitgutachtens.

Besonders möchte ich mich auch bei […] bedanken, da Du mir während meines Studiums als externer Biologie-Student den Einstieg in die Immunologie an der Universitätsmedizin Mainz ermöglicht hast und immer ein offenes Ohr für Fragestellungen aller Art hattest.

Außerdem möchte ich unseren Kooperationspartnern herzlich für die gemeinsame Arbeit danken.

Allen ehemaligen und jetzigen Mitarbeitern des Instituts für Immunologie danke ich für die Unterstützung jeglicher Art sowie die schöne gemeinsame Zeit am Institut.

Den Mitgliedern der Arbeitsgruppen Radsak, Schild und Stassen möchte ich für die intensive Zusammenarbeit, tatkräftige Unterstützung und die tolle Arbeitsatmosphäre in den letzten Jahren danken.

Ganz besonders möchte ich mich bei … bedanken. Im Laufe der Jahre ist eine tolle Freundschaft zu euch entstanden und ihr habt mich in den letzten Jahren bei meinem Projekt entscheidend unterstützt und standet immer mit tatkräftiger Hilfe zur Seite.

Außerdem möchte ich mich herzlich bei […] bedanken. Ihr habt mich in meiner Studien- und Promotionszeit immer unterstützt, an mich geglaubt und hattet immer ein offenes Ohr für mich.

Ein ganz besonderer Dank gilt meiner Frau […] Ich danke Dir von Herzen, dass Du mich in all meinem Handeln absolut unermüdlich unterstützt und immer für mich da bist. Danke, dass es Dich gibt!

Danke Euch allen!